COLLISION-INDUCED ABSORPTION SPECTRA OF MOLECULAR HYDROGEN IN THE SECOND OVERTONE REGION AT 77, 201 AND 298 K

FAN XIANG

COLLISION-INDUCED ABSORPTION SPECTRA OF MOLECULAR HYDROGEN IN THE SECOND OVERTONE REGION AT 77, 201 AND 298 K

by

© Fan Xiang

A thesis submitted to the School of Graduate Studies in partial fulfilment of the requirements for the degree of Master of Science

Department of Physics
Memorial University of Newfoundland

June 1992

St. John's Newfoundland

ISBN 0-315-78087-8

Abstract

The collision-induced absorption spectra of molecular hydrogen in its second overtone region were recorded with a $\sim$ 2.0 m high-pressure low-temperature absorption cell for gas densities up to 1000 amagat at 77, 201 and 298 K. The occurrence of the dip at $Q_3(1)$ with characteristic low- and high- wavenumber components Q_P and Q_R, observed for the first time in the 3-0 band at different temperatures, clearly shows the contribution of the short-range electron-overlap interaction of the collisions to the 3-0 band in contrast to the 2-0 band of H_2. In addition to the overlap components, the observed spectra consist of the long-range quadrupole-induced transitions of the type $Q_3(J) + Q_0(J)$, $S_3(J) + Q_0(J)$, $Q_3(J) + S_0(J)$, $Q_2(J)+Q_1(J)$, $S_2(J)+Q_1(J)$, $Q_2(J)+S_1(J)$ and $S_2(J)+S_1(J)$, where the subscripts 0 to 3 indicate Δv, the change in the vibrational quantum number.

An analysis of the observed profiles was performed by using the Levine-Birnbaum intracollisional line-shape function [Phys. Rev. 154, 86 (1967)] and the Van Kranendonk intercollisional line-shape function [Can. J. Phys. 46, 1173 (1968)] for the overlap-induced transitions, and the Lorentz line-shape function as well as the Birnbaum-Cohen line-shape function

[Can. J. Phys. 54, 593 (1976)] for the quadrupole-induced transitions. Very good agreement between the experimental absorption profiles and the calculated profiles was obtained by reducing the matrix elements of the quadrupolar moment $< 0J|Q|v'J' >$ for $\Delta v = 2$ and 3 by a factor 0.68 and by treating the relative intensities of the three groups of transitions, namely, the overlap transitions, the quadrupolar single transitions and the quadrupolar double transitions, as independent parameters. From this analysis the characteristic half-width parameters δ_d and δ_c for the overlap components, δ_q of the Lorentz line-shape function, and δ_1 and δ_2 of the Birnbaum-Cohen line-shape function for the quadrupole components have been determined.

The analysis of the profiles described above reveals some excess absorption in the band around 12,460 cm^{-1}. As the area under the absorption profile of this excess absorption is found to be proportional to the cube of the density of H_2, it is interpreted as arising from the triple transitions $Q_1(J) + Q_1(J) + Q_1(J)$. This represents the first observation of simultaneous transitions involving three molecules in collision-induced spectra. Profiles resulting from the triple-collision transitions were also analyzed satisfactorily by using the Lorentz line-shape function as well as Birnbaum-Cohen

line-shape function.

Acknowledgments

I am greatly indebted to my supervisor Dr. S. P. Reddy for suggesting the research project and for his valuable guidance, assistance, and encouragement throughout the progress of the research and in the preparation of this thesis.

I would like to thank Dr. G. Varghese for help in the experimental work and also for many rewarding discussions.

Help from the technical staff in the Department of Physics is gratefully acknowledged.

My thanks also go to the School of Graduate Studies, Memorial University of Newfoundland, for awarding me an Albert George Hatcher Memorial Scholarship, to the Department of Physics and to Dr. S. P. Reddy for providing me with teaching and research assistantships during my graduate studies.

I wish to express my sincere appreciation to my wife, Liya, for her understanding and inestimable help.

Finally, and most of all, I extend my heart-felt thanks to my parents for their support and encouragement throughout my academic career.

Contents

List of Tables

List of Figures

Chapter 1

INTRODUCTION

1.1 Collision-Induced Absorption Spectra of Molecular Hydrogen

Isolated homonuclear diatomic molecules, like hydrogen, in their electronic ground states have no permanent static or vibrational electric dipole moments on account of the symmetry of their charge configurations. Consequently, unlike polar molecules, they have no electric dipole absorption at their rotational or vibrational frequencies. However, a transient electric dipole moment is induced in two or more collid-

ing molecules by intermolecular forces because of an asymmetric distortion of the electron charge configuration during collisions. These transient induced-dipole moments interact with the electromagnetic field from an appropriate radiation source, and the colliding molecules absorb radiation in the spectral regions corresponding to vibration-rotation, pure rotation and translation. The resulting phenomenon is known as collision-induced absorption (CIA) in which normally forbidden transitions occur.

Collision-induced absorption was first observed in compressed oxygen and nitrogen by Crawford et al. (1949) in the regions of their fundamental bands. In the same year CIA was also identified in the fundamental vibrational band of gaseous hydrogen by Welsh et al. (1949). Since the discovery of this phenomenon, the collision-induced absorption spectra of the fundamental and overtone bands of gaseous H_2 have been studied in the pure gas and in binary mixtures with other simple gases under a variety of experimental conditions. The reasons for the greatest interest in the study of the spectra of hydrogen are many: the H_2 molecule is the simplest of all diatomic molecules; it can be treated more rigorously by theoretical calculations; various rotational components of the bands are somewhat separate in spite of their broad and diffuse nature because of its small moment of inertia; it is present in large quantities in the atmospheres of the major planets and in certain cold stellar atmospheres.

Thus the collision-induced absorption spectra of hydrogen have been instrumental in understanding the process involved and in verifying the results of theoretical studies. A comprehensive review of the experimental work done prior to 1971 on the CIA spectra of gaseous H_2 has been given by Welsh (1972). An exhaustive review of the more recent work on the collision-induced vibrational absorption of H_2, D_2 and HD in the gaseous phase was given by Reddy (1985). For further information on CIA the reader is also referred to the review by Reddy and the theses of van Nostrand (1983) and Gillard (1983), both from our laboratory. Comprehensive bibliographies on the subject have been compiled by Rich and McKellar (1976) and Hunt and Poll (1986). Van Kranendonk (1974), Poll (1980) and Birnbaum et al. (1982) have reviewed the theoretical aspects of collision-induced absorption.

Collision-induced absorption is usually represented by the theoretical model of Van Kranendonk (1957 and 1958) which assumes pairwise additivity of the intermolecular interactions, with the Lennard-Jones intermolecular pair potential, and the so-called "exponential-4" model for the induced-dipole moment. The reader is also referred to Poll and Van Kranendonk (1961), and Poll and Hunt (1976) for the angle-dependent expressions for the induced-dipole moment μ. On the basis of this exponential-4 model, the induced dipole moment μ of a pair of colliding molecules consists of two additive parts, $\mu_{overlap}(R)$ arising from the overlap of the electron clouds of the

colliding molecules, and $\mu_{quad}(R)$ resulting from the polarization of one molecule by the quadrupole field of the other, R being the intermolecular separation. The short-range, angle-independent, electron-overlap moment $\mu_{overlap}$ decreases exponentially with intermolecular separation R, and the long-range, angle-dependent, quadrupole-induced moment μ_{quad} varies asymptotically as R^{-4}. It should be emphasized that the existing theories concerning binary collisions take into account the pair potentials $\Phi(r_i, r_j, R_{ij})$. However, potentials involving terms such as $\Phi(r_i, r_j, r_k, R_{ij}, R_{jk}, R_{ki})$ should be considered to include the effect of higher order collisions.

The overlap induced-dipole moment $\mu_{overlap}(R)$ is mostly isotropic and gives rise to the broad $Q_{ov}(J)$ ($\Delta J = 0$) transitions (the anisotropic part of this induced-dipole moment also contributes to the intensity of the O ($\Delta J = -2$) and S ($\Delta J = +2$) transitions). A distinct feature of the overlap induction is a characteristic dip in the Q branch at the position of the corresponding free-molecular transition. This phenomenon was explained by Van Kranendonk (1968) in terms of a destructive interference between the induced dipoles in successive collisions, and the line-shape function for the dip will be discussed in Chapter 3. A detailed kinetic theory of the intercollisional interference dips in the overlap induced Q branch is given by Lewis and Van Kranendonk (1971, 1972a and 1972b) and Lewis (1972, 1973, 1976 and 1985).

The quadrupole induced-dipole moment μ_{quad} depends on the polarizability of the colliding molecules. The isotropic component of the polarizability of a colliding molecule contributes to the intensity of transitions $O_{\Delta v}(J_1) + Q_0(J_2)$, $Q_{\Delta v}(J_1) + Q_0(J_2)$, $S_{\Delta v}(J_1) + Q_0(J_2)$, $Q_{\Delta v}(J_1) + Q_{\Delta v}(J_2)$, $Q_{\Delta v}(J_1) + S_{\Delta v}(J_2)$ and $S_{\Delta v}(J_1) + Q_{\Delta v}(J_2)$. Here the subscript $\Delta v (= v' - v'')$, which takes values 0, 1, 2, 3, ..., etc., refers to the change in the vibrational quantum number v with $v'' = 0$, and the subscripts 1 and 2 refer to molecules 1 and 2 in a binary collision. The transitions O, Q and S correspond to the rotational selection rule $\Delta J = -2$, 0 and $+2$, respectively. The anisotropic component of the polarizability, on the other hand, contributes a small amount to the above transitions and also gives rise to the double transitions $S_{\Delta v}(J_1) + S_{\Delta v}(J_2)$. In the so-called "single transition", only one molecule of the colliding pair makes a vibration or a vibration-rotation transition while its collision partner makes an orientational transition denoted as $Q_0(J)$ with no change in the internal energy. In the "double transitions" both molecules of the collision pair simultaneously absorb a single photon. Line-shape functions used in the analysis of CIA spectra are reviewed by Reddy (1985, also see references therein). Birnbaum et al. (1976, 1982) also give the theory of line-shape functions for quadrupolar transitions. The line-shape functions used for the overlap as well as quadrupolar components in the present work will be given in Chapter 3.

In addition to the components $\mu_{overlap}(R)$ and $\mu_{quad}(R)$ discussed above, the induced dipole moment also includes two more components, $\mu_{hexa}(R)$ and $\mu_{tetra-hexa}(R)$. Of these, the intermediate-range component $\mu_{hexa}(R)$ results from the polarization of a molecule by the hexadecapole field of its collision partner, and is proportional to R^{-6}. It gives rise to much weaker transitions corresponding to the rotational selection rule $\Delta J = 0, \pm 2$ and ± 4. The transitions corresponding to $\Delta J = 4$ are known as U transitions and are of some interest for the hydrogens. The U branch consists of $U_{\Delta v}(J_1) + Q_0(J_2)$ and $Q_{\Delta v}(J_1) + U_{\Delta v}(J_2)$ transitions (and possibly $U_{\Delta v}(J_1) + S_{\Delta v}(J_2)$ transitions, which have not yet been observed). In the collision-induced fundamental band of H_2, the transitions $U_1(J) + Q_0(J)$ and $Q_1(J) + U_0(J)$, first observed by Gibbs et al. (1974), have been studied in detail by Reddy et al. (1980). The $\mu_{tetra-hexa}(R)$ component results from the polarization of a molecule by the tetra-hexadecapole field of its collision partner and is proportional to R^{-8}. This induced-dipole component gives rise to very weak transitions, corresponding to $\Delta J = 0, \pm 2, \pm 4$ and ± 6. The occurrence of the transition $W_0(J)$ corresponding to $\Delta J = +6$ in solid H_2 has been recently reported by Okumura et al. (1989).

Although the four types of induction mechanisms discussed here contribute to the hydrogen fundamental band (see for example Reddy et al., 1977, 1980 and Sen et al., 1980), the overlap induction does not appear to contribute to its first overtone

band (see for example McKellar and Welsh, 1971, van Nostrand, 1983, Varghese et al., 1987 and McKellar, 1988). But McKellar and Welsh (1971), and Gillard (1983) observed unexplained experimental absorption in the Q_3 region of the second overtone spectrum of H_2 at 85 K and 77 K, respectively. This was interpreted as evidence of the existence of an overlap-induction contribution to the second overtone band of H_2.

Collision-induced absorption spectra have components with broad transition half-widths. According to Van Kranendonk (1957), the width of the lines is due to the short duration of the induced dipole and the uncertainly principle, $\Delta E = \hbar/(\Delta t)$. If the collision duration is given by $\Delta t = \overline{R}/\overline{V}$ where $\overline{R}$ is the range of the induction mechanism and $\overline{V}$ is the relative speed of one molecule with respect to its collision partner, then the resulting width of the line in units of cm^{-1} is of the order of

$$\Delta\nu = \frac{1}{2\pi c\Delta t} = \frac{\overline{V}}{2\pi c\overline{R}} .$$

Because of the presence of $\overline{R}$, the short-range overlap induction will give rise to broader transitions than the long-range quadrupolar induction. Also the relative kinetic energy of the molecules is approximately $(1/2)m\overline{V}^2 \approx (3/2)kT$ and thus the half-width shows a $T^{1/2}$ dependence. This relation has been found to be valid in the fundamental (Reddy et al. 1977), and the first overtone (van Nostrand, 1983) bands of H_2.

The half-width of the collision-induced quadrupole-induced transitions also has a notable density dependence at high densities. De Remigis et al. (1971) observed a definite decrease in the halfwidth of the quadrupole-induced lines in the fundamental band of H_2 in H_2 - Ar mixtures for gas densities above 300 amagat. Zaidi and Van Kranendonk (1971) explained the line narrowing in terms of a diffusional effect in which the linewidth is proportional to the diffusion constant and thus is approximately proportional to density. Later, Mactaggart et al. (1973) studied in detail the same effect in the fundamental band in the binary mixtures H_2 - Ar, H_2 - Kr and H_2 - Xe. Lewis and Tjon (1978) showed that the simple explanation given by Zaidi and Van Kranendonk for narrowing of lines is sometimes inapplicable.

Although the collision-induced fundamental and first overtone bands of hydrogen have been studied over wide ranges of pressures and temperatures and their characteristics are well known, the properties of the absorption in the second overtone region have not been so precisely delineated. This is due to the weakness of absorption and the experimental difficulties in its investigation. The collision-induced absorption spectrum of hydrogen in the second overtone region was first observed in the laboratory by Herzberg (1952) who photographed the band at a gas pressure of 100 atm at 77 K with a path length of 80 m, and interpreted the spectrum as consisting of a pure second overtone band, in which one of the two colliding molecules makes a vibra-

tional transition $\Delta v = 3$, and a double vibrational band in which one molecule makes a vibrational transition $\Delta v = 2$ while its collision partner simultaneously makes a vibrational transition $\Delta v = 1$. Hunt (1959) recorded the 3-0 band of H_2 at room temperature and pressures up to 2200 atm. Prior to his observation in the laboratory, Herzberg (1951) identified a diffuse feature at 12,093 cm^{-1}, observed in the spectra of Uranus and Neptune by Kupier (1949), as the collision-induced $S_3(0)$ component of the second overtone band of hydrogen. McKellar and Welsh (1971) made the first quantitative measurement of the absorption spectrum of H_2 in the second overtone region at gas densities of about 37 amagat at 85 K with a path length of 137 m. Their analysis of the absorption profiles showed several discrepancies between the experimental and calculated profiles. Gillard (1983) met similar difficulty in the analysis of the CIA spectra of H_2 in the second overtone region which was recorded for gas densities in the range 500 - 930 amagat at 77 K with the 2 m absorption cell.

Representative collision-induced transitions in the second overtone region are shown in Figure 1.1. In the calculation of the term values (in cm^{-1}) for the rotational and vibrational levels of the free H_2 molecule, molecular constants given by Bragg et al. (1982) for $v = 0$, 1 and 2 and Foltz et al. (1966) for $v = 3$ were used. The single transitions $Q_3(J)$ and $S_3(J)$, and the double transitions $Q_3(J) + S_0(J)$ and $S_3(J) + S_0(J)$ are all representative of the pure second overtone band, whereas

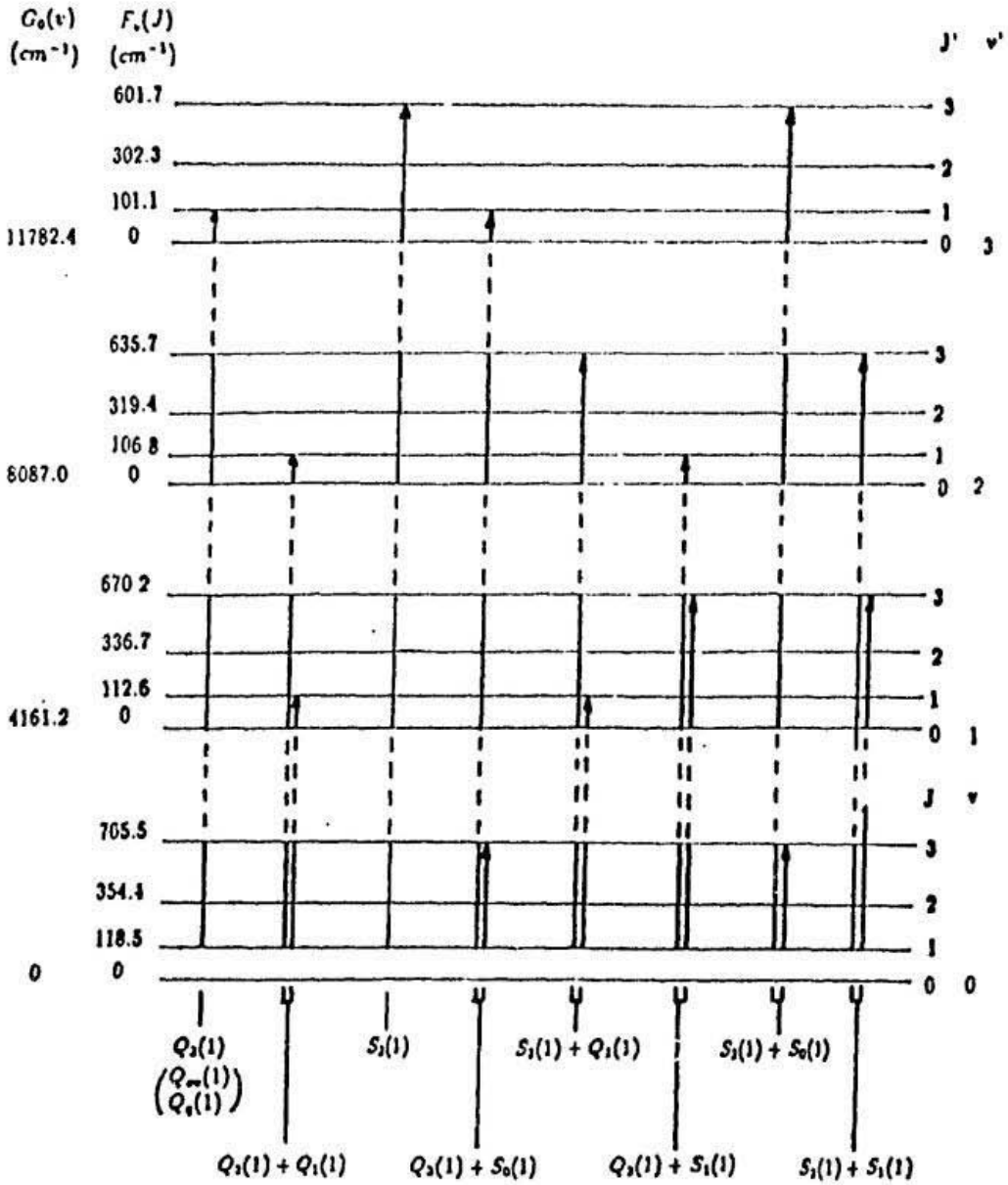

Figure 1.1: Energy level diagram of H_2 showing some representative collision-induced transitions in its second overtone region.

the $Q_2(J) + Q_1(J)$, $S_2(J) + Q_1(J)$, $Q_2(J) + S_1(J)$ and $S_2(J) + S_1(J)$ transitions correspond to the double vibrational band in which one molecule of the colliding pair makes the $v = 2 \leftarrow v = 0$ vibrational transition while its partner simultaneously makes the $v = 1 \leftarrow v = 0$ vibrational transition. The $S_3(J)+S_0(J)$ and $S_2(J)+S_1(J)$ transitions arise solely from the anisotropic component of the polarizability and their intensities are relatively weak compared to those arising from the isotropic part of the polarizability.

1.2 The Present Work

As mentioned in the previous section, quantitative measurements of CIA spectra of H_2 in the second overtone region were made for gas densities of about 37 amagat at 85 K by McKellar and Welsh (1971) and for gas densities up to 930 amagat at 77 K by Gillard (1983). The profile analyses of CIA of H_2 in both these studies showed several discrepancies between the experimental and calculated profiles.

One of the aims of the present work was to obtain accurate experimental CIA profiles of H_2 in its second overtone region at several temperatures and a wide range of gas densities, to analyze them with appropriate line-shape functions, and to find

whether it would be possible to obtain satisfactory agreement between the experimental and the calculated profiles. Another aim was to find whether it is possible to identify absorption resulting from triple transitions of the type $Q_1(J)+Q_1(J)+Q_1(J)$, which would fall in the spectral region of the second overtone band of H_2, and which would be an excess contribution not predicted by current theory.

The CIA spectra of H_2 were recorded with a 2 m low-temperature high-pressure stainless steel cell for gas densities up to 1000 amagat at 77, 201 and 298 K. The apparatus and the experimental technique are described in Chapter 2.

Chapter 3 presents representative experimental profiles of the CIA spectra of H_2 in the second overtone region. The occurrence of the dip at $Q_3(J)$ with characteristic low- and high- wavenumber components Q_P and Q_R clearly shows the presence of overlap induction of the collisions in the 3-0 band. In addition to the overlap components, several quadrupole-induced transitions of the type $Q_3(J) + Q_0(J)$, $S_3(J)+Q_0(J)$, and $Q_3(J)+S_0(J)$ of the pure 3-0 band and of the type $Q_2(J)+Q_1(J)$, $S_2(J)+Q_1(J)$, $Q_2(J)+S_1(J)$, and $S_2(J)+S_1(J)$ of the combination 2-0 + 1-0 band have been identified. Binary and ternary absorption coefficients of CIA in the second overtone region have been determined. Chapter 3 also presents the analysis of the observed profiles. The line-shape functions used are the Levine-Birnbaum (1967) intracollisional and the Van Kranendonk (1968) intercollisional line-shape functions

for the overlap-induced transitions, and the Lorentz line-shape function as well as the Birnbaum-Cohen (1976) line-shape function for quadrupole-induced transitions. In the calculation of the relative intensities of the quadrupole-induced transitions, the matrix elements for $\Delta v = 2$ and 3 are reduced by a factor of 0.68 to obtain satisfactory profile analysis. This is similar to the procedure used by van Nostrand (1983) in the analysis of the CIA spectra of H_2 in the first overtone region. Also, the relative intensities of the three groups of transitions, namely, the overlap transitions, the quadrupolar single transitions and quadrupolar double transitions, are treated as independent parameters in the analysis of the profile.

Analysis of the absorption profiles presented in Chapter 3 reveals some excess absorption, which is additional to theoretical prediction, in the spectral region around 12,460 cm^{-1}. As the area under the absorption profile of this excess absorption is found to be proportional to the cube of the density of the H_2 gas, it is interpreted as arising from triple transitions of the type $Q_1(J_1) + Q_1(J_2) + Q_1(J_3)$. This represents the first observation of the simultaneous triple transitions involving three molecules 1, 2 and 3 in the CIA spectra. Absorption profiles of the triple-collision transitions have also been analyzed satisfactorily by using the Lorentz line-shape function as well as the Birnbaum-Cohen line-shape function. The profiles of the triple-collision transitions and their analysis are presented in Chapter 4.

Conclusions of the present research work are summarized in Chapter 5.

Computer programs used in the analysis of the absorption profiles are listed in Appendix A. Matrix elements, of the quadrupole moment Q, polarizability α, and anisotropy of polarizability γ, used in the present work, are listed in Appendix B.

Chapter 2

APPARATUS AND EXPERIMENTAL TECHNIQUE

The infrared spectra of the collision-induced absorption of molecular hydrogen in its second overtone region was studied for gas pressures up to 1,700 atmospheres at 77, 201 and 298 K. The experimental data were obtained with a 2 m high-pressure low-temperature absorption cell, a high-pressure gas handling system and an infrared recording spectrometer. In this chapter, a brief description of the apparatus and the experimental procedure is presented.

2.1 The 2 m Absorption Cell

The 2 m transmission-type stainless steel absorption cell was originally designed by Reddy and Kuo (1971) for gas pressures up to 1000 atmospheres at room temperature. This cell was later modified for the work at low temperatures down to 77 K by providing a double-walled stainless steel jacket in which the space between the cell and inner wall of the jacket was used for the coolant and the space between two walls of the jacket was insulated with vermiculite (see for example Prasad, 1976). Finally to reduce the high consumption of the coolants used for low temperature work and to maintain uniform temperature over the entire cell, extensive modifications were made to the cell, including replacement of the vermiculite-filled insulating jacket with a stainless steel vacuum jacket (see Gillard, 1983).

A cross-sectional view of one end of the absorption cell is shown in Figure 2.1. The cell T was constructed from a type 303 stainless steel cylinder, 2 m long and 7.62 cm in outer diameter. It has a central bore of 2.54 cm. A polished stainless steel light guide L which passes through the full length of the cell has a rectangular cross sectional aperture 1.00 cm × 0.50 cm. It ensures good transmission of radiation through the cell and reduces the effective volume of the cell for economical use of the

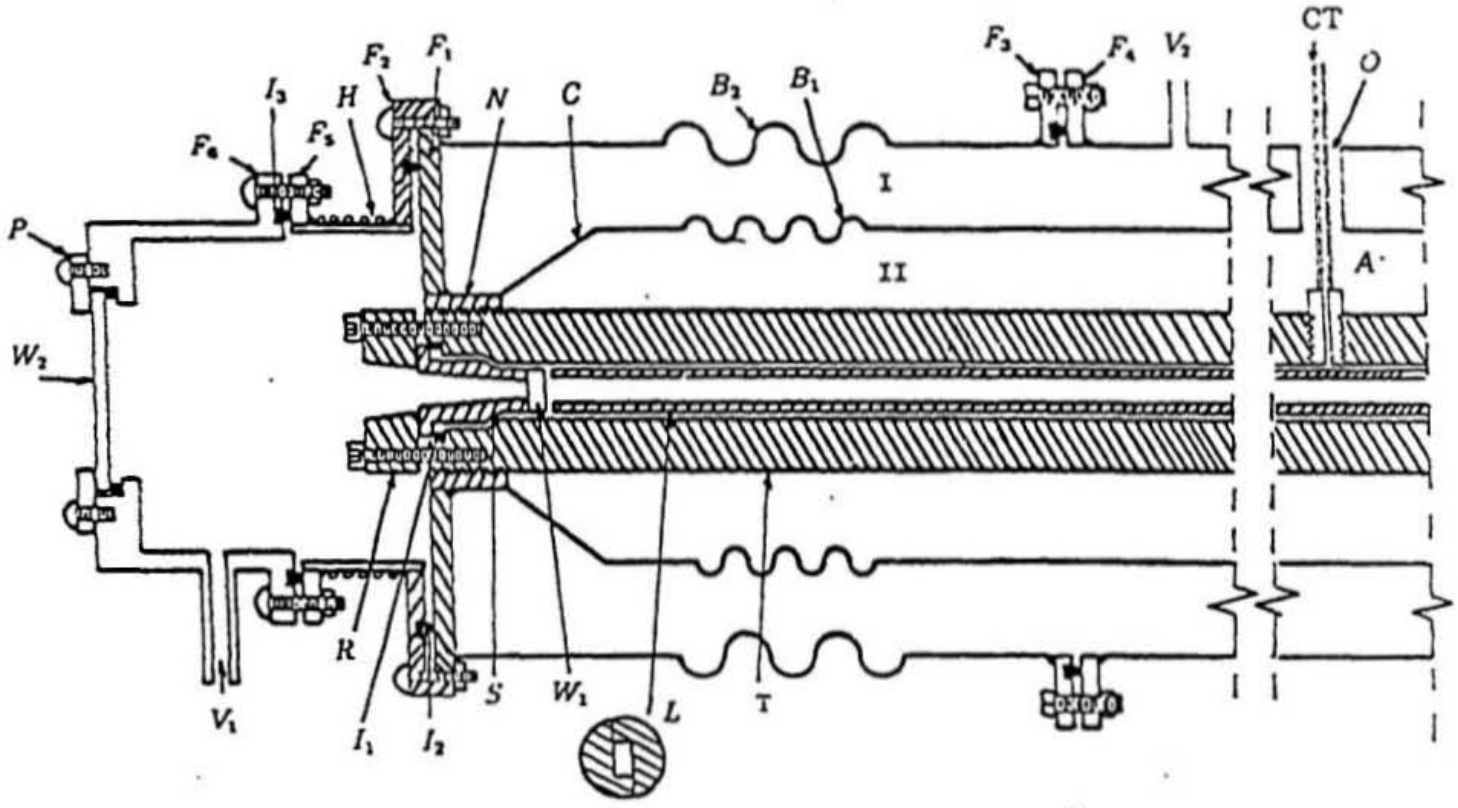

Figure 2.1: A cross-sectional view of one end of the 2 m low-temperature, high-pressure absorption cell.

experimental gas. The synthetic sapphire window W_1, 2.54 cm thick and the same in diameter, was attached to a stainless steel window seat S with a circular aperture of 1.00 cm by means of General Electric RTV-108 silicone adhesive sealant. The window seat was pressed firmly against an Invar O-ring I_1 by means of a stainless steel retaining block R which was held in position by eight 3/8 in. Allen head steel cap screws which pass through the holes in R and threaded into the face of the absorption cell. With this arrangement the Invar O-rings provide satisfactory seals for good vacuum as well as for high pressures in the cell at all experimental temperatures.

A nut N, 7.62 cm in internal diameter and 1.5 cm long and made of type 312 stainless steel was threaded onto each end of the cell. A solid flange F_1, and cone C both made of stainless steel were then welded to this nut as shown in Figure 2.1. The flange F_1 was also welded to a stainless steel bellows B_2 of diameter $\sim$ 16.5 cm. The bellows B_2 was then attached to the outer wall of the jacket by eight 1/4 in. - 20 screws and nuts by flanges F_3 and F_4. A 10.2 cm diameter stainless steel bellows B_1 was welded to the stainless steel cone to form the internal wall of the jacket and also to allow for relative expansion and contraction of the cell and the vacuum jacket. An RTV silicone rubber O-ring type seal I_2 was formed between F_1 and F_2 which were then held together by twelve 10 - 24 machine screws. Attached to F_2 was a short stainless steel tube and another flange F_5. Flange F_5 was sealed

with a neoprene O-ring I_3 to the flange F_6 of an end cap made of Delrin which was normally evacuated through vacuum port V_1 to prevent condensation of atmosphere water vapour on window W_1. A sapphire window W_2, 5.08 cm in diameter and 0.30 cm thick, was sealed to the end of the plastic end cap by a Plexiglas ring P. Heating tape H was wound around the end of the cell near flange F_2 so that the O-ring seal would not freeze. Chamber I was normally evacuated through a vacuum port V_2. Chamber II was filled with a coolant, either liquid nitrogen (77 K), or a mixture of ethanol (C_2H_5OH) and crushed dry ice (201 K), through an opening O in the central section of the jacket. The experimental gas was admitted into the cell through a 1.27 cm Aminco fitting A, attached to a stainless steel capillary tube CT. Figure 2.2 gives the photographs of (a) the assembled cell, (b) a view of one end of the cell, window seat and the retaining block before assembly, and (c) assembled end of the cell to which a vacuum chamber is attached to prevent condensation on the window.

2.2 The Gas Handling System

Matheson ultra-high-purity grade hydrogen gas with a stated purity of 99.999% was used in all experiments. The gas handling system for developing the required

Figure 2.2: Photographs of the 2 m low-temperature, high-pressure absorption cell used in the experiments.

(a) An overall view of the cell.

(b) An view of the one end of the cell (under construction) showing the inner jacket and the window mount.

(c) One end of the completed cell showing the Delrin end cap and the heating tapes.

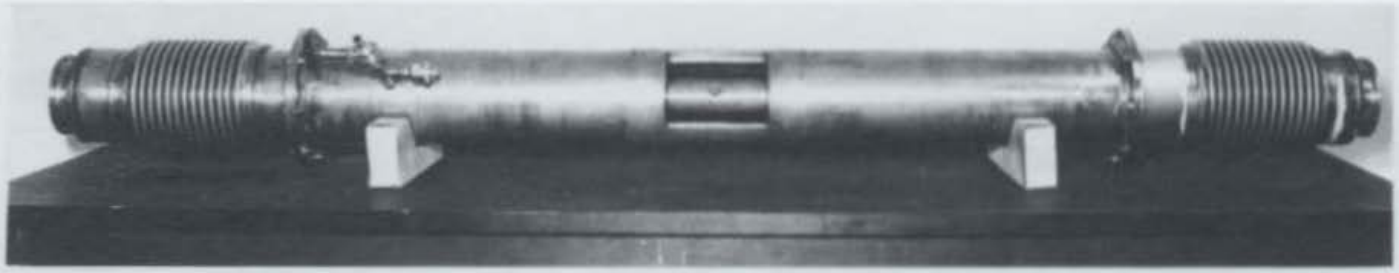

(a)

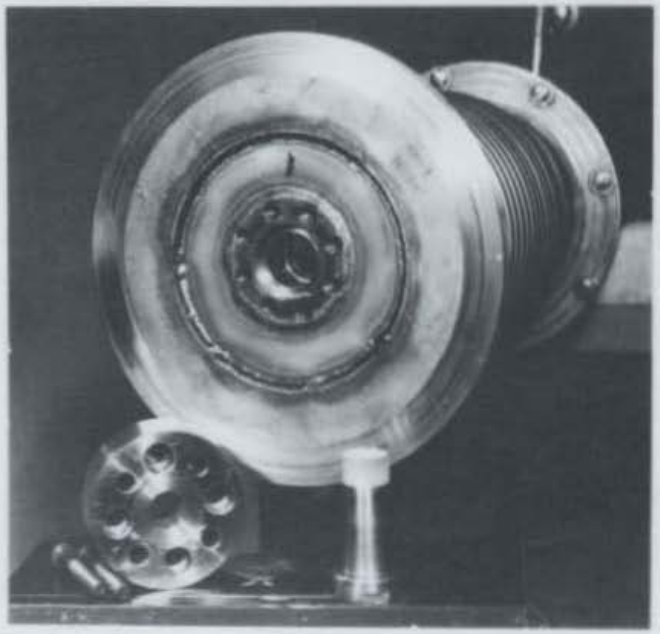

(b)

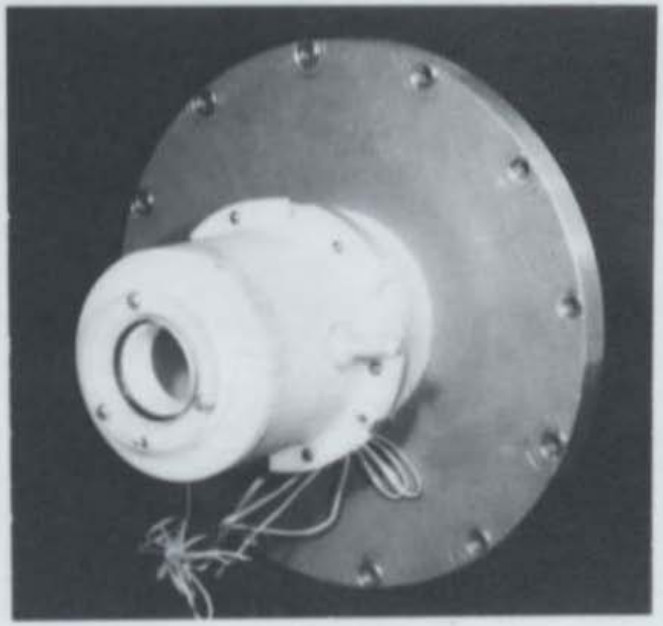

(c)

pressures in the absorption cell is shown schematically in Figure 2.3. A series of Aminco valves, fittings and capillary tubing, all made of stainless steel, copper tubing T_1 (0.62 cm in diameter), stainless steel thermal compressors T_2, T_3 and T_4 and Ashcroft Bourdon tube pressure gauges G_1 (range: 0 - 5,000 p.s.i.), G_2 (0 - 20,000 p.s.i.) and G_3 (0 - 30,000 p.s.i.) form the gas handling system between the Matheson hydrogen cylinder and the 2 m absorption cell as shown. All the Aminco components are rated for pressures up to 60,000 p.s.i. Before the H_2 gas was released from the cylinder, the gas handling system including the 2 m absorption cell was thoroughly evacuated. Hydrogen gas from the cylinder was then passed through T_1 immersed in liquid nitrogen to remove any impurities, then admitted into T_2. After closing the valve between the H_2 cylinder and T_1, cold H_2 from T_2 was admitted into high-pressure compressors T_3 and T_4 (each having a volume of 500 c.c) which were also immersed in liquid nitrogen. This process was repeated until sufficient gas was collected in T_3 and T_4. The gas in T_3 was then warmed to room temperature and admitted into T_4, which was still kept at 77 K. Finally T_4 was used as a high-pressure gas reservoir when it was warmed up to room temperature. In developing high pressures, the technique described here is simple in principle and avoids contamination of the experimental gas with impurities associated with instruments such as an oil gas compressor. By the present method, pressures up to $\sim$ 30,000 p.s.i. can be developed from a hydrogen cylinder with an

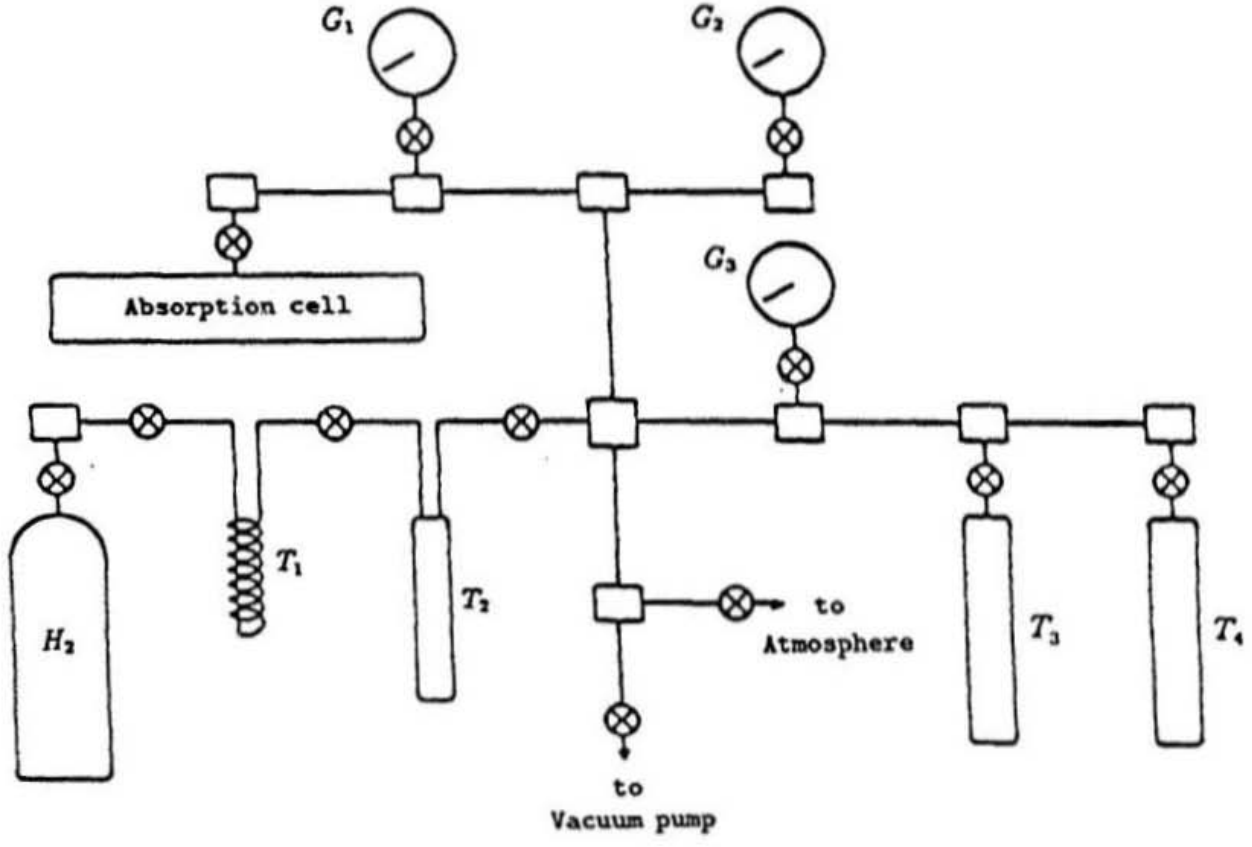

Figure 2.3: The gas-handling system.

initial pressure of $\sim$ 2,000 p.s.i. of H_2. Oil filled Bourbon tube test gauges which were calibrated against an Ashcroft dead weight pressure tester were used as calibration standards for the pressure gauges used in the gas handling system.

2.3 The Spectrometer and Optical Arrangement

The overall optical arrangement including the absorption cell is shown schematically in Figure 2.4. The source of continuous infrared radiation was a General Electric FFJ 600 W Quartzline projection lamp L housed in a water cooled brass jacket of special design and positioned close to the end of the absorption cell. The voltage across the lamp was adjusted between 60 - 90 volts to bring the signal to noise ratio to a satisfactory level. The voltage applied to the lamp was controlled by a Variac W10MT3A autotransformer which was fed by an a.c. voltage regulator. An f/4 aluminized concave spherical mirror M_1 with 15 cm diameter focused the radiation from the source on the entrance window of the absorption cell. Light passing through the absorption cell was then focused by a similar mirror M_2 onto the entrance slit S_1 of the spectrometer. The spectrometer was inclined at an angle of approximately 30^0 to the axis of the cell.

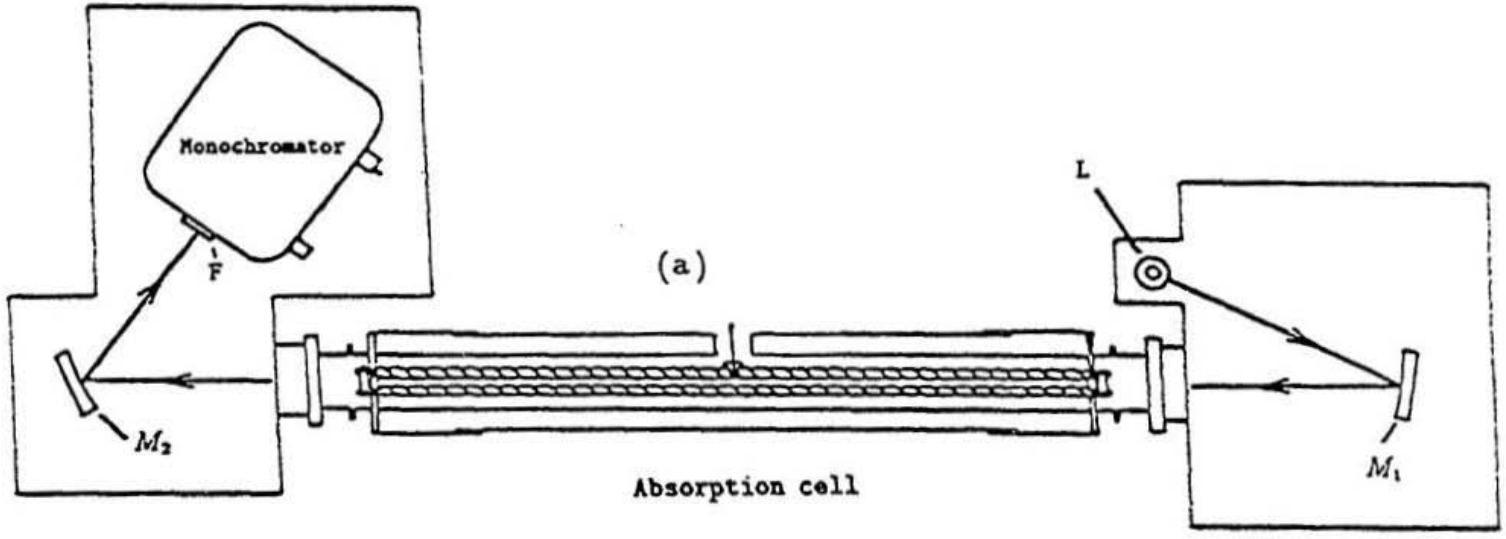

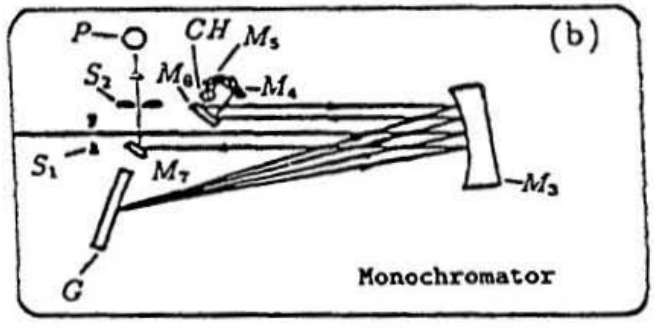

Figure 2.4: The optical arrangement.

A Perkin-Elmer model 112G double pass grating spectrometer whose optical layout is shown in Figure 2.4 (b) was used to record the spectra. This instrument contained a grating G ruled with 300 lines/mm, blazed at 3.0 μm in the first order. A Hamamatsu type R758 photomultiplier tube (PMT) P was housed directly behind the exit slit S_2 of the monochromator, inside the spectrometer box as shown. The PMT was mounted in a magnetic shield supplied by Hamamatsu and modified to fit inside the spectrometer. A light-tight box constructed of brass shimstock was fitted around the exit slit of the monochromator and the PMT housing to keep stray light to a minimum. To reduce scattered light in the spectrometer, the objects placed inside spectrometer housing were painted black. A Corning CS 2-64 filter F was used to eliminate unwanted radiation. The entrance slit width was maintained at 10 μm and gave a spectral resolution of about 2 cm^{-1} at 11782 cm^{-1}, the position of the $Q_3(0)$ transition.

2.4 The Signal Recording System

The radiation entering the spectrometer entrance slit S_1 from the absorption cell was dispersed by a grating. It was then chopped by a 260 Hz tuning fork chopper

CH between flat mirrors M_5 and M_6 where it was brought to a focus. The chopped radiation was reflected back to the grating by M_6, and was finally focused on the exit slit S_2 of the spectrometer (see Figure 2.4 (b)). The radiation passing through the exit slit was brought directly onto the PMT which consists of a photoemissive cathode (photocathode) followed by an electron multiplier section and a photoelectron collector (anode) in a vacuum tube. The electron multiplier section (called the dynode-string) has fast time-resolution, high amplification, and low noise. A constant voltage of 900 V was applied across the PMT, so that its output current was proportional to the intensity of the radiation incident upon it.

The signal from the PMT was directly connected to a model SR510 lock-in amplifier supplied by Stanford Research Systems. As the full scale current sensitivities of this lock-in amplifier range from 100 fA to 500 nA, no current sensitive preamplifier was needed. A reference signal was supplied to the lock-in amplifier from the power supply unit for the tuning fork chopper and the phasing adjustment is inherent in the lock-in amplifier. The output signal of the lock-in amplifier was recorded on a Hewlett-Packard model 7132A strip chart recorder.

2.5 Calibration of the Spectral Region and Reduction of Recorder Traces of the Spectra

The absorption spectra of H_2 in its second overtone region were recorded as intensity versus time by the chart recorder. However time was converted to wavenumbers (cm^{-1}) using the standard emission lines of neon and argon (Zaidel et al., 1970 and C.R.C. Handbook of Chemistry and Physics, 1985). The procedure of calibration is as follows: The distances $d(\nu)$ of the standard neon and argon emission peaks on the recorder charts were accurately measured. A second order polynomial function of wavenumber ν (cm^{-1})

$$d(\nu) = A + B\nu + C\nu^2$$

was found to represent the dependence of $d(\nu)$ on ν satisfactorily. A least-squares fit was performed to obtain the constants A, B and C, and these constants were in turn used to obtain wavenumbers against positions on a recorder trace at intervals of 10 cm^{-1}. A calibration chart was then drawn on tracing paper giving the position along the recorder trace at these intervals.

The absorption coefficient $\alpha(\nu)$ at a given wavenumber ν (in cm^{-1}) of an absorbing

gas is given by

$$\alpha(\nu) = (2.303/l)\log_{10}[I_0(\nu)/I(\nu)]$$

where $I_0(\nu)$ and $I(\nu)$ are the intensities of radiation transmitted by the evacuated cell of sample path length l, and by the cell filled with the absorbing gas at density ρ, respectively. The intensities are measured from the infinite absorption line. A proper matching of chart recorder traces taken with evacuated cell at the beginning and end of an experiment ensures the stability of the source of radiation and the signal recording system during the experiment. At each gas pressure, two or more recorder traces were taken until they matched well with each other. The wavenumber calibration chart was positioned on the recorder traces and the quantity $\log_{10}[I_0(\nu)/I(\nu)]$ was measured at the marked intervals on the chart with the help of a standard logarithmic scale. Absorption profiles were obtained by plotting $\log_{10}[I_0(\nu)/I(\nu)]$ against ν. The areas under the absorption profiles represent the integrated absorption coefficients $\int \alpha(\nu)d\nu$.

2.6 Isothermal Data

In this thesis, the densities of the gases are expressed in amagat units. An amagat

unit is defined as the ratio of the density of a gas at a given temperature and pressure to its density at the standard temperature and pressure (S.T.P.). Recorded pressures of hydrogen at the three experimental temperatures were converted to the density using its pressure-density data. Densities of hydrogen at 77 K, 201 K and 298 K were first obtained by linear interpolation of the data given by McCarty et al. (1981) at temperature 75 K and 80 K, 200 K and 220 K, and 280 K and 300 K, respectively. These data were least-squares fitted to a polynomial of degree 5 to allow interpolation of the densities for the experimental pressures of the gas. The densities of hydrogen for pressures above the available data were obtained by the method of extrapolation using the coefficients of the polynomial.

Chapter 3

ABSORPTION SPECTRA OF H_2 IN THE SECOND OVERTONE REGION

3.1 Introduction

A brief survey of the previous work on the collision-induced infrared absorption of H_2 in the fundamental, first overtone and second overtone regions has been given in Chapter 1. The high pressure absorption cell and the experimental procedure have

been described in Chapter 2. In the present work, the collision-induced absorption spectra of H_2 in the second overtone region were recorded at 77, 201 and 298 K with a 2 m absorption cell for a number of gas densities up to 1000 amagat. The experimental conditions under which the spectra were recorded are summarized in Table 3.1. The rest of this chapter is devoted to the absorption profiles of H_2 and their analysis.

Table 3.1: Summary of the experiments on the H_2 second overtone band

Temperature (K)	Absorption path length (cm)	Number of gas densities studied	Maximum density of the gas (amagat)
77	194.2	8	1002
201	194.5	5	866
298	194.8	6	752

3.2 Experimental Absorption Profiles

Three typical absorption profiles of normal hydrogen in the pure gas at each of the

temperatures 77, 201 and 298 K in the second overtone region are shown in Figures 3.1, 3.2 and 3.3, respectively, by plotting $\log_{10}[I_0(\nu)/I(\nu)]$ against wavenumber ν. The positions of several transitions calculated from the constants of the free hydrogen molecule (Foltz et al., 1966 for $v = 3$ and Bragg et al., 1982 for v=0, 1 and 2) are marked along the wavenumber axis in these figures. The absorption peak positions and the assignments of the transitions contributing to these peaks are listed in Tables 3.2, 3.3 and 3.4. A characteristic dip in the Q branch with associated maxima Q_P and Q_R in the 3-0 band of H_2 is observed at the position of $Q_3(1)$ at all the three experimental temperatures. The occurrence of the dip has been interpreted in terms of the density-dependent intercollisional interference effect which arises from the negative correlations existing between the short-range overlap dipole moments induced in successive collisions (Van Kanendonk, 1968; Mactaggart and Welsh, 1973; and Reddy et al., 1977). The presence of the dip in the Q branch of the second overtone band of hydrogen is a positive indication of the overlap contribution to the intensity of the band. It is also apparent from the profiles in Figures 3.1, 3.2 and 3.3 that the separation $\Delta\nu_{PR}$ between the Q_P and Q_R maxima increases with increasing density of the gas. For example, for the profiles presented in Figure 3.3, $\Delta\nu_{PR}$ has values 190, 220 and 256 cm^{-1}. It should be noted that the isotropic overlap contribution is predominant in the collision-induced fundamental band of H_2 (see

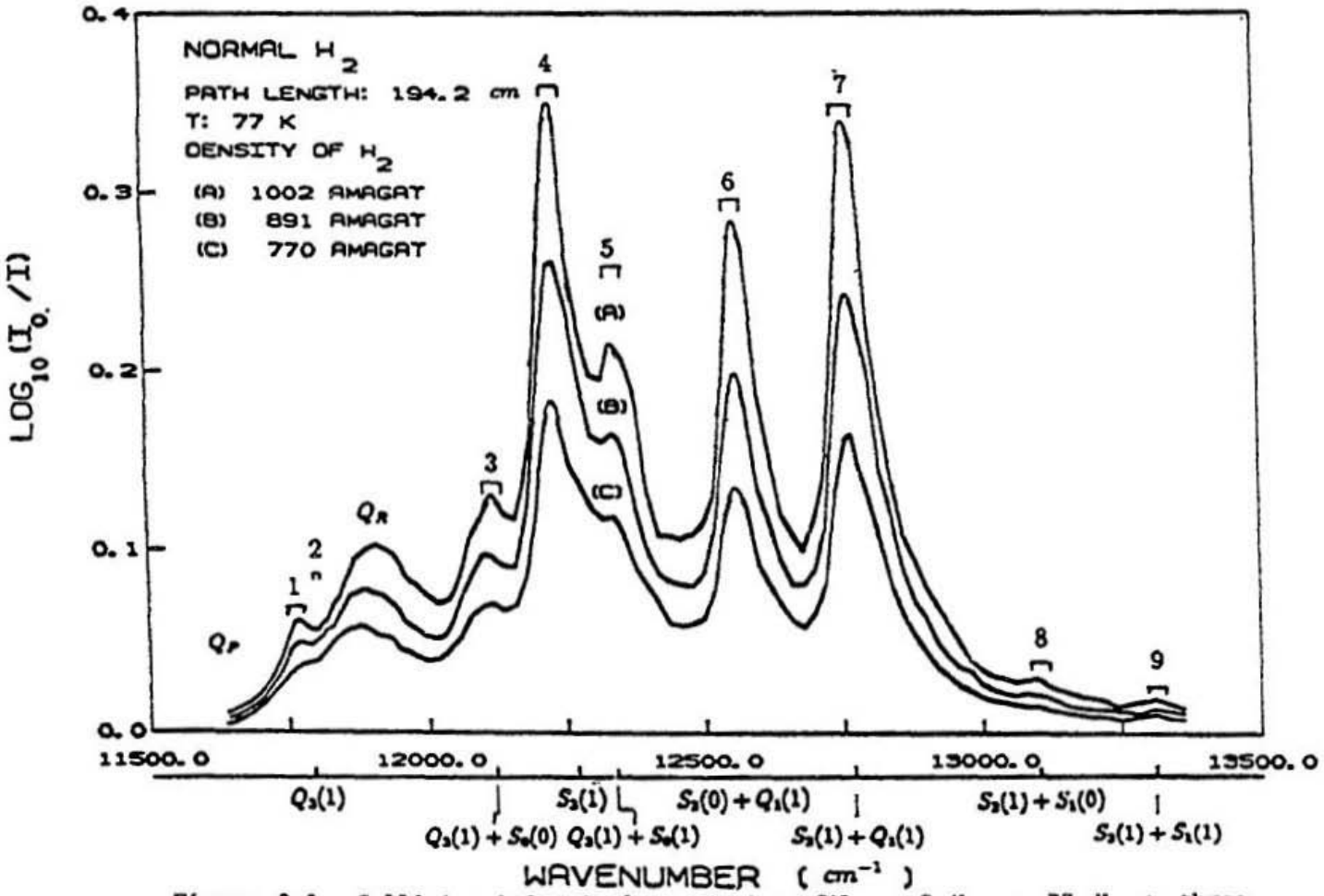

Figure 3.1: Collision-induced absorption profiles of H_2 at 77 K at three different densities of the gas in the second overtone region. Calculated positions of a few transitions are marked along the wavenumber axis. The extents of various transitions are marked in groups 1-9. See Table 3.2 for other details.

Table 3.2: Assignment of the observed absorption peaks of the H_2 second overtone region at 77 K

Peak number	Wavenumber of observed peak (cm^{-1})	Assignment
1	11773	$Q_3(J) + Q_0(J)$
2	11798	$Q_3(J)_{overlap}$ dip
3	12120	$S_3(0) + Q_0(J)$, $Q_3(J) + S_0(0)$
4	12226	$S_3(1) + Q_0(J)$, $Q_2(J) + Q_1(J)$
5	12345	$Q_3(J) + S_0(1)$
6	12560	$S_2(0) + Q_1(J)$, $Q_2(J) + S_1(0)$
7	12762	$S_2(1) + Q_1(J)$, $Q_2(J) + S_1(1)$
8	13107	$S_2(1) + S_1(0)$, $S_2(0) + S_1(1)$
9	13310	$S_2(1) + S_1(1)$

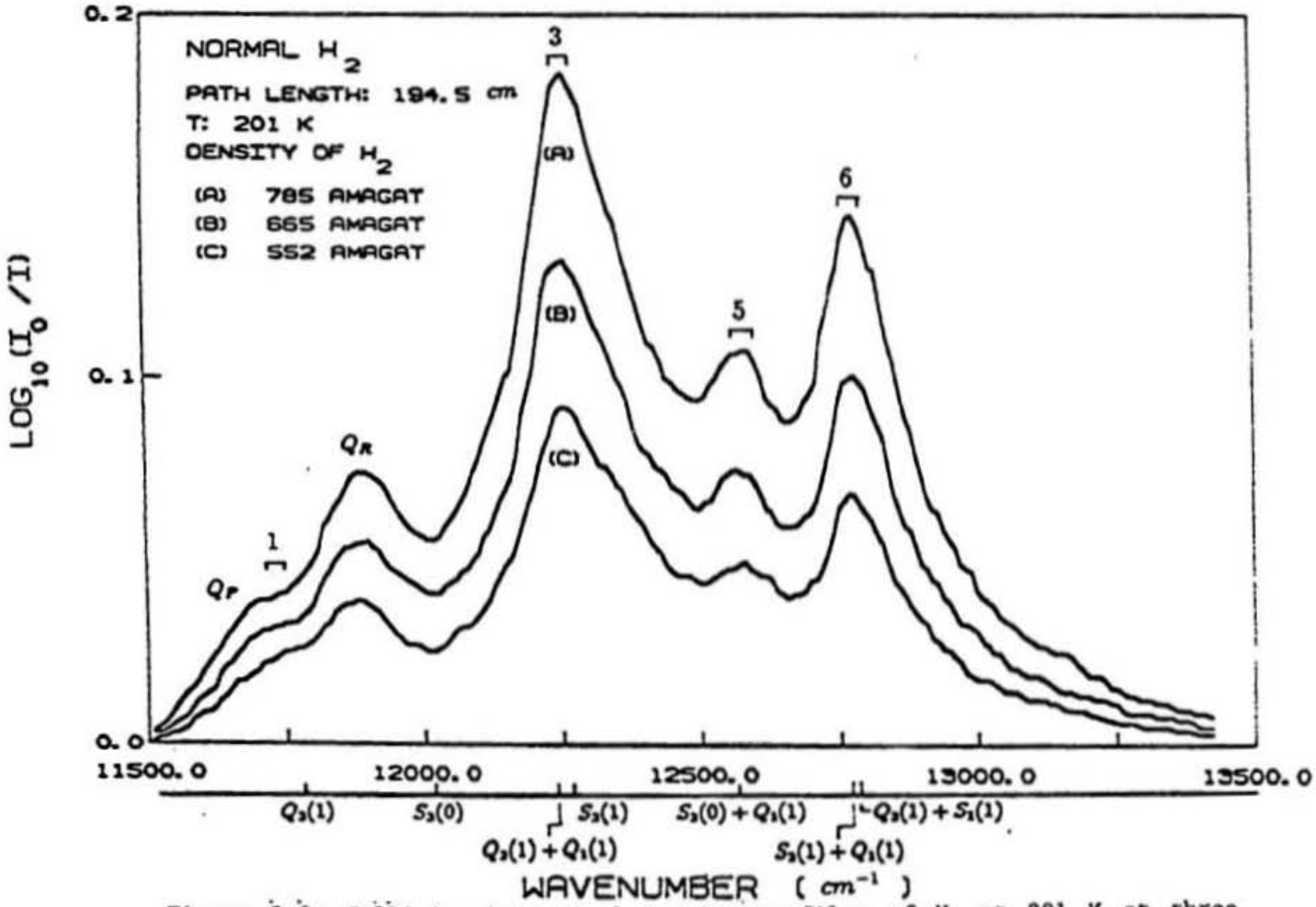

Figure 3.2: Collision-induced absorption profiles of H_2 at 201 K at three different densities of the gas in the second overtone region. Calculated positions of a few transitions are marked along the wavenumber axis. The extents of various transitions are marked in groups 1-6. See Table 3.3 for other details.

Table 3.3: Assignment of the observed absorption peaks of the H_2 second overtone region at 201 K

Peak number	Wavenumber of observed peak (cm^{-1})	Assignment
1	11732	$Q_3(J) + Q_0(J)$,$Q_3(J)_{overlap}$
2	-	$S_3(0) + Q_0(J)$,
3	12255	$S_3(1) + Q_0(J)$, $Q_2(J) + Q_1(J)$
4	-	$Q_3(1) + S_0(1)$
5	12572	$S_2(0) + Q_1(J)$, $Q_2(J) + S_1(0)$
6	12786	$S_2(1) + Q_1(J)$, $Q_2(J) + S_1(1)$

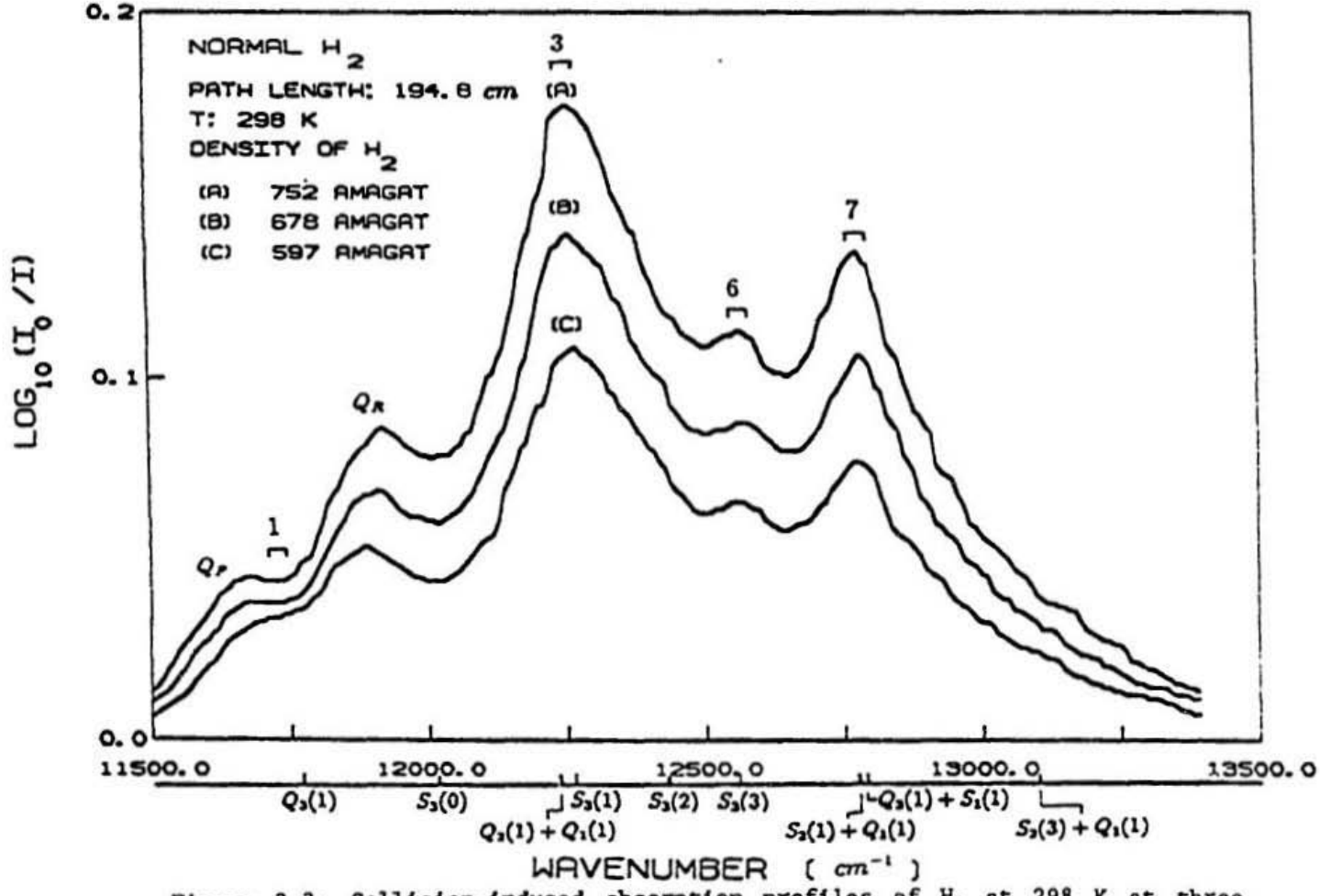

Figure 3.3: Collision-induced absorption profiles of H_2 at 298 K at three different densities of the gas in the second overtone region. Calculated positions of a few transitions are marked along the wavenumber axis. The extents of various transitions are marked in groups 1-7. See Table 3.4 for other details.

Table 3.4: Assignment of the observed absorption peaks of the H_2 second overtone region at 298 K

Peak number	Wavenumber of observed peak (cm^{-1})	Assignment
1	11740	$Q_3(J) + Q_0(J)$,$Q_3(J)_{overlap}$
2	-	$S_3(0) + Q_0(J)$,
3	12255	$S_3(1) + Q_0(J)$, $Q_2(J) + Q_1(J)$
4	-	$Q_3(1) + S_0(1)$
5	-	$S_3(2) + Q_0(J)$
6	12571	$S_2(0) + Q_1(J)$, $Q_2(J) + S_1(0)$ $S_3(3) + Q_0(J)$
7	12780	$S_2(1) + Q_1(J)$, $Q_2(J) + S_1(1)$

Reddy et al., 1977) but is absent in its 2-0 band (see van Nostrand, 1983, and Varghese et al., 1987). It may be noted that the absorption profiles of H_2 in its second overtone region at 85 K presented by McKellar and Welsh (1971) show no dip in the Q branch because of the low gas densities used and have five peaks. But in the present work we have observed three more additional peaks at 12,345, 13,107 and 13,310 cm^{-1} in the second overtone region of the hydrogen at 77 K (see also Gillard, 1983). For each of the profiles at 201 K and 298 K, in addition to the dip in the Q branch with associated Q_P and Q_R maxima, three absorption peaks are observed. For the collision-induced absorption in the second overtone region resulting from the quadrupolar contribution, the isotropic part of the polarizability contributes to the intensity of the pure overtone single transitions $Q_3(J)$ $(=Q_3(J)+Q_0(J))$ and $S_3(J)$ $(=S_3(J)+Q_0(J))$, pure overtone double transitions $Q_3(J)+S_0(J)$ and $S_3(J)+S_0(J)$, and double vibrational transitions $Q_2(J)+Q_1(J)$, $S_2(J)+Q_1(J)$, and $Q_2(J)+S_1(J)$, whereas the anisotropic part of the polarizability contributes to the double S transitions $S_2(J)+S_1(J)$ which were observed clearly at the high wavenumber wing of the absorption profiles of H_2 at 77 K; the absorption peak at 13,107 cm^{-1} is assigned to the transitions $S_2(1)+S_1(0)$ and $S_2(0)+S_1(1)$ and the one at 13,310 cm^{-1} is assigned to $S_2(1)+S_1(1)$.

3.3 The Absorption Coefficients

The absorption coefficient $\alpha(\nu)$ at wavenumber ν (in cm^{-1}) was obtained from the relation

$$\alpha(\nu) = (1/l)\ln[I_0(\nu)/I(\nu)] \tag{3.1}$$

where l is the sample pathlength, $I_0(\nu)$ is the intensity of radiation incident on the sample, and $I(\nu)$ is the intensity of radiation transmitted through the sample. The integrated absorption coefficients $\int(\alpha(\nu)/\nu)d\nu$ etc., and higher moments are of great interest as they are time-independent equilibrium quantities and as such are much more theoretically tractable than the frequency-dependent absorption coefficients ($\alpha(\nu)$) themselves. Over a limited range of low gas densities, only binary collisions account for almost all the absorption of the band, and the integrated absorption coefficient of the band varies quadratically with the gas density. However, at higher gas densities the effects of ternary and higher-order collisions must be taken into account. More generally, the integrated absorption coefficient of a given transition or a set of transitions can be expanded as a power series in density as

$$\int \alpha(\nu)d\nu = \alpha_{1a}\rho^2 + \alpha_{2a}\rho^3 + \cdots, \tag{3.2}$$

where the temperature-dependent quantities α_{1a} (in cm^{-2} $amagat^{-2}$) and α_{2a} (in

cm^{-2} $amagat^{-3}$) are the binary and ternary absorption coefficients, respectively, and ρ is the density of the gas.

The integrated absorption coefficients can also be represented by the relation

$$c\int \tilde{\alpha}(\nu)d\nu = \tilde{\alpha}_{1a}\rho^2 n_0^2 + \tilde{\alpha}_{2a}\rho^3 n_0^3 + \cdots , \tag{3.3}$$

where c is the speed of light, $\tilde{\alpha}(\nu) = \alpha(\nu)/\nu$, and n_0 is Loschmidt's number (2.687×10^{-19} cm^{-3}). The new binary and ternary absorption coefficients $\tilde{\alpha}_{1a}$ (in $cm^6 s^{-1}$) and $\tilde{\alpha}_{2a}$ (in $cm^9 s^{-1}$) are related to α_{1a} and α_{2a}, respectively, by the relations

$$\tilde{\alpha}_{1a} = (c/n_0^2)\alpha_{1a}/\bar{\nu} \tag{3.4}$$

and

$$\tilde{\alpha}_{2a} = (c/n_0^3)\alpha_{2a}/\bar{\nu} \ . \tag{3.5}$$

The quantity $\bar{\nu}$ in the above equations is the band center, given by the relation

$$\bar{\nu} = \frac{\int \alpha(\nu)d\nu}{\int \alpha(\nu)\nu^{-1}d\nu} \ . \tag{3.6}$$

The integrated absorption coefficients $\int \alpha(\nu)d\nu$ of the band were determined by integrating the areas under the experimental profiles, and these can be expressed in terms of density by Eq. (3.2). Plots of $(1/\rho^2)\int \alpha(\nu)d\nu$ versus ρ for the profiles at three experimental temperatures are shown in Figure 3.4 and are found to be straight

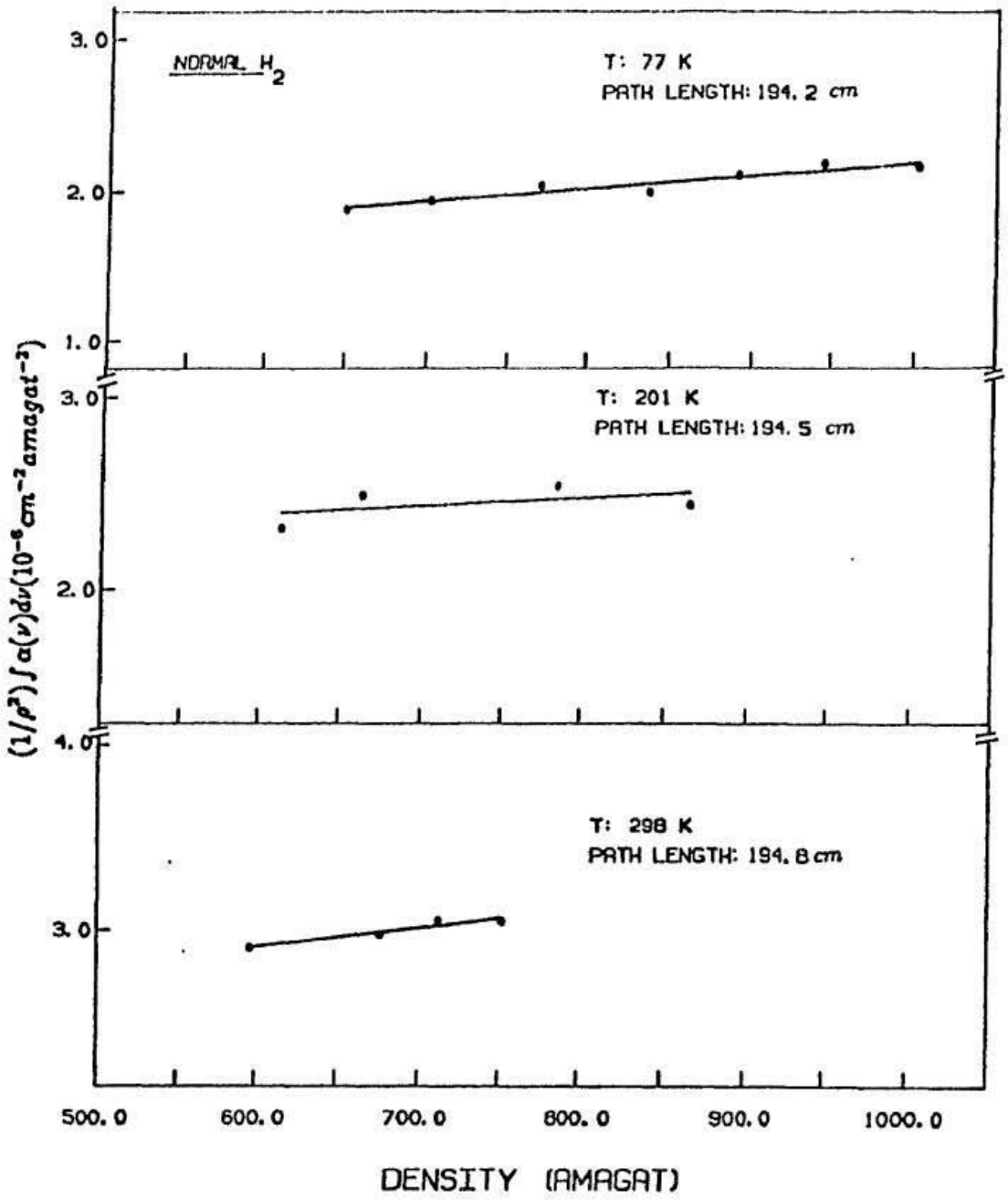

Figure 3.4: Plots of $(1/\rho^2)\int\alpha(\nu)d\nu$ versus ρ for normal H_2 in the pure gas at 77, 201 and 298 K in the second overtone region.

lines. The intercepts and the slopes of the straight lines, which give the binary and the ternary absorption coefficients, respectively, are calculated by a least-squares fit of the experimental data and their values are listed in Table 3.5. The experimental errors in the integrated absorption coefficients (i.e., the areas under the absorption profiles) are believed to be around 1 to 2 % and these are too small to be shown in Figure 3.4.

3.4 Absorption Coefficients of Individual Lines

For comparison with theory, it is more convenient to calculate a quantity proportional to the integrated transition probability than the integrated absorption coefficient. The theory of collision-induced absorption of Van Kranendonk (1957, 1958) allows the relative intensities of the various H_2 transitions to be specified for the overlap-induced transitions. The relative intensities for the overlap components, $Q_{overlap}(J)$, are given by

$$\tilde{\alpha}^0_{ov,m} \propto P_J \ , \tag{3.7}$$

where P_J is the normalized Boltzmann factor, which satisfies the relation $\sum_J P_J = 1$

Table 3.5: Absorption coefficients[a] of the fundamental, first overtone, and second overtone bands of normal H_2

Band	Temper -ature (K)	Binary absorption coefficient α_{1a} ($cm^{-2}amagat^{-2}$)	Binary absorption coefficient $\bar{\alpha}_{1a}$ (cm^6s^{-1})	Ternary absorption coefficient α_{2a} ($cm^{-2}amagat^{-3}$)	Ratio $\alpha_{1a}/\alpha_{1a}(1-0)$ at a given T	Reference
1-0	77	$(1.42 \pm 0.05) \times 10^{-3}$	1.32×10^{-35}	$(1.5 \pm 1.5) \times 10^{-6}$	1.0	Reddy et al. (1976)
	196	$(1.87 \pm 0.05) \times 10^{-3}$	1.74×10^{-35}	$(4.9 \pm 1.3) \times 10^{-6}$	1.0	..
	298	$(2.46 \pm 0.03) \times 10^{-3}$	2.30×10^{-35}	$(4.7 \pm 0.7) \times 10^{-6}$	1.0	..
2-0	77	$(4.31 \pm 0.09) \times 10^{-5}$	2.86×10^{-37}	$(-0.3 \pm 0.3) \times 10^{-9}$	3.0×10^{-2}	Van Nostrand (1983)
	201	$(4.99 \pm 0.08) \times 10^{-5}$	2.44×10^{-37}	$(1.9 \pm 0.3) \times 10^{-9}$	2.7×10^{-2}	..
	298	$(5.8 \pm 0.1) \times 10^{-5}$	2.1×10^{-37}	$(1.2 \pm 0.3) \times 10^{-9}$	2.4×10^{-2}	..
3-0	77	$(1.35 \pm 0.04) \times 10^{-6}$	4.53×10^{-39}	$(0.8 \pm 0.2) \times 10^{-9}$	1.0×10^{-3}	Present work
	201	$(2.13 \pm 0.02) \times 10^{-6}$	7.11×10^{-39}	$(0.4 \pm 0.1) \times 10^{-9}$	1.1×10^{-3}	..
	298	$(2.33 \pm 0.02) \times 10^{-6}$	7.88×10^{-39}	$(0.9 \pm 0.3) \times 10^{-9}$	1.0×10^{-3}	..

[a]The errors indicated are standard deviations

and is expressed as

$$P_J = \frac{g_T(2J+1)\exp(-E_J/kT)}{\sum_J g_T(2J+1)\exp(-E_J/kT)}\,, \tag{3.8}$$

where g_T is the nuclear statistical weight of the molecule in a given rotational state and E_J is the energy of the Jth rotational level. For hydrogen g_T is 1 and 3 for the even and odd J rotational states, respectively. For normal H_2 the conversion of the ortho to para species or vice versa is forbidden and the relation

$$\sum_{evenJ} P_J / \sum_{oddJ} P_J = 1/3 \tag{3.9}$$

is satisfied. Therefore Eq. (3.8) is written as

$$\left.\begin{aligned} P_{evenJ} &= \frac{(2J+1)\exp(-E_J/kT)}{\sum_J(2J+1)\exp(-E_J/kT)}\,\frac{C_p}{C_p+C_o}\,, \\ P_{oddJ} &= \frac{(2J+1)\exp(-E_J/kT)}{\sum_J(2J+1)\exp(-E_J/kT)}\,\frac{C_o}{C_p+C_o}\,, \end{aligned}\right\} \tag{3.10}$$

where $C_p/(C_p+C_o) = 1/4$ and $C_o/(C_p+C_o) = 3/4$ are the para-H_2 (J even) and ortho-H_2 (J odd) concentrations of normal H_2, respectively. The normalized Boltzmann factors for H_2 at 77, 201 and 298 K are listed in Table 3.6.

For quadrupolar induction, the integrated binary absorption coefficient can be expressed as (Poll, 1971, Karl et. al., 1975 and Reddy, 1985)

$$\int \alpha(\nu)\frac{d\nu}{\nu} = \int \tilde{\alpha}(\nu)d\nu = \tilde{\alpha}_{1qm}\rho^2 + \tilde{\alpha}_{2qm}\rho^3 + \cdots. \tag{3.11}$$

The new binary absorption coefficient (in cm^{-1} $amagat^{-2}$) for a given band due to quadrupolar induction and arising from binary collisions is expressed as (Reddy, 1985)

Table 3.6: Normalized Boltzmann factors for normal hydrogen

J	P_J		
	77 K	201 K	298 K
0	0.2483	0.1789	0.1292
1	0.7500	0.7247	0.6587
2	0.0017	0.0708	0.1167
3	–	0.0253	0.0903
4	–	0.0004	0.0041
5	–	–	0.0010

(the subscript 1 is omitted)

$$\tilde{\alpha}_{qm} = (\frac{1}{\rho^2})\int \frac{\alpha_m(\nu)}{\nu} d\nu \tag{3.12}$$

$$= \frac{8\pi^3 e^2}{3hc} n_0^2 a_0^5 (\frac{a_0}{\sigma})^5 J_q X_{qm} \, , \tag{3.13}$$

where ρ is the density of the gas in amagat units, e is the electron charge, n_0 is the Loschmidt constant, a_0 is the Bohr radius, and the temperature-dependent dimensionless integral $J_q(T^*)$ represents the average dependence of the square of the induced dipole moment on the intermolecular separation R. This integral is given by

Van Kranendonk (1958) as

$$J_q = 12\pi \int_0^\infty x^{-8} g_0(x) x^2 dx \ . \tag{3.14}$$

Here $x = R/\sigma$, where R denotes the separation between two interacting molecules and σ is the intermolecular separation corresponding to the intermolecular potential $V(\sigma) = 0$; $g_0(x)$ is the low density limit of the pair correlation function which in the classical limit is given by $\exp(-V^*(x)/T^*)$ with $V^*(x) = V(x)/\epsilon$, where $V(x)$ denotes the Lennard-Jones potential $V(x) = 4\epsilon(x^{-12} - x^{-6})$; and the quantity $T^* = kT/\epsilon$, where ϵ is the depth of the potential well. Equation (3.14) gives classical values of J_q $(=J_q^{cl})$ which are applicable at high temperatures. But at intermediate temperatures, quantum corrections have to be applied, and the quantity J_q is expressed as

$$J_q = J^{cl} + \Lambda^{*2} J^{(1)} + \Lambda^{*4} J^{(2)} + \cdots \ , \tag{3.15}$$

where $J^{(1)}$ and $J^{(2)}$ are quantum corrections, Λ^* $(=h/(2\mu\epsilon\sigma^2)^{1/2})$ is the reduced mean de Broglie wave-length (De Boer, 1949). Here μ is the reduced mass of the colliding pair of molecules. $J^{(1)}$ and $J^{(2)}$ (expressions for $J^{(1)}$ and $J^{(2)}$ are given by Van Kranendonk (1958)) were evaluated by us and found to agree with the values given by Gibbs et al. (1979). In our calculations of the absorption coefficients of the individual components, values of J_q with the quantum corrections are used. The

quantity X_{qm} is given by

$$\begin{aligned} X_{qm} &= \sum P_{J_1} P_{J_2} \quad [C(J_1 2 J_1'; 00)^2 C(J_2 0 J_2'; 00)^2 < v_1 J_1 | Q_1 | v_1' J_1' >^2 < v_2 J_2 | \alpha_2 | v_2' J_2' >^2 \\ &+ \qquad C(J_2 2 J_2'; 00)^2 C(J_1 0 J_1'; 00)^2 < v_2 J_2 | Q_2 | v_2' J_2' >^2 < v_1 J_1 | \alpha_1 | v_1' J_1' >^2 \\ &+ \qquad Y_{qm}] \,, \end{aligned} \tag{3.16}$$

where the subscripts 1 and 2 refer to the two colliding molecules and vJ and $v'J'$ are their initial and final vibrational and rotational quantum numbers; the summation is taken over all individual transitions that contribute to the band. The quantities P_J are the normalized Boltzmann factors as expressed in Eq. (3.8), and $C(J\lambda J'; 00)$ with $\lambda = 0$ and 2 are Clebsch-Gordan coefficients and are functions of J (Rose, 1957; also listed by Reddy, 1985). The quantities $< vJ|Q|v'J' >$ and $< vJ|\alpha|v'J' >$ (with $v = 0$ in the present case) are quadrupole moment and polarizability matrix elements, respectively, of the hydrogen molecule and are expressed in atomic units. The term Y_{qm} in Eq. (3.16) is included to account for the effects of the anisotropy of the polarizability, and is given by

$$\begin{aligned} Y_{qm} &= C(J_1 2 J_1'; 00)^2 C(J_2 2 J_2'; 00)^2 \\ &\times \left[\frac{2}{9} < 0 J_1 | Q_1 | v_1' J_1' >^2 < 0 J_2 | \gamma_2 | v_2' J_2' >^2 \right. \\ &+ \left. \frac{2}{9} < 0 J_2 | Q_2 | v_2' J_2' >^2 < 0 J_1 | \gamma_1 | v_1' J_1' >^2 \right. \end{aligned}$$

$$- \frac{4}{15} < 0J_1|Q_1|v_1'J_1' >< 0J_2|Q_2|v_2'J_2' >$$

$$\times \ < 0J_1|\gamma_1|v_1'J_1' >< 0J_2|\gamma_2|v_2'J_2' >] \ , \qquad (3.17)$$

where the $< 0J|\gamma|v'J' >$ are matrix elements of the anisotropy of the polarizability. In general, Y_{qm} is small compared to the rest of expression for X; it not only contributes a small amount to the transitions which mainly arise from the isotropic polarizability, but exclusively gives rise to weak double transitions of the form $S(J_1)+S(J_2)$. A computer program was written to calculate the integrated binary absorption coefficients for all the individual quadrupolar transitions in terms of Eq. (3.13) and is listed in Appendix A. The matrix elements[1] of the quadrupole, polarizability, and anisotropic polarizability, of H_2 used in these calculations were numerically calculated by Hunt et al. (1984) and are listed in Appendix B. Tables 3.7, 3.8 and 3.9 present the transition intensities of H_2 due to the quadrupolar induction in the second overtone region at 77, 201 and 298 K.

[1]One-half of the numerical values of $< Q >$ given by these authors are used because of the difference in the definition of $< Q >$.

Table 3.7: Calculated intensities for H_2 transitions in the second overtone region at 77 K.

Transition	Wavenumber (cm^{-1})	Absolute Intensity ($cm^{-1}amagat^{-2}$)	Relative Intensity	"Improved" Relative Intensity
$Q_3(1) + Q_0(J)$	11765.0	0.1678e-10	0.4683	0.5719
$Q_3(0) + Q_0(J)$	11782.4	0.1014e-11	0.0283	0.0611
$S_3(0) + Q_0(J)$	12084.6	0.1628e-10	0.4544	0.4555
$Q_3(1) + S_0(0)$	12119.3	0.2853e-11	0.0796	0.1664
$Q_3(0) + S_0(0)$	12136.7	0.8439e-12	0.0236	0.0508
$Q_2(1) + Q_1(1)$	12230.6	0.1488e-10	0.4153	0.5836
$Q_2(1) + Q_1(0)$	12236.5	0.3026e-11	0.0845	0.0843
$Q_2(0) + Q_1(1)$	12242.3	0.1727e-11	0.0482	0.1040
$S_3(1) + Q_0(J)$	12265.6	0.3583e-10	1.0000	1.0000
$Q_3(1) + S_0(1)$	12352.0	0.5216e-11	0.1456	0.3043
$Q_3(0) + S_0(1)$	12369.4	0.1542e-11	0.0430	0.0929
$S_3(0) + S_0(0)$	12439.0	0.2200e-12	0.0061	0.0079
$S_2(0) + Q_1(1)$	12561.6	0.8540e-11	0.2383	0.2369
$S_2(0) + Q_1(0)$	12567.5	0.2696e-11	0.0752	0.0751
$Q_2(1) + S_1(0)$	12573.2	0.3787e-11	0.1057	0.2166
$Q_2(0) + S_1(0)$	12584.8	0.1135e-11	0.0317	0.0684
$S_3(1) + S_0(0)$	12619.9	0.3845e-12	0.0107	0.0125
$S_3(0) + S_0(1)$	12671.7	0.4038e-12	0.0113	0.0145
$S_2(1) + Q_1(1)$	12759.5	0.1592e-10	0.4443	0.4419
$S_2(1) + Q_1(0)$	12765.4	0.5038e-11	0.1406	0.1403
$Q_2(1) + S_1(1)$	12788.2	0.5850e-11	0.1633	0.3331
$Q_2(0) + S_1(1)$	12800.0	0.1739e-11	0.0485	0.1048
$S_3(1) + S_0(1)$	12852.6	0.7062e-12	0.0197	0.0230
$S_2(0) + S_1(0)$	12904.2	0.2731e-12	0.0076	0.0069
$S_2(1) + S_1(0)$	13102.1	0.4849e-12	0.0135	0.0123
$S_2(0) + S_1(1)$	13119.3	0.4574e-12	0.0128	0.0116
$S_2(1) + S_1(1)$	13317.1	0.8127e-12	0.0227	0.0206

Table 3.8: Calculated intensities for H_2 transitions in the second overtone region at 201 K.

Transition	Wavenumber (cm^{-1})	Absolute Intensity ($cm^{-1}amagat^{-2}$)	Relative Intensity	"Improved" Relative Intensity
$Q_3(3) + Q_0(J)$	11678.5	0.4686e-12	0.0126	0.0165
$Q_3(2) + Q_0(J)$	11730.3	0.1345e-11	0.0362	0.0469
$Q_3(1) + Q_0(J)$	11765.0	0.1760e-10	0.4734	0.5821
$Q_3(0) + Q_0(J)$	11782.4	0.8270e-12	0.0222	0.0480
$S_3(0) + Q_0(J)$	12084.6	0.1259e-10	0.3386	0.3396
$Q_3(2) + S_0(0)$	12084.6	0.2050e-12	0.0055	0.0116
$Q_3(1) + S_0(0)$	12119.3	0.2131e-11	0.0573	0.1198
$Q_3(0) + S_0(0)$	12136.7	0.4698e-12	0.0126	0.0273
$Q_2(3) + Q_1(1)$	12172.5	0.4215e-12	0.0113	0.0172
$Q_2(2) + Q_1(2)$	12195.5	0.1024e-12	0.0028	0.0039
$Q_2(1) + Q_1(3)$	12201.2	0.4599e-12	0.0124	0.0162
$Q_2(2) + Q_1(1)$	12207.3	0.1202e-11	0.0323	0.0484
$Q_2(2) + Q_1(0)$	12213.2	0.1596e-12	0.0043	0.0043
$Q_2(1) + Q_1(2)$	12218.8	0.1303e-11	0.0350	0.0464
$Q_2(1) + Q_1(1)$	12230.6	0.1491e-10	0.4010	0.5634
$Q_2(1) + Q_1(0)$	12236.5	0.2260e-11	0.0608	0.0607
$Q_2(0) + Q_1(1)$	12242.3	0.1290e-11	0.0347	0.0749
$Q_3(3) + S_0(1)$	12265.6	0.1824e-12	0.0049	0.0104
$S_3(1) + Q_0(J)$	12265.6	0.3718e-10	1.0000	1.0000
$Q_3(2) + S_0(1)$	12317.3	0.5027e-12	0.0135	0.0285
$Q_3(1) + S_0(1)$	12352.0	0.5226e-11	0.1406	0.2937
$Q_3(0) + S_0(1)$	12369.4	0.1152e-11	0.0310	0.0669
$S_3(2) + Q_0(J)$	12424.5	0.3657e-11	0.0984	0.0982
$S_3(0) + S_0(0)$	12439.0	0.1225e-12	0.0033	0.0042
$S_2(0) + Q_1(3)$	12532.2	0.2227e-12	0.0060	0.0060
$S_2(0) + Q_1(2)$	12549.8	0.6187e-12	0.0166	0.0166
$Q_2(2) + S_1(0)$	12549.8	0.2726e-12	0.0073	0.0152

Table 3.8: (continued)

$S_3(3) + Q_0(J)$	12560.0	0.1384e-11	0.0372	0.0371
$S_2(0) + Q_1(1)$	12561.6	0.6379e-11	0.1716	0.1705
$S_2(0) + Q_1(0)$	12567.5	0.1501e-11	0.0404	0.0403
$Q_2(1) + S_1(0)$	12573.3	0.2828e-11	0.0761	0.1558
$Q_3(1) + S_0(2)$	12579.4	0.4434e-12	0.0119	0.0249
$Q_2(0) + S_1(0)$	12584.8	0.6318e-12	0.0170	0.0367
$S_3(1) + S_0(0)$	12619.9	0.2872e-12	0.0077	0.0090
$S_3(0) + S_0(1)$	12671.7	0.3016e-12	0.0081	0.0104
$Q_2(3) + S_1(1)$	12730.1	0.2044e-12	0.0055	0.0114
$S_2(1) + Q_1(3)$	12730.1	0.5573e-12	0.0150	0.0149
$S_2(1) + Q_1(2)$	12747.7	0.1548e-11	0.0416	0.0414
$S_2(1) + Q_1(1)$	12759.5	0.1595e-10	0.4290	0.4266
$Q_2(2) + S_1(1)$	12764.9	0.5637e-12	0.0152	0.0314
$S_2(1) + Q_1(0)$	12765.4	0.3762e-11	0.1012	0.1010
$Q_2(1) + S_1(1)$	12788.2	0.5862e-11	0.1577	0.3216
$Q_3(1) + S_0(3)$	12799.6	0.1494e-12	0.0040	0.0084
$Q_2(0) + S_1(1)$	12799.9	0.1299e-11	0.0349	0.0754
$S_3(1) + S_0(1)$	12852.6	0.7076e-12	0.0190	0.0222
$S_2(0) + S_1(0)$	12904.2	0.1520e-12	0.0041	0.0037
$S_2(2) + Q_1(2)$	12929.0	0.1314e-12	0.0035	0.0035
$S_2(2) + Q_1(1)$	12940.8	0.1353e-11	0.0364	0.0362
$S_2(2) + Q_1(0)$	12946.7	0.3197e-12	0.0086	0.0086
$Q_2(1) + S_1(2)$	12992.3	0.4141e-12	0.0111	0.0226
$S_2(1) + S_1(0)$	13102.1	0.3622e-12	0.0097	0.0089
$S_2(3) + Q_1(1)$	13104.0	0.4483e-12	0.0121	0.0120
$S_2(3) + Q_1(0)$	13109.9	0.1060e-12	0.0029	0.0028
$S_2(0) + S_1(1)$	13119.3	0.3416e-12	0.0092	0.0084
$Q_2(1) + S_1(3)$	13183.7	0.1144e-12	0.0031	0.0062
$S_2(1) + S_1(1)$	13317.1	0.8144e-12	0.0219	0.0199
$Q_3(3) + S_0(0)$	12032.9			0.0042
$Q_2(0) + Q_1(2)$	12230.5			0.0052
$Q_2(3) + S_1(0)$	12515.0			0.0055
$Q_3(0) + S_0(2)$	12596.8			0.0057
$Q_2(0) + S_1(2)$	13004.0			0.0053

Table 3.9: Calculated intensities for H_2 transitions in the second overtone region at 298 K.

Transition	Wavenumber (cm^{-1})	Absolute Intensity ($cm^{-1}amagat^{-2}$)	Relative Intensity	"Improved" Relative Intensity
$Q_3(3) + Q_0(J)$	11678.5	0.1816e-11	0.0497	0.0653
$Q_3(2) + Q_0(J)$	11730.3	0.2407e-11	0.0659	0.0856
$Q_3(1) + Q_0(J)$	11765.0	0.1735e-10	0.4748	0.5858
$Q_3(0) + Q_0(J)$	11782.4	0.6563e-12	0.0180	0.0388
$S_3(0) + Q_0(J)$	12084.6	0.9832e-11	0.2691	0.2699
$Q_3(2) + S_0(0)$	12084.6	0.2638e-12	0.0072	0.0152
$Q_3(3) + S_0(0)$	12032.9	0.2072e-12	0.0057	0.0120
$Q_3(1) + S_0(0)$	12119.3	0.1512e-11	0.0414	0.0865
$Q_3(0) + S_0(0)$	12136.7	0.2618e-12	0.0072	0.0156
$Q_2(3) + Q_1(3)$	12143.1	0.1726e-12	0.0047	0.0067
$Q_2(3) + Q_1(2)$	12160.7	0.2272e-12	0.0062	0.0089
$Q_2(3) + Q_1(1)$	12172.5	0.1478e-11	0.0404	0.0614
$Q_2(2) + Q_1(3)$	12177.9	0.2289e-12	0.0063	0.0087
$Q_2(3) + Q_1(0)$	12178.4	0.1513e-12	0.0041	0.0041
$Q_2(2) + Q_1(2)$	12195.5	0.3009e-12	0.0082	0.0116
$Q_2(1) + Q_1(3)$	12201.2	0.1613e-11	0.0441	0.0557
$Q_2(2) + Q_1(1)$	12207.3	0.1947e-11	0.0533	0.0799
$Q_2(2) + Q_1(0)$	12213.2	0.2055e-12	0.0056	0.0056
$Q_2(1) + Q_1(2)$	12218.8	0.2110e-11	0.0577	0.0764
$Q_2(0) + Q_1(2)$	12230.5	0.1661e-12	0.0032	0.0069
$Q_2(1) + Q_1(1)$	12230.6	0.1331e-10	0.3643	0.5120
$Q_2(1) + Q_1(0)$	12236.5	0.1604e-11	0.0439	0.0438
$Q_2(0) + Q_1(1)$	12242.3	0.9152e-12	0.0250	0.0541
$Q_3(3) + S_0(1)$	12265.6	0.6395e-12	0.0175	0.0369
$S_3(1) + Q_0(J)$	12265.6	0.3654e-10	1.0000	1.0000
$Q_3(2) + S_0(1)$	12317.3	0.8144e-12	0.0223	0.0470
$Q_3(1) + S_0(1)$	12352.0	0.4667e-11	0.1277	0.2670

Table 3.9: (continued)

$Q_3(0) + S_0(1)$	12369.4	0.8173e-12	0.0224	0.0483
$S_3(2) + Q_0(J)$	12424.5	0.6520e-11	0.1784	0.1782
$Q_2(3) + S_1(0)$	12515.0	0.2755e-12	0.0075	0.0157
$S_2(0) + Q_1(3)$	12532.2	0.6203e-12	0.0170	0.0169
$Q_3(2) + S_0(2)$	12544.7	0.1253e-12	0.0034	0.0072
$S_2(0) + Q_1(2)$	12549.8	0.7963e-12	0.0218	0.0217
$Q_2(2) + S_1(0)$	12549.8	0.3508e-12	0.0096	0.0200
$S_3(3) + Q_0(J)$	12560.0	0.5338e-11	0.1461	0.1458
$S_2(0) + Q_1(1)$	12561.6	0.4526e-11	0.1239	0.1231
$S_2(0) + Q_1(0)$	12567.5	0.8461e-12	0.0232	0.0231
$Q_2(1) + S_1(0)$	12573.2	0.2007e-11	0.0549	0.1125
$Q_3(1) + S_0(2)$	12579.4	0.7184e-12	0.0197	0.0441
$Q_2(0) + S_1(0)$	12584.8	0.3562e-12	0.0097	0.0210
$Q_3(0) + S_0(2)$	12596.8	0.1257e-12	0.0034	0.0074
$S_1(1) + S_0(0)$	12619.9	0.2037e-12	0.0056	0.0065
$S_3(0) + S_0(1)$	12671.7	0.2140e-12	0.0059	0.0075
$Q_2(3) + S_1(1)$	12730.1	0.7169e-12	0.0196	0.0408
$S_2(1) + Q_1(3)$	12730.1	0.1954e-11	0.0535	0.0532
$S_2(1) + Q_1(2)$	12747.7	0.2508e-11	0.0686	0.0683
$S_2(1) + Q_1(1)$	12759.5	0.1425e-10	0.3900	0.3877
$Q_2(2) + S_1(1)$	12764.9	0.9132e-12	0.0250	0.0518
$S_2(1) + Q_1(0)$	12765.4	0.2669e-11	0.0730	0.0729
$Q_2(1) + S_1(1)$	12788.2	0.5235e-11	0.1433	0.2923
$Q_3(1) + S_0(3)$	12799.6	0.5240e-12	0.0143	0.0300
$Q_2(0) + S_1(1)$	12799.9	0.9217e-12	0.0252	0.0544
$S_3(1) + S_0(1)$	12852.6	0.6319e-12	0.0173	0.0202
$S_2(2) + Q_1(3)$	12911.4	0.3009e-12	0.0082	0.0082
$S_2(2) + Q_1(2)$	12929.0	0.3862e-12	0.0106	0.0105
$S_2(2) + Q_1(1)$	12940.8	0.2193e-11	0.0600	0.0597
$S_2(2) + Q_1(0)$	12946.7	0.4116e-12	0.0113	0.0112
$Q_2(2) + S_1(2)$	12969.0	0.1167e-12	0.0032	0.0066
$Q_2(1) + S_1(2)$	12992.3	0.6708e-12	0.0184	0.0373
$Q_2(0) + S_1(2)$	13004.0	0.1169e-12	0.0032	0.0069
$S_2(3) + Q_1(3)$	13074.6	0.2158e-12	0.0059	0.0059
$S_2(3) + Q_1(2)$	13092.2	0.2770e-12	0.0076	0.0076

Table 3.9. (continued)

$S_2(1) + S_1(0)$	13102.1	0.2570e-12	0.0070	0.0064
$S_2(3) + Q_1(1)$	13104.0	0.1572e-11	0.0430	0.0429
$S_2(3) + Q_1(0)$	13109.9	0.2954e-12	0.0081	0.0081
$S_2(0) + S_1(1)$	13119.3	0.2424e-12	0.0066	0.0060
$Q_2(1) + S_1(3)$	13183.7	0.4010e-12	0.0110	0.0221
$S_2(1) + S_1(1)$	13317.1	0.7273e-12	0.0200	0.0181
$S_2(2) + S_1(1)$	13498.5	0.1075e-12	0.0029	
$S_2(1) + S_1(2)$	13521.2	0.1025e-12	0.0028	
$Q_2(0) + Q_1(3)$	12212.9			0.0050
$Q_3(3) + S_0(2)$	12493.0			0.0057
$Q_3(2) + S_0(3)$	12765.0			0.0053
$Q_3(0) + S_0(3)$	12817.0			0.0054
$Q_2(3) + S_1(2)$	12934.2			0.0052

3.5 Lineshape Functions

It is clear from Section 3.2 that the H_2 collision-induced second overtone band consists of the superposition of several overlapping transitions, namely, the overlap-induced Q lines and the quadrupole-induced Q and S lines, including many double transitions. To effect a full analysis of the absorption spectra it is necessary to transform the results of the preceding discussions into a convenient form that can be applied to the experimental profiles. For computational purposes it is convenient to express the dimensionless absorption coefficient $\tilde{\alpha}(\nu)(\equiv \alpha(\nu)/\nu)$, following Van Kranendonk (1968), Mactaggart and Welsh (1973) and Reddy (1985), in the form

$$\tilde{\alpha}(\nu) = \sum_{m,n} \frac{\alpha^0_{nm} W_n(\Delta\nu)}{1 + \exp(-hc\Delta\nu/kT)} , \tag{3.18}$$

where $\Delta\nu = \nu - \nu_m$, m represents a particular transition of the H_2 molecule, n stands for the overlap (ov), quadrupolar (q), or hexadecpolar (hexa) induction mechanism; α^0_{nm} is twice the maximum absorption coefficient at molecular frequency ν_m (in cm^{-1}) and the term $1 + \exp(-hc\Delta\nu/kT)$ in the denominator satisfies the detailed balance condition and converts the 'symmetric' line form $W_n(\Delta\nu)$ into the observed asymmetric line-shape. It was shown by Poll (1960) that transitions arising from the same induction mechanism have the same line-shape.

The line-shape function in Eq. (3.18) for the overlap transitions is expressed as

$$W_{ov}(\Delta\nu) = W^0_{ov}(\Delta\nu)D(\Delta\nu)\ . \tag{3.19}$$

Here the intracollisional line-shape function W^0_{ov}, which is the Fourier transform of the autocorrelation function of the induced dipole moment for a single binary collision, is represented by the Levine-Birnbaum (1967) expression as

$$W^0_{ov} = (2\Delta\nu/\delta_d)^2 K_2(2\Delta\nu/\delta_d)\ , \tag{3.20}$$

where K_2 is the modified Bessel function of the second kind and δ_d is the intracollisional half-width at half-height. The intercollisional line form $D(\Delta\nu)$, which takes into account of the negative correlations existing between the dipole moments induced in successive collisions, is represented by Van Kranendonk (1968) as

$$D(\Delta\nu) = 1 - \gamma[1 + (\Delta\nu/\delta_c)^2]^{-1}\ , \tag{3.21}$$

where γ is a constant which is normally assumed to be unity to give zero absorption at the dip occurring at the molecular frequency ν_m and $\delta_c = 1/2\pi c\tau_c$ is the intercollisional half-width at half-height, where τ_c is the mean time between collisions. Lewis (1985) discussed the asymmetry in W_{ov}, resulting from phase shifts.

The line-shape function in Eq. (3.18) for the quadrupolar transitions is represented by the dispersion-type function, also known as the Lorentz line-shape function,

as (see Sen et al., 1980)

$$W_q^L(\Delta\nu) = 1/[1 + (\Delta\nu/\delta_q)^2] \,, \tag{3.22}$$

where δ_q is the quadrupolar half-width at half-height. Reddy et al. (1980) included a $(\Delta\nu/\delta_{q_4})^4$ term in the denominator of the dispersion-type function to account satisfactorily for the contribution of the quadrupolar wing in the region of the hexadecapolar U transitions in the fundamental band of H_2. Gillard et al. (1984) used the same model in the analysis of S + S transitions of the fundamental band of D_2 at 77 K. The $(\Delta\nu/\delta_{q_4})^4$ term is particularly useful when analysing the weaker transitions in the high wavenumber wings of the spectra at high gas densities. In the present profile analysis, the dispersion type function given by Eq. (3.22) was shown to adequately describe the quadrupolar contribution to the hydrogen second overtone band.

Another line-shape function for the quadrupolar induced lines in Eq. (3.18) is due to Birnbaum and Cohen (1976). This line-shape function (hereafter to be denoted as BC line-shape function), W_q^{BC}, can be expressed as

$$W_q^{BC}(\Delta\nu) = \frac{\tau_1}{\pi} \exp(\frac{\tau_2}{\tau_1}) \exp(\frac{hc\Delta\nu}{2kT}) \frac{zK_2(z)}{1 + (2\pi c\Delta\nu\tau_1)^2} \,, \tag{3.23}$$

where the quantity z is given by

$$z = [1 + (2\pi c\Delta\nu\tau_1)^2]^{1/2}[(\frac{\tau_2}{\tau_1})^2 + (\frac{h}{4\pi kT\tau_1})^2]^{1/2} \,, \tag{3.24}$$

where $K_2(z)$ is the modified Bessel function of the second kind, and τ_1 and τ_2 are the characteristic time parameters for the collisions. One can also use half-width parameters δ_1 and δ_2 instead of τ_1 and τ_2 in the $W_q^{BC}(\Delta\nu)$ expression as these are related by the equations $\delta_1 = 1/2\pi c\tau_1$ and $\delta_2 = 1/2\pi c\tau_2$. Hence $W_q^{BC}(\Delta\nu)$ and z can also be expressed as

$$W_q^{BC}(\Delta\nu) = \frac{1}{2\pi^2 c\delta_1} \exp(\frac{\delta_1}{\delta_2}) \exp(\frac{hc\Delta\nu}{2kT}) \frac{zK_2(z)}{1+(\Delta\nu/\delta_1)^2} \tag{3.25}$$

and

$$z = [1 + (\frac{\Delta\nu}{\delta_1})^2]^{1/2}[(\frac{\delta_1}{\delta_2})^2 + (\frac{hc\delta_1}{2kT})^2]^{1/2} . \tag{3.26}$$

Goorvitch et al. (1981) compared this line-shape function with the Lorentz line-shape function in the analysis of the fundamental band of H_2 and found that the observed spectra were equally well fitted by both functions. Dore et al. (1983) and Silvaggio et al. (1981) used the BC line-shape function in analysis of the 1-0 and 2-0 bands of H_2, respectively. In the present work both the Lorentz and the Birnbaum-Cohen line-shape functions are used to fit the observed profiles.

3.6 Method of Profile Analysis

The objective of the profile analysis is to obtain a satisfactory fit of the experimental absorption profiles with the synthetic profile computed from the superposition of the individual components with appropriate line-shape functions, and to derive certain characteristic molecular parameters from the analysis. The half-width parameters δ_d, and δ_c for the overlap components, and either δ_q for the Lorentz line-shape function or δ_1 and δ_2 for the BC line-shape function for the quadrupolar components are adjustable parameters in the least-squares computer fitting program listed in Appendix A. For the best fit of the computed profiles to the experimental profiles, the computations in present analysis included three independent intensity parameters – one for each group of the overlap components, the quadrupolar single transition components, and the quadrupolar double transition components. In addition, a shift parameter for the molecular frequency ν_m was also introduced to account for any possible perturbations in the energy levels. Thus, when Lorentz line-shape function is used in the analysis of experimental profiles, there are seven adjustable parameters – three relative intensity parameters, three half-width parameters and one frequency shift parameter. When the BC line-shape function is used, there is an additional

half-width parameter, making the total number of parameters eight. The synthetic profile thus obtained was fitted to the experimental profile using the criterion that the sum of the squares of the deviations between the calculated and observed values of $\log_{10}[I_0(\nu)/I(\nu)]$ at equally spaced data points over the entire experimental profile be a minimum. Visual verification of the quality of the fit was also made by plotting the experimental and synthetic profiles on the same frequency scale on the computer.

3.7 Results of Profile Analysis

Initially, attempts were made to fit the observed profiles to the synthetic profiles calculated from Eq. (3.18) by means of the Lorentz line shape function, considering only two independent intensity parameters, one for the overlap components, and the other for all the quadrupolar components (i.e., considering the single and double transitions as one group). However, the fit between the observed and synthetic profiles was poor, as shown in Figure 3.5 for H_2 at 77 K. It was noticed that the synthetic profile showed greater intensity than the observed profile in the region of the quadrupolar single transition components $Q_3(1)$, $S_3(0)$ and $S_3(1)$ and less intensity in the region of the quadrupolar double transition components. A similar trend was

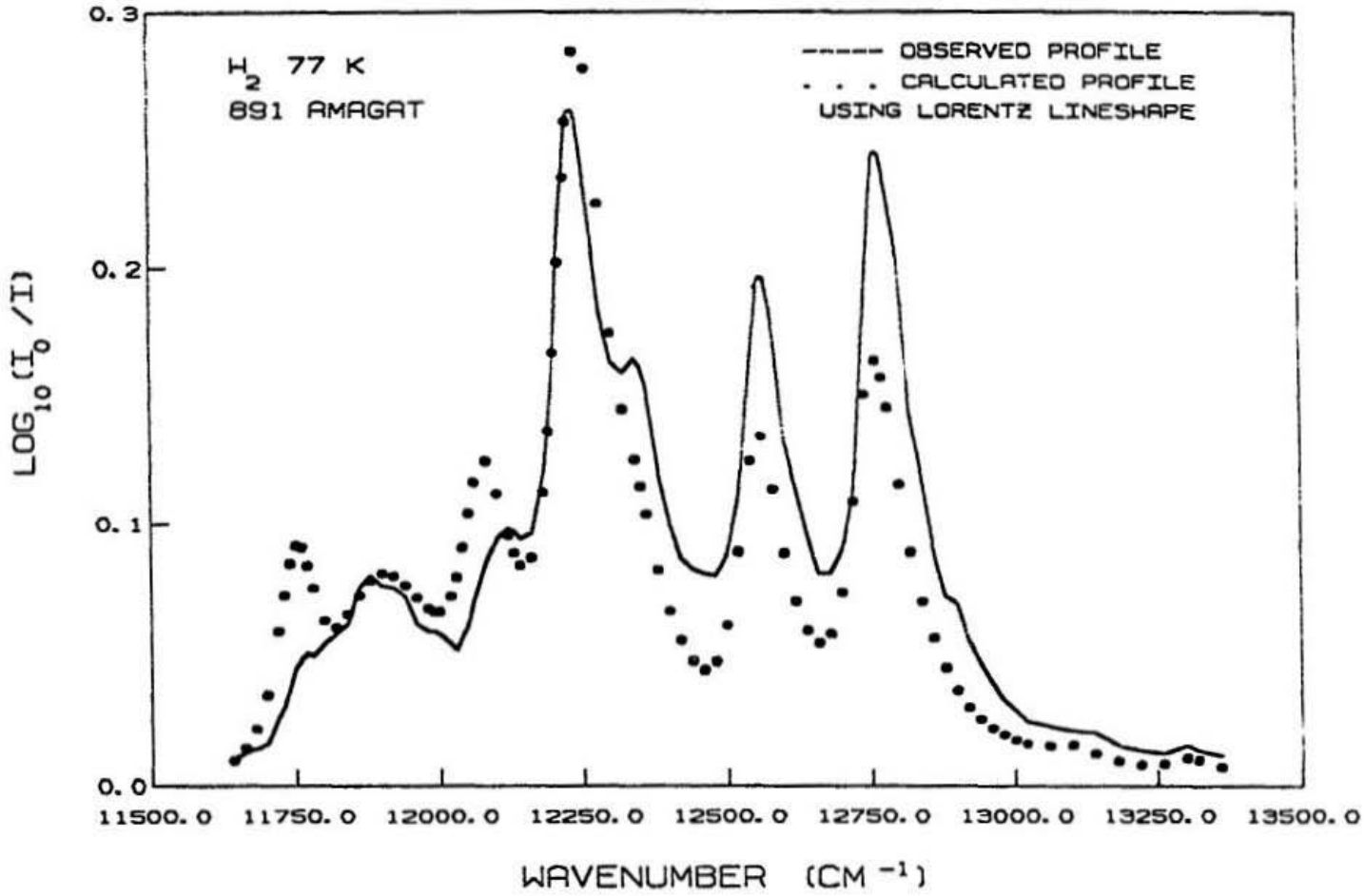

Figure 3.5: Initial analysis of an absorption profile of normal H_2 in the pure gas at 891 amagat and 77 K in the second overtone region.

observed in the case of the absorption profiles of H_2 at 201 and 298 K. Earlier, in the analysis of the collision-induced absorption of H_2 in the first-overtone region, similar discrepancies were observed by Watanabe (1971). It was suggested by him that these discrepancies could be explained in terms of different density dependences for the single and double transitions. At low densities binary collisions are predominant, whereas at higher densities the ternary and higher-order collisions must be taken into account, so that the cancellation effect (Van Kranendonk, 1958, 1959) causes the single transitions to have a negative ternary absorption coefficient, whereas the double transitions have a positive ternary absorption coefficient of nearly equal magnitude. Van Kranendonk calculated the ternary absorption coefficient for temperatures in the range 200-350 K in terms of a hard sphere model (which is only approximate) for the intermolecular potential, and found that the positive and negative parts were of exactly equal magnitude for the quadrupolar induction mechanism. On the basis of this model, the relative intensities of the single and double quadrupolar transitions were treated as independent parameters in the present analysis. An example of the result of such an analysis for the absorption profile at 77 K is shown in Figure 3.6. It is clear from this figure that the agreement between the observed and synthetic profiles is better than in Figure 3.5. However, some discrepancies still exist around the positions of $Q_3(J) + S_0(J)$, $Q_2(J) + S_1(J)$, $Q_2(J) + Q_1(J)$ and $S_2(J) + Q_1(J)$.

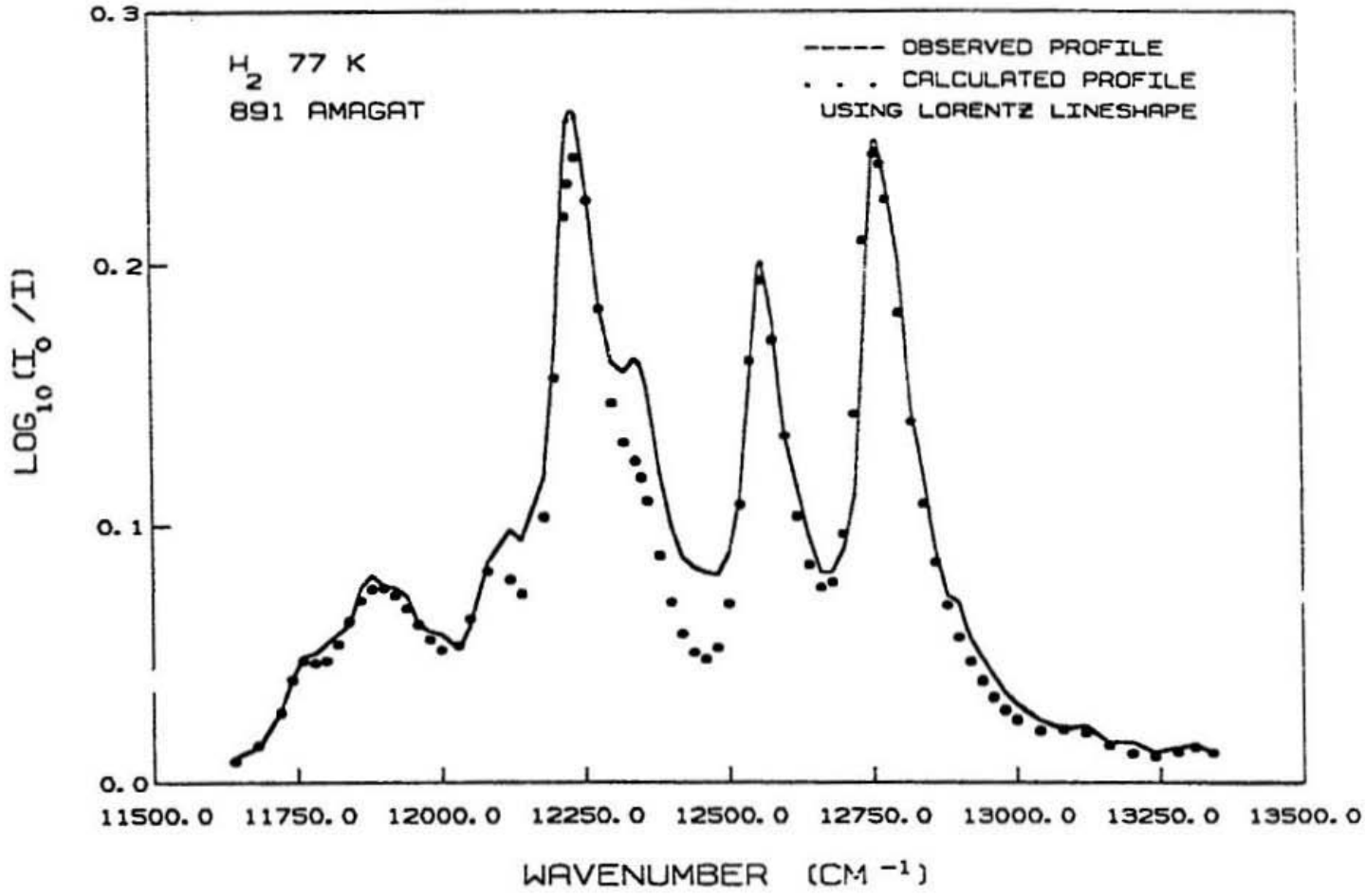

Figure 3.6: Analysis of an absorption profile of normal H_2 in the pure gas at 891 amagat and 77 K in the second overtone region, considering the quadrupolar single and double transitions separately.

In the analysis of absorption profiles of H_2 in the first overtone region, similar discrepancies were observed by van Nostrand (1983) in our laboratory in the transitions which involve the $v = 2$ vibrational state. The best fit between the observed and synthetic profiles was obtained by him by reducing the values of the $\Delta v = 2$ quadrupole moment matrix elements by a factor of 0.68. Also, McKellar (1988) found that in the first overton band of H_2 around 27 K, the standard theory of quadrupole-induced absorption overestimates the strength of the Δv=2 transitions. We now find that, after several trials with different adjustment factors, the same adjustment factor of 0.68 for the both $\Delta v = 2$ and $\Delta v = 3$ quadrupole matrix elements gives the best agreement between the observed and synthetic profiles of H_2 in the second overtone region as well at all the three experimental temperatures. Result of such an analysis for the experimental profile at 77 K (given also in Figures 3.5 and 3.6) is shown in Figure 3.7. The final results of analyses of typical profiles at 201 and 298 K are shown in Figures 3.8 and 3.9, respectively. The improved relative intensities for the transitions after application of the factor 0.68 to the quadrupolar matrix elements are also listed in Tables 3.6, 3.7 and 3.8 for 77, 201 and 298 K, respectively. It is seen from Figures 3.7, 3.8 and 3.9 that the experimental profiles have more intensity than the calculated profiles in the region near 12,460 cm^{-1}. This excess absorption is interpreted by us as arising from triple transitions $Q_1(J) + Q_1(J) + Q_1(J)$, which

Figure 3.7: Analysis of an absorption profile of normal H_2 in the pure gas at 891 amagat and 77 K in the second overtone region. The solid curves (a) is the experimental profile. The dashed curve (b) represent the individual overlap and quadrupolar computed components and the dots (c) represent the summation of these. An adjustment factor of 0.68 is used for the $\Delta v = 2$ and $\Delta v = 3$ quadrupolar matrix elements (see text for details). The curve represented by the open circle (d) around 12,460 cm^{-1} is the difference between the experimental and calculated profiles and is attributed to the triple transitions of the type $Q_1(J) + Q_1(J) + Q_1(J)$. The individual components for the transitions of the type $S_2(J) + S_1(J)$ which are relatively weak are not shown for the sake of clarity. (Note that the Lorentz line-shape function is used for the quadrupolar components.)

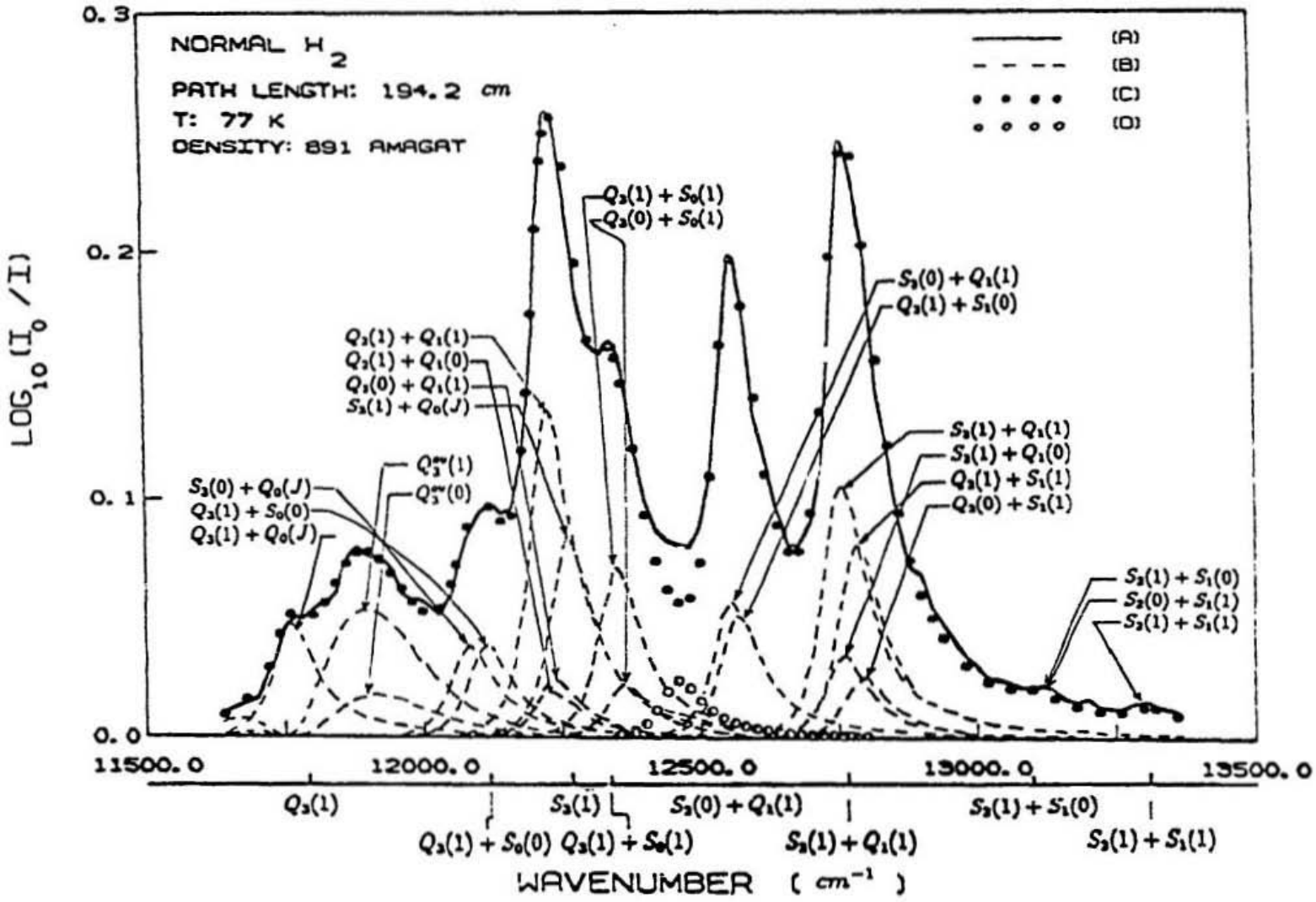
NORMAL H_2
PATH LENGTH: 194.2 cm
T: 77 K
DENSITY: 891 AMAGAT
(A)
(B)
(C)
(D)
$Q_3(1) + S_0(1)$
$Q_3(0) + S_0(1)$
$S_3(0) + Q_1(1)$
$Q_3(1) + S_1(0)$
$Q_3(1) + Q_1(1)$
$Q_3(1) + Q_1(0)$
$Q_3(0) + Q_1(1)$
$S_3(1) + Q_0(J)$
$S_3(1) + Q_1(1)$
$S_3(1) + Q_1(0)$
$Q_3(1) + S_1(1)$
$Q_3(0) + S_1(1)$
$Q_3^{ev}(1)$
$Q_3^{ev}(0)$
$S_3(0) + Q_0(J)$
$Q_3(1) + S_0(0)$
$Q_3(1) + Q_0(J)$
$S_3(1) + S_1(0)$
$S_3(0) + S_1(1)$
$S_3(1) + S_1(1)$
$LOG_{10}(I_0/I)$
0.3
0.2
0.1
0.0
11500.0
12000.0
12500.0
13000.0
13500.0
$Q_3(1)$
$S_3(1)$
$S_3(0) + Q_1(1)$
$S_3(1) + S_1(0)$
$Q_3(1) + S_0(0)$
$Q_3(1) + S_0(1)$
$S_3(1) + Q_1(1)$
$S_3(1) + S_1(1)$
WAVENUMBER (cm^{-1})

Figure 3.8: Analysis of an absorption profile of normal H_2 in the pure gas at 785 amagat and 201 K in the second overtone region. Here the rotational quantum number J takes the values 0 to 3. The solid curves (a) is the experimental profile. The dashed curve (b) represents the computed overlap-induced profile and quadrupolar-induced profile. The dots (c) represent the sum of the computed overlap and quadrupolar components. The difference between curve (a) and (c) represented by curve (d) is the contribution due to triple transitions of the type $Q_1(J) + Q_1(J) + Q_1(J)$. (Note the Lorentz line-shape function is used for the quadrupolar components.)

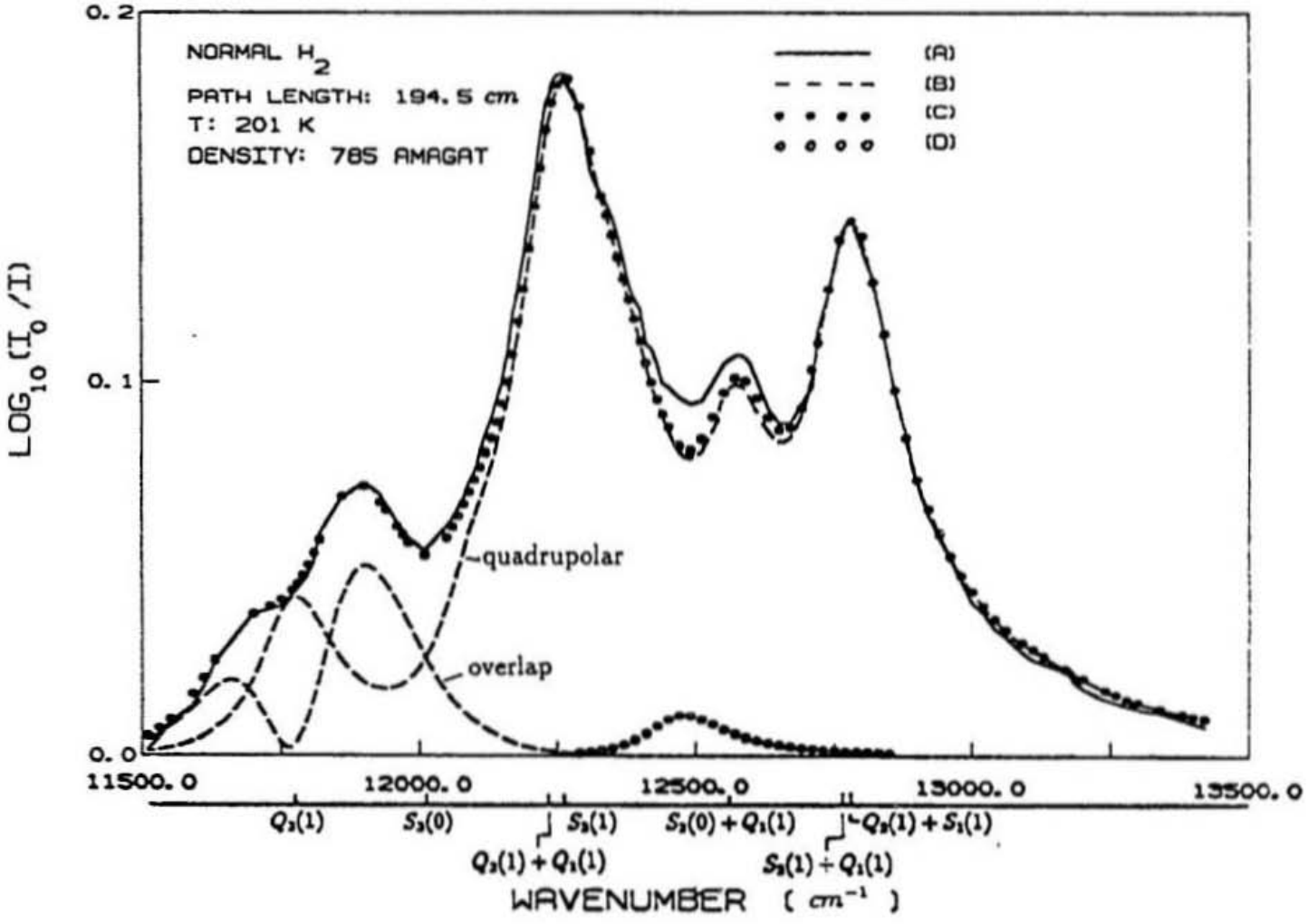
NORMAL H_2
PATH LENGTH: 194.5 cm
T: 201 K
DENSITY: 785 AMAGAT
(A)
(B)
(C)
(D)
quadrupolar
overlap
0.2
0.1
0.0
$LOG_{10}(I_0/I)$
11500.0
12000.0
12500.0
13000.0
13500.0
$Q_2(1)$
$S_2(0)$
$S_2(1)$
$S_2(0)+Q_1(1)$
$Q_2(1)+S_1(1)$
$Q_2(1)+Q_1(1)$
$S_2(1)+Q_1(1)$
WAVENUMBER (cm^{-1})

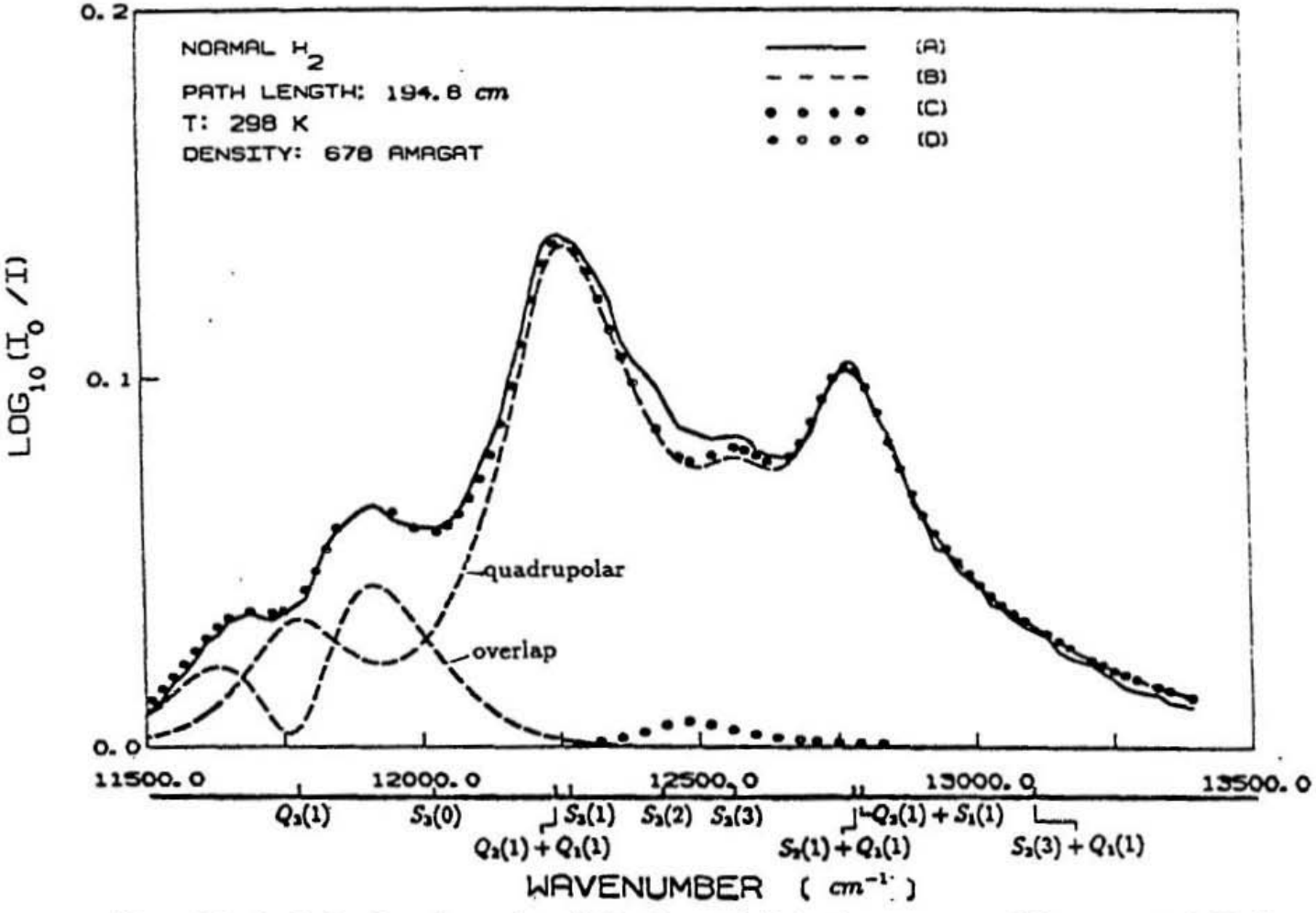

Figure 3.9: Analysis of an absorption profile of normal H_2 in the pure gas at 678 amagat and 298 K. Refer to the caption of Figure 3.8 for other details.

will be treated in Chapter 4.

In order to test the hypothesis of the cancellation effect, the ratio of the intensities of the single and double transitions, $R(\rho)$, was calculated from the following equation (Watanabe, 1971)

$$R(\rho) = R(0) - \Delta R\rho \,, \tag{3.27}$$

where $R(0)$ is the value of the ratio at zero density, and ΔR is a positive number which is essentially the sum of the absolute magnitudes of the density dependences of the single and double transitions. The variation of the ratio of the intensities of the single and double transitions with density ρ at 77, 201 and 298 K is plotted in Figure 3.10. The values of the normalized slopes $\Delta R/R(0)$ are listed in Table 3.10. The values 4.8×10^{-4} and 4.5×10^{-4} amagat^{-1} obtained in the present work at 77 and 201 K, respectively, are close to 4×10^{-4} amagat^{-1} predicted by the theory of Van Kranendonk as stated by Watanabe (1971).

The results obtained from the profile analysis are presented in Table 3.11. It can be seen from this table that the overlap contribution increases from 11% to 19% as the temperature increases from 77 to 298 K; equivalently, the quadrupolar contribution decreases from 89% at 77 K to 81% at 298 K. From the values of the characteristic half-widths δ_d and δ_q, the collision durations τ_d and τ_q were calculated from the rela-

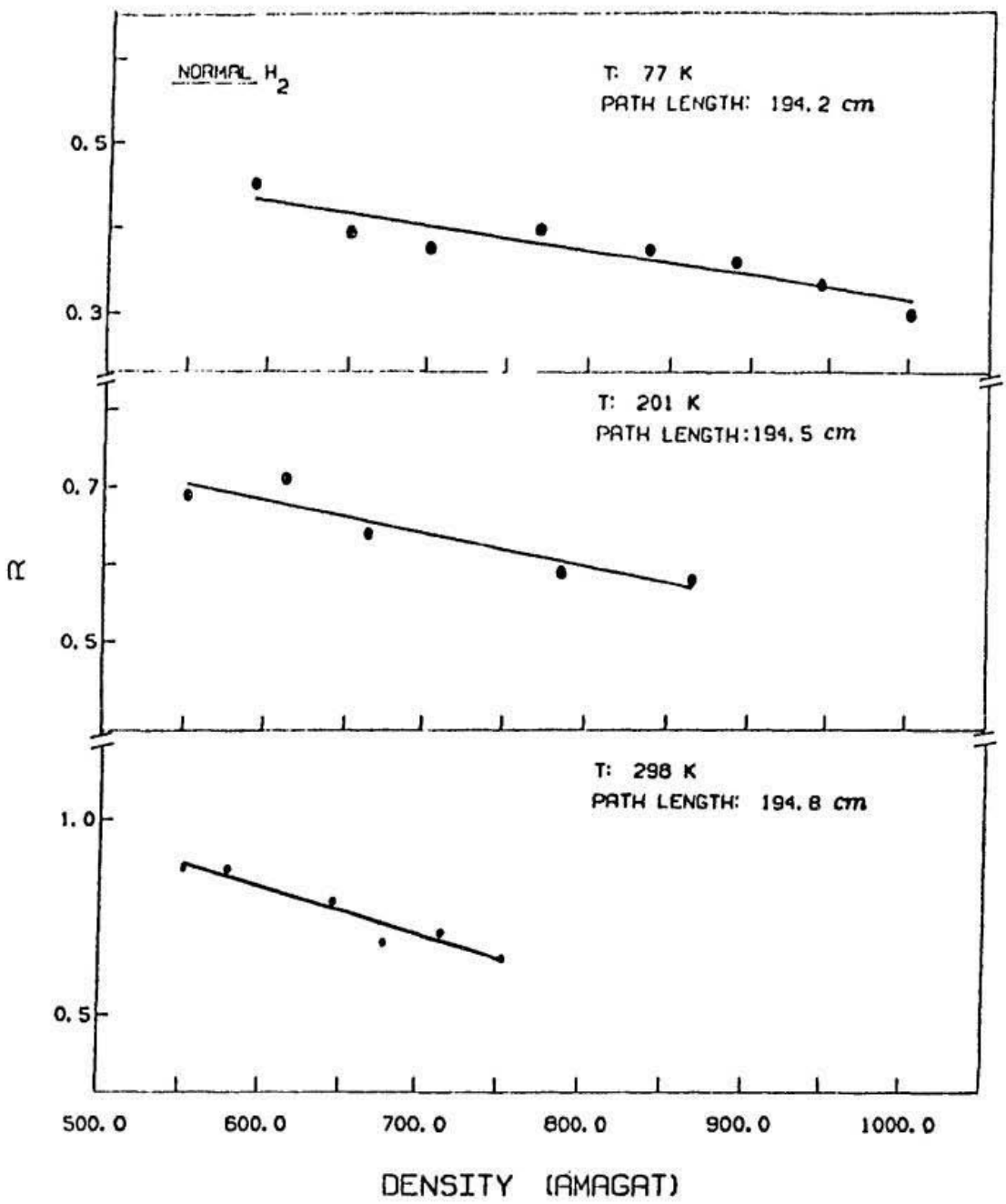

Figure 3.10: Variation of the ratio of the intensities of the quadrupolar single and double transitions at 77, 201 and 298 K.

Table 3.10: Values of the normalized slope $\Delta R/R(0)$ (in amagat^{-1}) of Eq. 3.27

Temperature (K)	Hunt & Welsh (1964)	Watanabe (1971)	Present work
20.4		5.8×10^{-3}	
77			4.8×10^{-4}
85	3.9×10^{-3}		
195	6.0×10^{-3}		
201			4.5×10^{-4}
298			8.6×10^{-4}
300	8.8×10^{-3}		

tions $\tau_d = 1/2\pi c\delta_d$ and $\tau_q = 1/2\pi c\delta_q$ and are also listed in the same table. The half-widths δ_d and δ_q have been plotted against the square root of absolute temperature in Figure 3.11. In Table 3.11, the value of $\delta_q = 50\pm1$ cm^{-1} for the profiles at 77 K is for those recorded at the densities 651, 702 and 770 amagat. However, δ_q at 77 K decreases from 50 to 42 cm^{-1} as the gas density increases to 1002 amagat. This decrease can be attributed to diffusional narrowing (see, for example, De Remigis et al., 1971). Narrowing of δ_q is not observed for the absorption profile at 201 K and

Table 3.11: Results[a] of profile analysis of normal H_2 in the second overtone region

T (K)	Intracollisional half-width δ_d (cm^{-1})	Collision duration τ_d (10^{-14} sec)	Quadrupolar half-width δ_q (cm^{-1})	Collision duration τ_q (10^{-14} sec)	BC profile parameter δ_1 (cm^{-1})	BC profile parameter δ_2 (cm^{-1})	Overlap contribution (%)	Quadrupolar contribution (%)
77	98±3	5.4	50±1[b]	11.1	47±3	315±4	11	89
201	104±3	5.1	82±1	6.5	100±1	297±3	15	85
298	118±6	4.5	106±3	5.0	135±5	264±4	19	81

[a]The errors indicated are standard deviations.
[b]The value is taken from the lower density profiles.

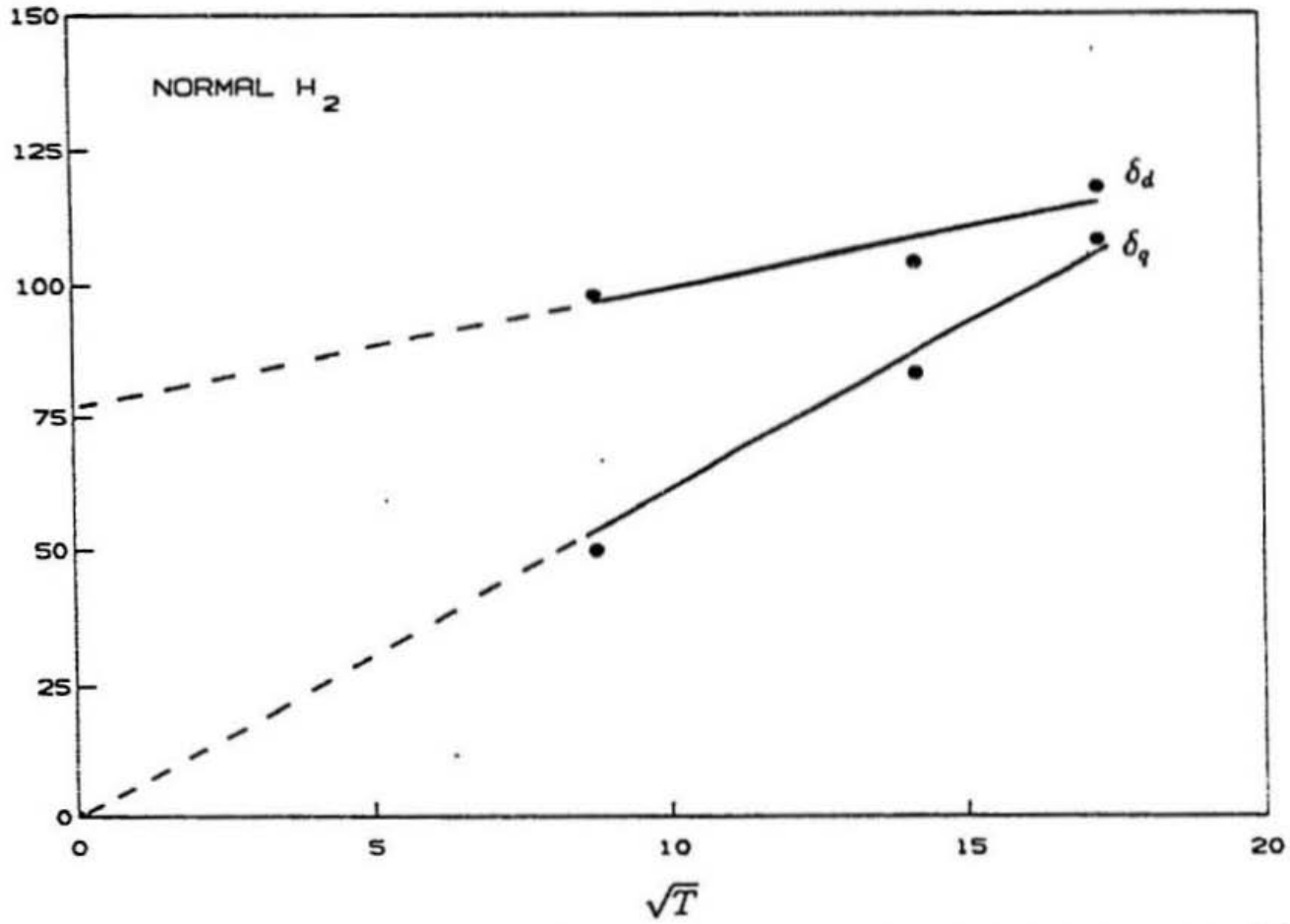

Figure 3.11: Halfwidth parameters δ_d and δ_q against the square root of the absolute temperature T.

298 K. The quadrupolar half-widths δ_q are found to satisfy the linear relation $\delta_q = 6.15\sqrt{T}$. The corresponding relations for the fundamental and first overtone bands of H_2 are $\delta_q = 6.16\sqrt{T}$ (Reddy et al. 1977) and $\delta_q = 6.4\sqrt{T}$ (van Nostrand, 1983), respectively. The intracollisional halfwidth δ_d which varies linearly with $\sqrt{T}$, when extrapolated to T = 0 gives a value of 77 cm^{-1}, which means that even at T = 0 the duration of the collision is still small because the overlap induction occurs mainly in the region of the strong repulsive forces between the molecules of the colliding pairs. From the H_2 fundamental band in H_2-rare gas mixtures it was found that the intercollisional half-width δ_c increases with increasing density of the perturbing gas (Mactaggart and Welsh, 1973 and Prasad, 1976). As the present experiments with pure H_2 gas were limited to densities up to 1000 amagat only, it was difficult to derive a definite expression for the density dependence of δ_c. The values of δ_c for the maximum experimental densities of the gas at 77, 201 and 298 K were 125, 200 and 210 cm^{-1}, respectively

The profile analyses as shown above were made by using the Lorentz line-shape function for the quadrupolar transitions. The BC line-shape function, W_q^{BC} in Eq. (3.25), was also applied in analysis of these profiles. The results are presented in Figures 3.12, 3.13 and 3.14 for profiles at 77, 201 and 298 K. From these figures it

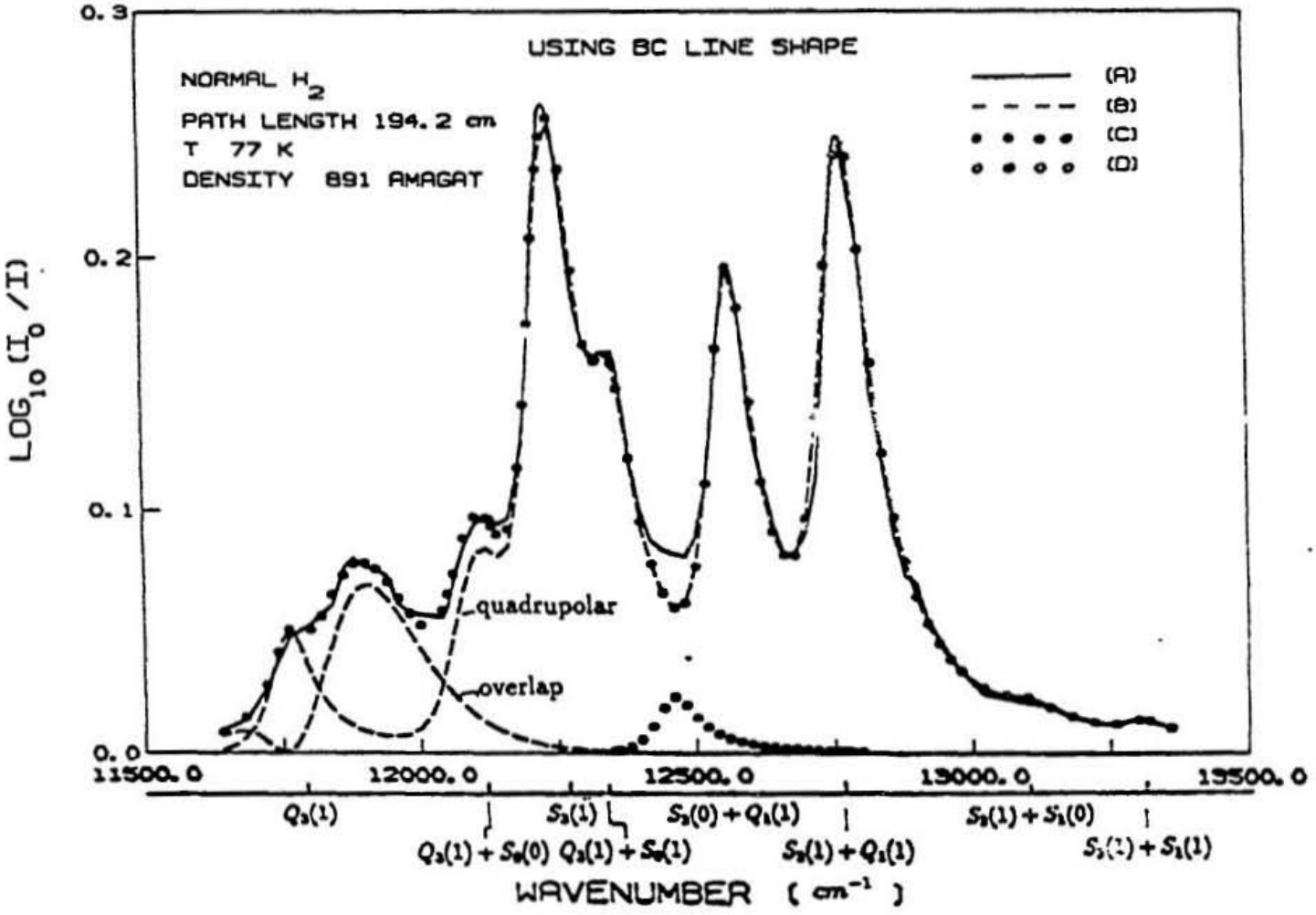

Figure 3.12: Re-analysis of the absorption profile shown in Figure 3.7 using BC line-shape function for the quadrupolar components. Refer to the caption of Figure 3.8 for other details.

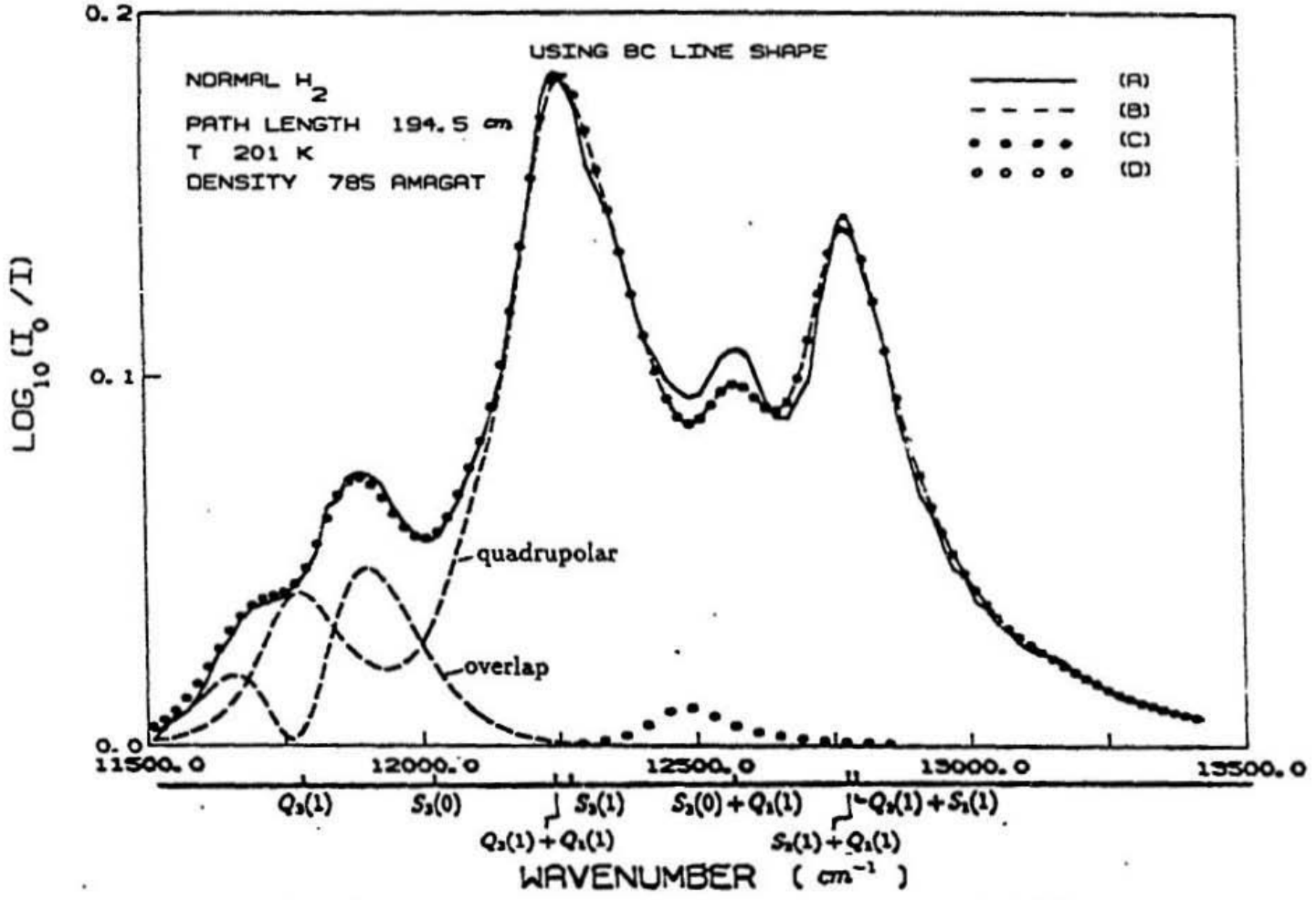

Figure 3.13: Re-analysis of the absorption profile shown in Figure 3.8 using BC line-shape function for the quadrupolar components. Refer to the caption of Figure 3.8 for other details.

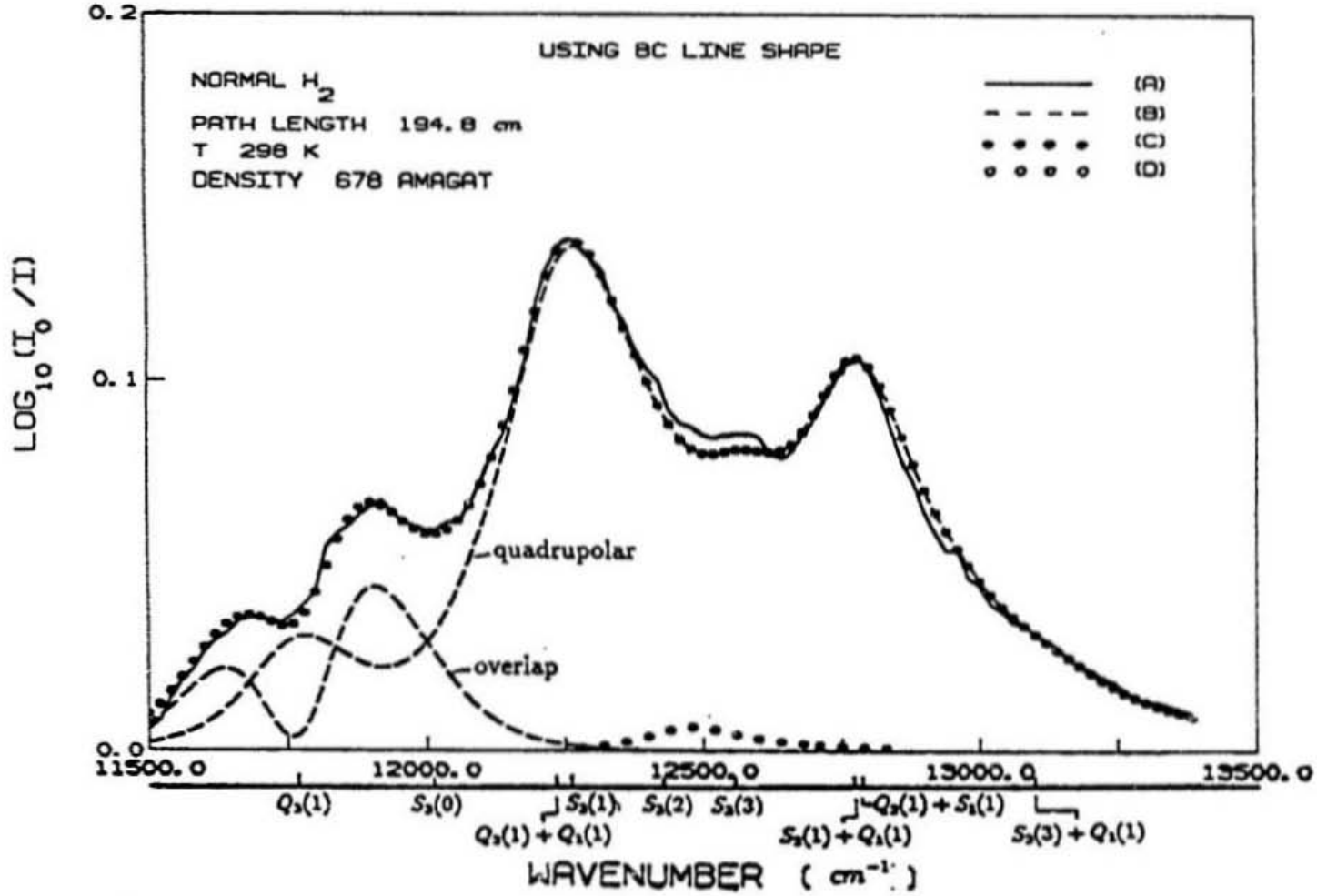

Figure 3.14: Re-analysis of the absorption profile shown in Figure 3.9 using BC line-shape function for the quadrupolar components. Refer to the caption of Figure 3.8 for other details.

was shown that the collision-induced spectra of H_2 in its second overtone region can be fitted very well with either the Birnbaum-Cohen line-shape function or the Lorentz line-shape function. However, the Birnbaum-Cohen line-shape function gives better fits of the calculated profiles to the experimental ones in the high wavenumber tails of the spectra.

As mentioned earlier, in the computer program for the profile analysis, provision was made to adjust the molecular wavenumbers ν_m of H_2. For the spectra of the second overtone of H_2 at 201 and 298 K, the best fits of the calculated profiles to the observed profiles were obtained for an unshifted molecular frequency ν_m (in cm^{-1}). However, for the spectra at 77 K, a wavenumber shift of $\sim$ -10 cm^{-1} for the quadrupolar lines is required for the best fits within the range of the experimental gas densities; no shift is required for the overlap lines.

3.8 Discussion

Very good agreement between the calculated absorption profiles and the experimental profiles of the CIA spectra of H_2 in its second overtone region has been obtained as seen in Section 3.7. One of the factors used in the analysis of the profiles

is the reduction of the matrix elements of the quadrupolar moment of H_2 for $\Delta v = 2$ and 3 by a factor of 0.68, and it is essential to explain the physical basis for this reduction. Private discussions with professors J.D. Poll (University of Guelph) and A. Dalgarno (Harvard University) have indicated that such a direct reduction of the quadrupolar matrix elements is not appropriate in the first instance and that there must be a different mechanism for the reduced intensity of the quadrupolar lines involving $\Delta v = 2$ and 3. We give an account for this in the following paragraph.

According to Poll and Van Kranendonk (1961) and Poll and Hunt (1976) (see also Reddy, 1985), a spherical component μ_ν of the induced dipole moment $\vec{\mu}$ in a pair of colliding molecules 1 and 2 can be expanded as a sum of components with definite angular dependence and is written as

$$\mu_\nu(\vec{r}_1, \vec{r}_2, \vec{R}) = \frac{(4\pi)^{3/2}}{3^{1/2}} \sum_{\lambda_1 \lambda_2 \Lambda L} A_\Lambda(\lambda_1 \lambda_2 L; r_1 r_2 R) \Psi_{1\nu}^{\lambda_1 \lambda_2 \Lambda L}(\omega_1 \omega_2 \Omega) \qquad (3.28)$$

where the intermolecular separation $\vec{R} \equiv (R, \Omega)$, internuclear separations $\vec{r}_1 \equiv (r_1, \omega_1)$ and $\vec{r}_2 \equiv (r_2, \omega_2)$, the functions $\Psi_{1\nu}^{\lambda_1 \lambda_2 \Lambda L}$ transform like vectors under rotation and involve Clebsch-Gordan coefficients and spherical harmonics, and the expansion coefficients $A_\Lambda(\lambda_1 \lambda_2 L; r_1 r_2 R)$ characterize the possible contributions of a given symmetry under rotation. The quantities λ take only even values, 0 for the overlap induction, and 2 for the quadrupolar induction, etc., and L takes odd values 1 and 3. The

expansion coefficients A_Λ (abbreviated as $A_\Lambda(\lambda_1\lambda_2 L)$) are replaced by the matrix elements $B_{L\lambda}(R)$ by the relation

$$B_{L\lambda}(R) = < v_1 J_1 v_2 J_2 | A_\Lambda(\lambda_1\lambda_2 L) | v_1' J_1' v_2' J_2' > \ . \tag{3.29}$$

The $B_{L\lambda}$ matrix elements can be explicitly written in terms of atomic units ea_0 as (see Poll et al., 1975)

$$B_{10}(R)/ea_0 = \lambda_{10} \exp[-(R-\sigma)/\rho_{10}] \tag{3.30}$$

$$B_{12}(R)/ea_0 = \lambda_{12} \exp[-(R-\sigma)/\rho_{12}] \tag{3.31}$$

$$\begin{aligned} B_{32}(R)/ea_0 &= \lambda_{32} \exp[-(R-\sigma)/\rho_{32}] \\ &+ \sqrt{3} < vJ|Q|v'J' >< vJ|\alpha|v'J' > (R/a_0)^{-4} \ . \end{aligned} \tag{3.32}$$

Here ρ's are the ranges of the induced dipole. Of the three $B_{L\lambda}$ terms, the B_{10} term refers to the short-range isotropic overlap contribution and the B_{12} term refers to the short-range anisotropic overlap contribution. The B_{32} term in Eq. 3.32 evidently consists of two terms. The first of these is expected to be considerably smaller than the second. The intensity of absorption of the quadrupolar lines is proportional to the square of $B_{32}(R)$, i.e., it depends on two square terms, $\lambda_{32}^2 \exp[-2(R-\sigma)/\rho_{32}]$ (which is very small), and $3 < vJ|Q|v'J' >^2 < vJ|\alpha|v'J' >^2 \ (R/a_0)^{-8}$ (the major term)

and a mixed term $2\sqrt{3}\lambda_{32}\exp[-(R-\sigma)/\rho_{32}] < vJ|Q|v'J' >< vJ|\alpha|v'J' > (R/a_0)^{-4}$. We interpret our results to indicate that the mixed term contributes negatively to the intensity of absorption of the quadrupolar transitions involving $\Delta v = 2$ and 3. We now conclude that the *apparent* reduction factor of 0.68 applied to the matrix elements of the quadrupolar moment used in the profile analysis presented in this chapter is *indirectly* due to the *negative* contribution to the intensity of absorption by the mixed term proposed here. Thus the reason for the apparent reduction of the $\Delta v = 2$ and 3 quadrupole moment matrix elements is due to the limitations of the "exponential-4" model for the induced-dipole moment. We are grateful to Professor J.D. Poll of the University of Guelph for helpful discussions in this matter.

Chapter 4

TRIPLE TRANSITIONS

$Q_1(J) + Q_1(J) + Q_1(J)$ of H_2

4.1 Introduction

Prior to the present work there has been no experimental observation of spectral transitions in collision-induced absorption corresponding to simultaneous collisions among three molecules. We now propose that the excess absorption around 12,460 cm^{-1} in the collision-induced absorption spectra of H_2 in the second overtone region (see Figures 3.7, 3.8 and 3.9) does arise from the transitions $Q_1(J) + Q_1(J) + Q_1(J)$

of H_2 due to three-body collisions of H_2. The existing theories of collision-induced absorption (see, for example, Van Kranendonk, 1957, 1958, 1959) assume the pair-wise additivity of potentials in calculating the total intermolecular potential, i.e., $V_{total} = \sum V_{ij}$. However, when the density of the gas is high enough, triple-wise and higher order potentials should also be taken into account, and V_{total} can be expressed as

$$V_{total} = \sum V_{ij} + \sum V_{ijk} + \sum V_{ijkl} + \cdots , \tag{4.1}$$

where the terms V_{ijk}, etc., represent potentials due to triple collisions, etc. Thus triple transitions in collision-induced absorption occur due to the contribution of triple and possibly higher order dipole moment terms. The higher order interaction terms depend simultaneously on the relative translational, rotational and vibrational motions of the molecules in triple and higher order collisions.

For the positive confirmation of the occurrence of the triple-collision transitions it is indeed necessary to establish (1) that the absorption intensity is proportional to the cube of the gas density (i.e., $\int \alpha(\nu)d\nu \propto \rho^3$), (2) that the spectral region of the excess absorption coincides with the calculated frequencies of the triple collisions, and (3) that the excess absorption profile can be satisfactorily fitted with the calculated profile of triple-collision transitions. The first two of these criteria are satisfactorily

applied for all the excess absorption profiles of H_2 at 77, 201 and 298 K in this chapter. We also estimate here the relative intensities for the $Q_1(J) + Q_1(J) + Q_1(J)$ transitions. Profile analysis of the excess absorption is then carried out using the methods described in Chapter 3, thus satisfying the criterion 3. The rest of this chapter is devoted to the presentation of the absorption profiles and their analyses.

4.2 Absorption Profiles and Absorption Coefficients

Typical absorption profiles of the triple-collision transitions obtained at 77, 201 and 298 K are presented in Figures 4.1, 4.2 and 4.3, respectively. Experimental details for the profiles presented in these figures are summarized in Table 4.1.

As seen in Chapter 3, in normal H_2 at 77 K only the $J = 0$ and 1 levels of $v = 0$ of the ground electronic state are populated appreciably. The calculated wavenumbers of the three possible Q type triple transitions, namely, $Q_1(1) + Q_1(1) + Q_1(1)$ and $Q_1(1) + Q_1(1) + Q_1(0)$ and $Q_1(1) + Q_1(0) + Q_1(0)$, from the constants of the free H_2

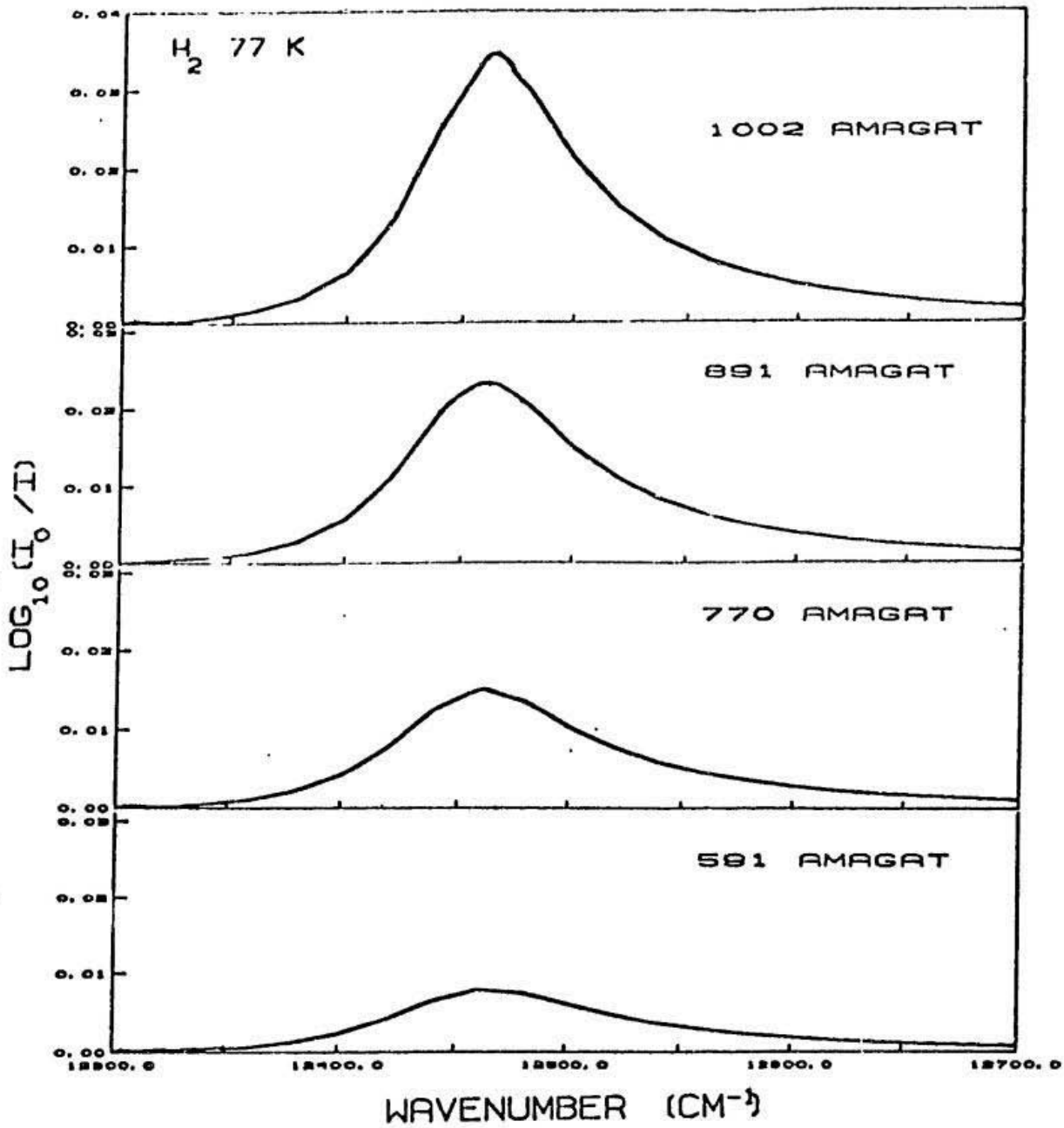

Figure 4.1: Absorption profiles of the triple transitions of the type $Q_1(J) + Q_1(J) + Q_1(J)$ of H_2 at 77 K at four different densities of the gas in the second overtone region.

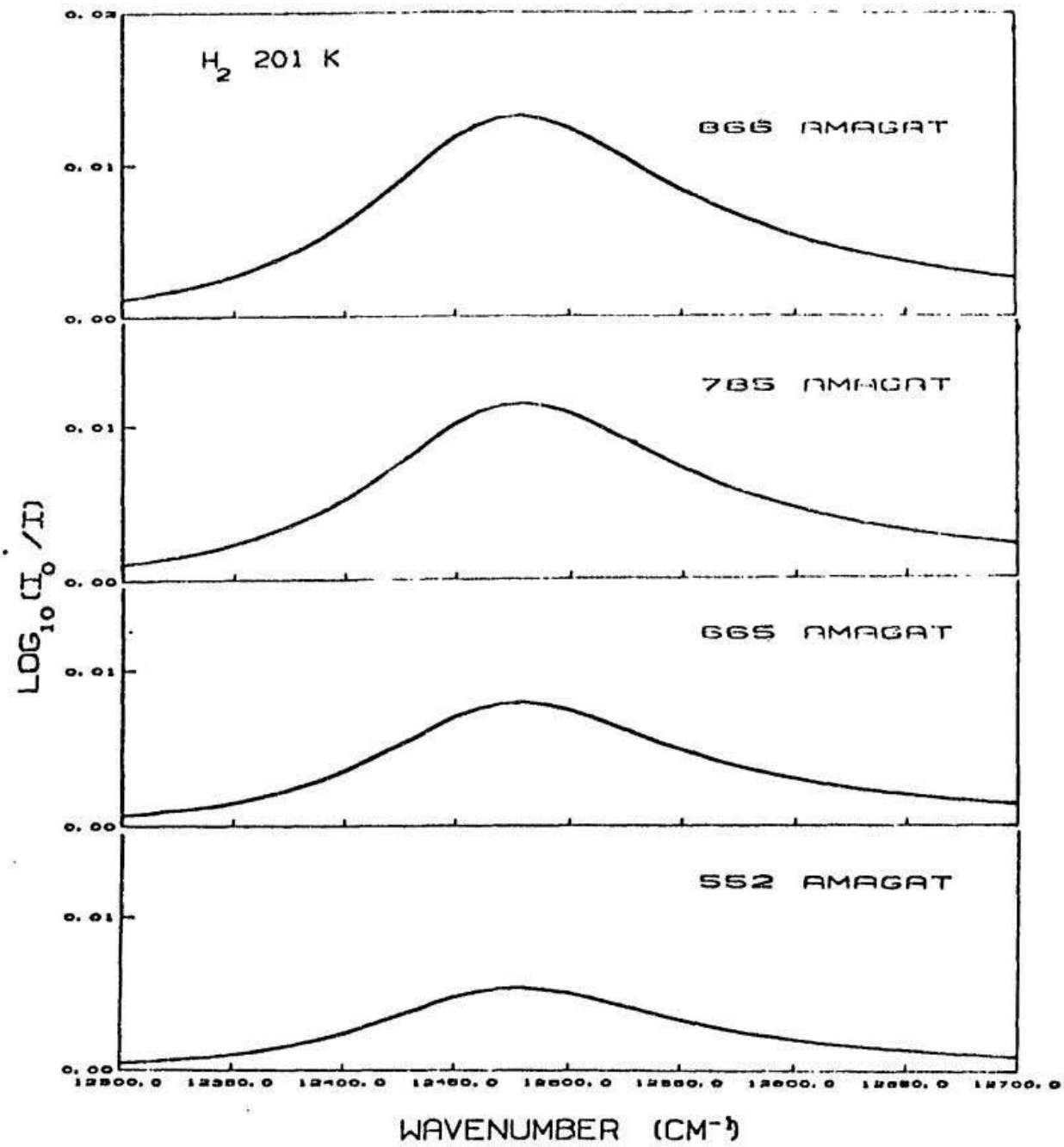

Figure 4.2: Absorption profiles of the triple transitions of the type $Q_1(J) + Q_1(J) + Q_1(J)$ of H_2 at 201 K at four different densities of the gas in the second overtone region.

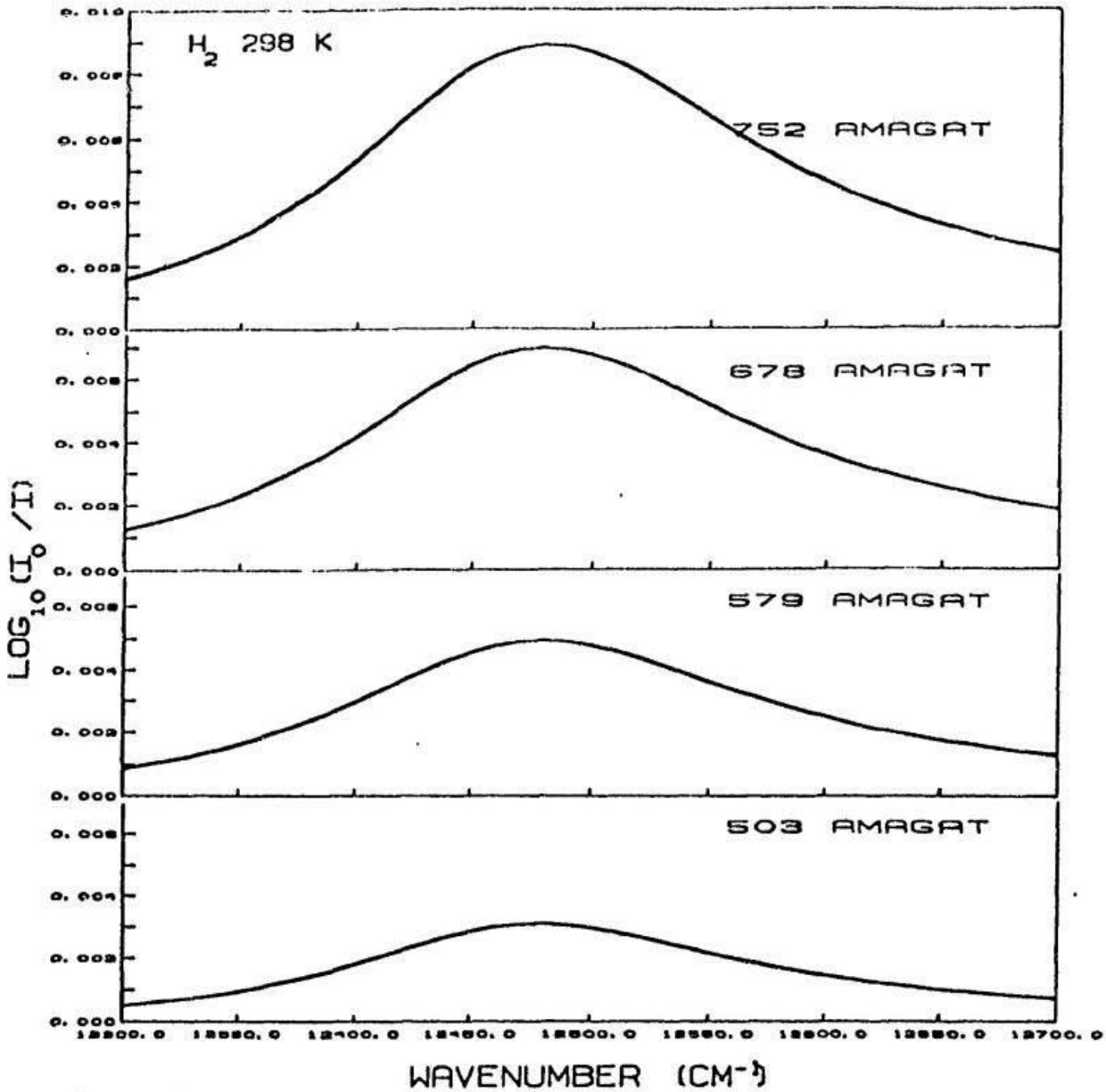

Figure 4.3: Absorption profiles of the triple transitions of the type $Q_1(J) + Q_1(J) + Q_1(J)$ of H_2 at 298 K at four different densities of the gas in the second overtone region.

Table 4.1: Experimental details for the excess absorption

Figure	Temperature (K)	Absorption path length (cm)	Gas density (amagat)
4.1	77	194.2	591, 770, 891, 1002
4.2	201	194.5	552, 665, 785, 866
4.3	298	194.8	503, 579, 678, 752

molecule (Bragg et al., 1982) are 12,465.8, 12,471.7 and 12,477.6 cm^{-1}, respectively, and these are listed in Table 4.2. For the sake of information, calculated wavenumbers of four possible S type triple transitions of the type $S_1(J) + S_1(J) + S_1(J)$ are also given in the same table. We note here that the absorption in Figures 4.1, 4.2 and 4.3 occurs in the vicinity of the $Q_1(J) + Q_1(J) + Q_1(J)$ transitions.

The integrated absorption coefficients $\int \alpha(\nu)d\nu$ of the *excess* absorption profiles can be expressed as

$$\int \alpha(\nu)d\nu = \alpha_3\rho^3 + \alpha_4\rho^4 + \cdots \tag{4.2}$$

where ρ is the density of the gas and α_3 (in $cm^{-2}amagat^{-3}$) is the triple-collision absorption coefficient and α_4 (in $cm^{-2}amagat^{-4}$) is the four-body collision absorption

coefficient. Plots of $(1/\rho^3)\int \alpha(\nu)d\nu$ against ρ for the three experimental temperatures are shown in Figure 4.4. The intercepts and slopes obtained from the least-squares fit give the ternary and quaternary absorption coefficients and the values of these are listed in Table 4.3. Figure 4.4 definitely establishes ρ^3 and ρ^4 dependence of the integrated absorption coefficient.

Table 4.2: Wavenumbers and relative intensities for triple transitions in the second overtone region of H_2 at 77 K

Transition	Wavenumber (cm^{-1})	Relative Intensity
$Q_1(1) + Q_1(1) + Q_1(1)$	12465.8	1.000
$Q_1(1) + Q_1(1) + Q_1(0)$	12471.7	0.331
$Q_1(1) + Q_1(0) + Q_1(0)$	12477.6	0.109
$S_1(0) + S_1(0) + S_1(0)$	13493.4	
$S_1(1) + S_1(0) + S_1(0)$	13708.5	
$S_1(1) + S_1(1) + S_1(0)$	13923.6	
$S_1(1) + S_1(1) + S_1(1)$	14138.7	

Table 4.3: Absorption coefficients[a] of the triple transitions in the second overtone region of H_2

Temperature (K)	Ternary absorption coefficient α_3 (10^{-11}cm^{-2}amagat^{-3})	Quaternary absorption coefficient α_4 (10^{-14}cm^{-2}amagat^{-4})
77	8.8 ± 0.1	-4.4 ± 1.2
201	11.0 ± 0.3	-4.2 ± 1.4
298	11.0 ± 0.6	-6.2 ± 1.6

[a]The errors indicated are standard deviations.

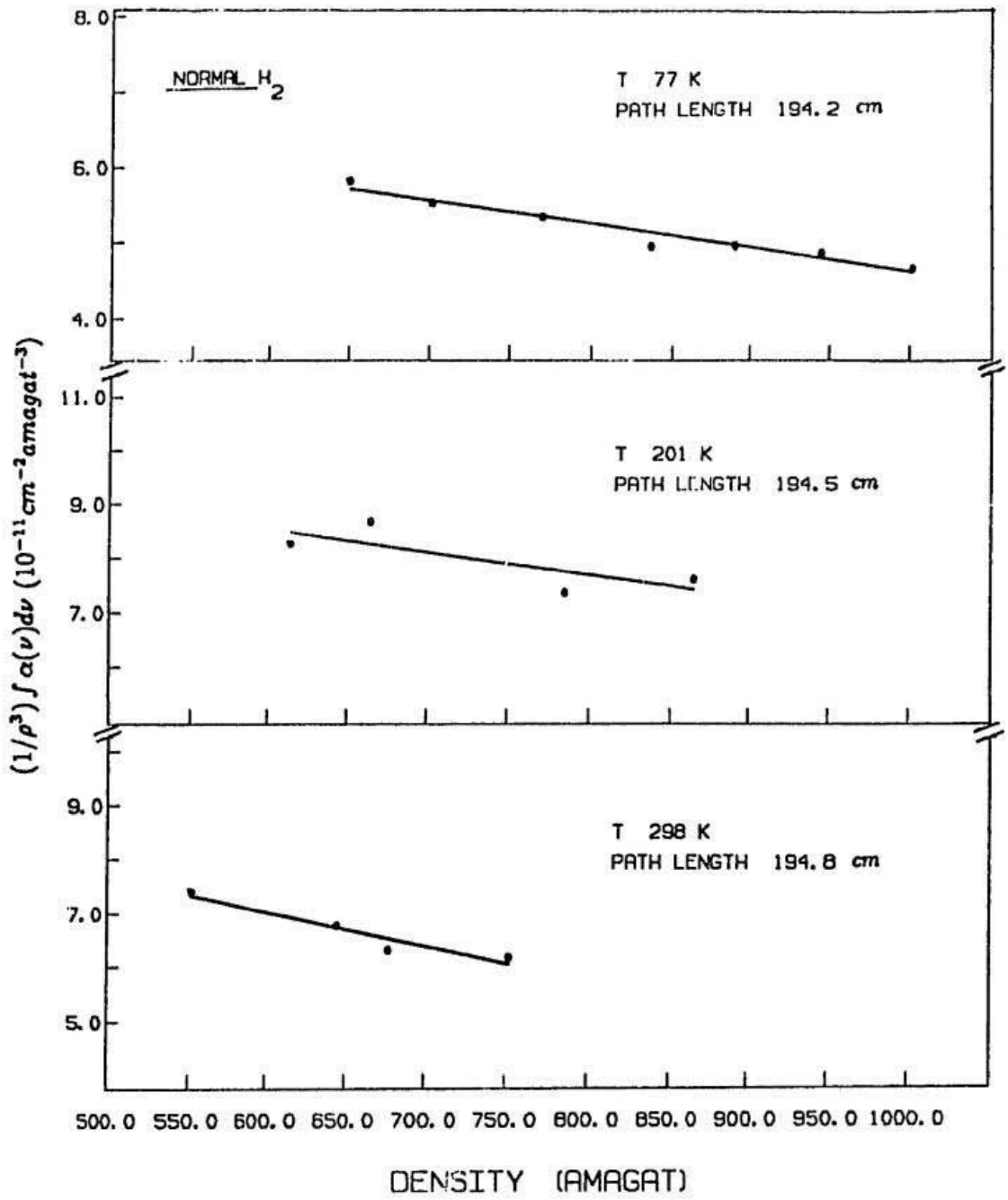

Figure 4.4: Plots of $(1/\rho^3)\int\alpha(\nu)d\nu$ versus ρ for the triple transition profiles of H_2 in the pure gas at 77, 201 and 298 K in the second overtone region.

4.3 Profile Analysis

A theoretical expression for the intensity of the triple transitions is not available in the literature. However, since the relative intensities of the transitions depend mostly on the populations, i.e. the normalized Boltzmann factor P_J, one can estimate the relative intensities of the triple transitions from the values of P_J. The estimated relative intensities for the $Q_1(J) + Q_1(J) + Q_1(J)$ transitions are also listed in Table 4.2.

The analysis of the absorption profiles of the $Q_1(J)+Q_1(J)+Q_1(J)$ transitions at 77 K were performed using the Lorentz line-shape function as well as the Birnbaum-Cohen line-shape function, as described in Chapter 3. A typical example of the profile analysis at 77 K using the Lorentz line-shape function is given in Figure 4.5. The analysis of the same profile using the BC line-shape function is shown in Figure 4.6. In each of these figures the calculated profile is in excellent agreement with the experimental profile. The halfwidth parameter, δ_q, for the Lorentz line-shape function is 49 cm^{-1}. The parameters, δ_1 and δ_2, for the BC line-shape function are 48 and 316 cm^{-1}. Thus it is concluded that the excess absorption is due to $Q_1(J)+Q_1(J)+Q_1(J)$ transitions of H_2.

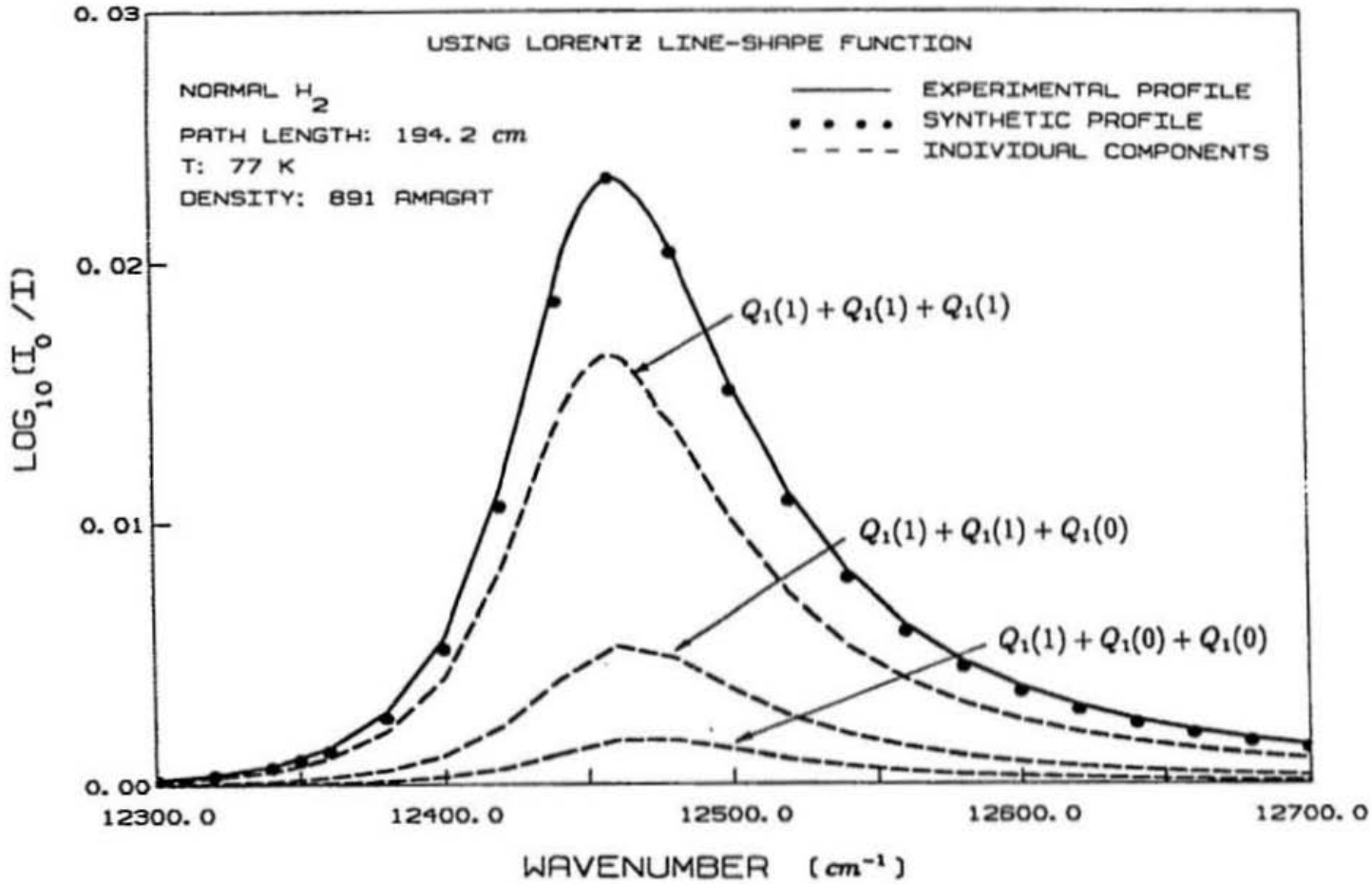

Figure 4.5: Analysis of an absorption profile of the triple transition of normal H_2 in the pure gas at 891 amagat and 77 K in the second overtone region, using the Lorentz line-shape function.

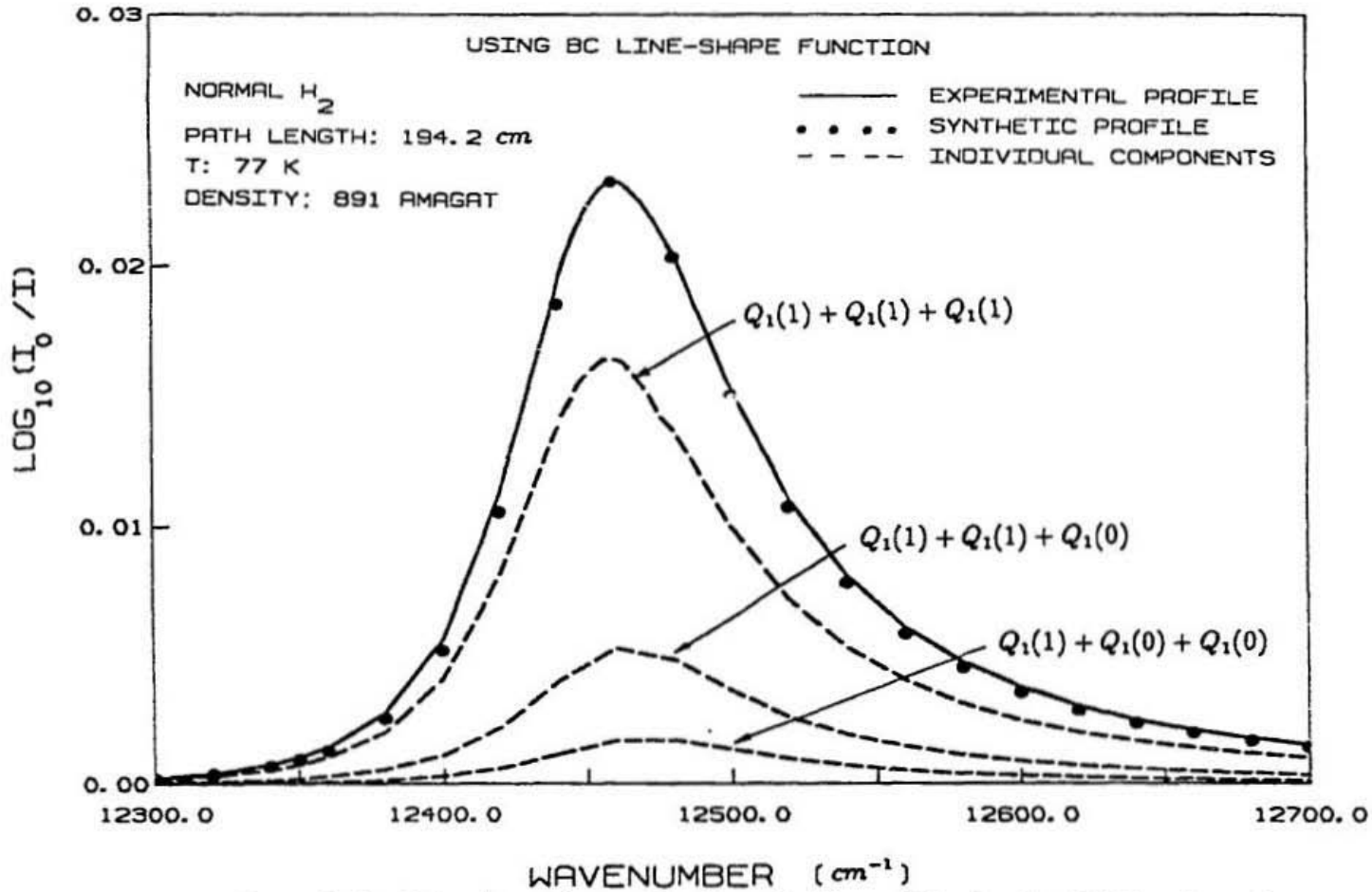

Figure 4.6: Re-analysis of the absorption profile shown in Figure 4.5 using the BC line-shape function.

Chapter 5

CONCLUSIONS

The research project for the present thesis consisted of a detailed experimental investigation of the collision-induced infrared absorption of normal H_2 in its second overtone region at 77, 201 and 298 K for gas densities up to 1000 amagat with a 2 m stainless steel absorption cell.

The observed absorption profiles show a dip in the Q branch in the overlap-induced transitions $Q_3(J)$ with characteristic low- and high- wavenumber components Q_P and Q_R and several quadrupole-induced single transitions $Q_3(J)$ (=$Q_3(J) + Q_0(J)$) and $S_3(J)$ (=$S_3(J) + Q_0(J)$), and double transitions $Q_3(J) + S_0(J)$ and $S_3(J) + S_0(J)$ of the pure 3-0 band, and many quadrupole-induced double transitions $Q_2(J) + Q_1(J)$,

$S_2(J)+Q_1(J)$, $Q_2(J)+S_1(J)$ and $S_2(J)+S_1(J)$ of the combination 2-0 + 1-0 band. The observation of the dip in the Q branch clearly indicates the contribution of the isotropic overlap interaction to the intensity of the band. The earlier work on the fundamental and first overtone bands of H_2 and the present work on the second overtone band of H_2 show that $< 0J|\mu_{ov}|v'_{odd}J' > \neq 0$, but $< 0J|\mu_{ov}|v'_{even}J' >= 0$. This implies that the overlap contribution to the Q branch of the induced 4–0 band of H_2 will be negligible. It is suggested that a theoretical treatment of this feature in the CIA spectra will be interesting.

The line-shape function $W_{ov}(\Delta\nu)$ for the overlap components and either the Lorentz line-shape function $W_q^L(\Delta\nu)$ or the Birnbaum-Cohen line-shape function $W_q^{BC}(\Delta\nu)$ for the quadrupolar components were used in the analyses of the absorption profiles. Also, it was found necessary to treat the relative intensities of the groups of quadrupolar single and double transitions as independent parameters and to reduce the quadrupole matrix elements of H_2, $< 0J|Q|v'J' >$ for $v' = 2$ and 3 by a factor 0.68. This *apparent* reduction is interpreted as due to the negative contribution of the mixed term $2\sqrt{3}\lambda_{32}\exp[-(R-\sigma)/\rho_{32}] < vJ|Q|v'J' >< vJ|\alpha|v'J' > (R/a_0)^{-4}$ to the total absorption. Both line-shape functions $W_q^L(\Delta\nu)$ and $W_q^{BC}(\Delta\nu)$ gave good fits of the synthetic profiles to the experimental profiles. However, BC line-shape function gave a better fit in the high wavenumber wing of the band. The reason

for the *apparent* reduction in the values of the matrix elements of the quadrupole moment of H_2 for $\Delta v = 2$ and 3 is interpreted as being due to a *negative* interference between the quadrupole-induced dipole moment and an anisotropic overlap-induced dipole moment in the collision process.

To explain the triple transitions, potential terms such as V_{ijk} and V_{ijkl} are invoked. The excess absorption around 12,460 cm^{-1} in the absorption profiles is assigned to the triple transitions $Q_1(J) + Q_1(J) + Q_1(J)$ of H_2, resulting from simultaneous collision of three H_2 molecules. The absorption profiles due to these transitions were analyzed using the line-shape functions $W_q^L(\Delta\nu)$ and $W_q^{BC}(\Delta\nu)$.

Bibliography

Birnbaum, G. and Cohen, E.R. *Can. J. Phys.* **54**, *593* (1976).

Birnbaum, G., Guillot, B. and Bratos, S. *Adv. Chem. Phys.* **51**, *49* (1982).

Bragg, S.L., Brault, J.W. and Smith, W.H. *Astrophys. J.* **263**, *999* (1982).

Crawford, M.F., Welsh, H.L. and Locke, J.L. *Phys. Rev.* **75**, *1607* (1949).

C.R.C. Handbook of Chemistry and Physics edited by R.C. Weast (Chemical Rubber Co.) 66th Edition (1985-1986).

De Boer, J. *Repts. Progr. Phys.* **12**, *305* (1949).

De Remigis, J., MacTaggart, J.W. and Welsh, H.J. *Can. J. Phys.* **49**, *381* (1971).

Dore, P., Nencini, L. and Birnbaum, G. *JQSRT* **30**, *245* (1983).

Foltz, J.V., Rank, D.H. and Wiggins, T.A. *J. Mol. Spect.* **21**, *203* (1966).

Gibbs, P.W., Gray, C.G., Hunt, J.L., Reddy, S.P., Tipping, R.H. and Chang, K.S. *Phys. Rev. Lett.* **33**, *256* (1974).

Gibbs, P.W., Hunt, J.L. and Poll, J.D. *Can. J. Phys.* **57** *981* (1979).

Gillard, P.G. *Ph.D Thesis, Memorial University of Newfoundland, St. John's, Newfoundland,* (1983).

Gillard, P.G., Prasad, R.D.G. and Reddy, S.P. *J. Chem. Phys.* **81**, *3458* (1984).

Goorvitch, D., Silvaggio, P.M. and Boese, R.W. *JQSRT* **25**, *237* (1981).

Herzberg. G. *J. Roy. Astron. Soc. Can.* **45**, *100* (1951).

Herzberg, G. *Astrophys. J.* **115**, *337* (1952).

Hunt, J.L. *Ph.D. Thesis, University of Toronto.* (1959).

Hunt, J.L. and Welsh, H.L. *Can. J. Phys.* **42**, *873* (1964).

Hunt, J.L., Poll, J.D. and Wolniewicz, L. *Can. J. Phys.* **62**, *1719* (1984).

Hunt, J.L. and Poll, J.D. *Mol. Phys.* **59**, *163* (1986).

Karl, G., Poll, J.D. and Wolniewicz, L. *Can. J. Phys.* **53**, *1781* (1975).

Kupier, G.P. *Astrophys. J.* **109**, *540* (1949).

Levine, H.B. and Birnbaum, G. *Phys. Rev.* **154**, *72* (1967).

Lewis, J.C. and Van Kranendonk, J. *Phys. Rev. Lett.* **24**, *802* (1971).

Lewis, J.C. and Van Kranendonk, J. *Can. J. Phys.* **50**, *952* (1972a).

Lewis, J.C. and Van Kranendonk, J. *Can. J. Phys.* **50**, *2881* (1972b).

Lewis, J.C. *Can. J. Phys.* **50**, *2902* (1972).

Lewis, J.C. *Can. J. Phys.* **51**, *2455* (1973).

Lewis, J.C. *Physica A* **82**, *500* (1976).

Lewis, J.C. and Tjon, J.A. *Physica A* **91**, *161* (1978).

Lewis, J.C., in **Phenomena induced by intermolecular interactions. NATO ASI Series, Series B: Physics. Vol. 127,** Edited by G. Birnbaum (Plenum Press, New York), *215* (1985).

Mactaggart, J.W. and Welsh, H.L. *Can. J. Phys.* **51**, *158* (1973).

Mactaggart, J.W., De Remegis, J. and Welsh, H.L. *Can. J. Phys.* **51**, *1971* (1973).

McCarty, R.D., Hord, J. and Roder, H.M. *Natl. Bur. Standards Monograph* **168** (1981).

McKellar, A.R.W. and Welsh, H.L. *Proc. Roy.Soc. London, A* **322**, (1971).

McKellar, A.R.W. *Can. J. Phys.* **66**, *155* (1988).

Okumura, M., Chan, M. and Oka, T. *Phys. Rev. Lett.* **62**, *32* (1989).

Poll, J.D. *Ph.D. Thesis, University of Toronto* (1960).

Poll, J.D. and Van Kranendonk, J. *Can. J. Phys.* **39**, *189* (1961).

Poll, J.D., in **Proceedings I.A.U. Symposium 40 on Planetary atmospheres** (Reidel, Dordrecht, Holland), *384* (1971).

Poll, J.D., Hunt, J.L. and Mactaggart, J.W. *Can. J. Phys.* **53**, *954* (1975).

Poll, J.D. and Hunt, J.L. *Can. J. Phys.* **54**, *461* (1976).

Poll, J.D., in **Proceedings of the International School of Physics Enrico Fermi, Course LXXV, Intermolecular Spectroscopy and Dynamical Properties of Dense Systems** Edited by J. Van Kranendonk (North-Holland Publishing Company, New York), *45* (1980).

Prasad, R.D.G. *Ph.D thesis, Memorial University of Newfoundland, St. John's, Newfoundland,* (1976).

Reddy, S.P. and Kuo, C.Z. *J. Mol. Spectrosc.* **37**, *327* (1971).

Reddy, S.P., Varghese, G. and Prasad, R.D.G. *Phys. Rev. A* **15**, *975* (1977).

Reddy, S.P. and Prasad, R.D.G. *J. Chem. Phys.* **66**, *5259* (1977).

Reddy, S.P., Sen, A. and Prasad, R.D.G. *J. Chem. Phys.* **72**, *6102* (1980).

Reddy, S.P., in **Phenomena induced by intermolecular interactions. NATO ASI Series, Series B: Physics. Vol. 127,** Edited by G. Birnbaum (Plenum Press, New York), *129* (1985).

Rich, N.H. and McKellar, A.R.W. *Can. J. Phys.* **54**, *486* (1976).

Rose, M.E. **Elementary Theory of Angular Momentum** (John Wiley and Sons, Inc., New York) (1957).

Sen, A., Prasad, R.D.G. and Reddy, S.P. *J. Chem. Phys.* **72**, *1716* (1980).

Silvaggio, P.M., Goorvitch, D. and Boese, R.W. *JQSRT* **26**, *103* (1981).

Varghese, G., Prasad, R.D.G. and Reddy, S.P. *Phys. Rev. A* **35**, *701* (1987).

van Nostrand, E. *M.Sc. Thesis, Memorial University of Newfoundland, St. John's, Newfoundland,* (1983).

Van Kranendonk, J. *Physica* **23**, *825* (1957).

Van Kranendonk, J. *Physica* **24**, *947* (1958).

Van Kranendonk, J. *Physica* 25, *337* (1959).

Van Kranendonk, J. *Can. J. Phys.* **46**, *1173* (1968).

Van Kranendonk, J. *Physica* **73**, *156* (1974).

Watanabe, A. *Can. J. Phys.* **49**, *1320* (1971).

Welsh, H.L., Crawford, M.F. and Locke, J.L. *Phys. Rev.* **76**, *580* (1949).

Welsh, H.L., in **MTP International Review of Science, Spectroscopy, Physical Chemistry, Series one, Vol. 3,** Edited by D.A. Ramsay (Butterworths, London), *33* (1972) and references therein.

Zaidel, A.N., Prokofer, V.K., Raisku, S.M., Slavnyi, V.A. and Shreider, E.Ya. **Tables of Spectral Lines** (IFI/Plenum, New York-London.) (1970).

Zaidi, H.R. and Van Kranendonk, J. *Can. J. Phys.* **49**, *385* (1971).

Appendix A

FORTRAN PROGRAM FOR PROFILE ANALYSIS

A.1 Calculation of Absolute Intensities for H_2 in the Second Overtone Band

```
c       PROGRAM TO CALCULATE ABSOLUTE INTENSITIES FOR H2
c       IN TERMS OF EQUATION (3.13)
c       ---------------------------------------------------------------
        implicit real *8 (a-h,o-z)
        real*8 mat(3,3,6,6),p(8),e(8),pc,sum1,sum2,sum,jstar
        real*8 x,y,cq,cs,co
        integer v,v1,v2,j1,j2
        character*60 spec

        t = 298.0
        c = 2.9979246e+10
        h = 6.6260755e-27
        bolz = 1.380658e-16
        sigma = 2.95886
        eps = 5.067e-15
        pi = 3.14159265
c       e = 4.80324e-10 (esu), a0 = 0.529177249 (angstrom)
c       n0 = 2.686763e+19 (1/cm**3)
```

```
c       const = (8*pi**3*e**2*a0**5*n0**2)*(a0/sigma)**5/(3*h*c)
c       const = 0.52632e-07

c       read the matrix elements
c       specification of matrix elements mat(k,i,v,j)
c       k=1(quadrupole),k=2(polarizability),k=3(anisotropic polar)
c       i=1(Q branch),i=2(S branch),i=3(O branch)
c       v=vibrational QN, j=rotational QN
        open (unit = 8,file = 'h2matrix',status = 'old')
        rewind (8)
        do 70 k = 1, 3
          read (8,*)
          read (8,80) spec
          do 60 i = 1, 3
            read (8,*)
            read (8,80) spec
            do 50 v = 1,6
              read (8,90) (mat(k,i,v,j),j = 1, 6)
50          continue
60        continue
70      continue
80      format (a60)
90      format (x,f9.6,5(2x,f9.6))

c       calculate the Normalized Boltzmann factors p for molecule in
c       tempreture t. b, d, h1 are molecular rotational constant

        b = 59.334510
        d = 0.45651E-1
        h1 = 0.456E-4

        sum1 = 0.0
        sum2 = 0.0
        do 100 j = 1, 8
          f = b*(j-1)*j - d*((j-1)*j)**2 + h1*((j-1)*jj)**3
```

```
          e(j) = exp(-h*c*f/bolz/t)
          if ((-1)**(j-1) .gt. 0) then
            sum1 = sum1 + (2*(j-1)+1)*e(j)
          else
            sum2 = sum2 + 3*(2*(j-1)+1)*e(j)
          end if
100       continue
          pc = 0.0
          do 110 j = 1, 8
            if ((-1)**(j-1) .gt. 0) then
              p(j) = (2*(j-1)+1)*e(j)/sum1/4
            else
              p(j) = 3*(2*(j-1)+1)*e(j)/sum2*3/4
            end if
            pc = pc + p(j)*j*(j-1)/(2*j-3)/(2*j+1)
110       continue

          open (unit = 9,file = 'h2int',status = 'new')

c         calculate Q single transition

          write(9,400) 'Q transition'
400       format(a20)
          do 200 j = 1, 4
            x = p(j)*cq(j)*mat(1,1,4,j)**2*mat(2,1,1,1)**2 + p(j)*pc*
     +      mat(1,1,1,1)**2*mat(2,1,4,j)**2
            y = p(j)*cq(j)*pc*(2.0/9.0*mat(1,1,4,j)**2*mat(3,1,1,1)**2+
     +      2.0/9.0*mat(3,1,4,j)**2*mat(1,1,1,1)**2 - 4.0/15.0*
     +      mat(1,1,4,j)*mat(3,1,1,1)*mat(3,1,4,j)*mat(1,1,1,1))
            QS = const*jstar(t,sigma,eps,pi,bolz)*(x+y)
            write(9,210) 'Q3(',j-1,')=',QS
200       continue
210       format(2x,a3,i1,a2,g11.4)

c         calculate S single transition
```

```
      write(9,*)
      write(9,400) 'S transition'
      do 220 j = 1, 4
        x = p(j)*cs(j)*mat(1,2,4,j)**2*mat(2,1,1,1)**2
        y = P(j)*cs(j)*pc*(2.0/9.0*mat(1,2,4,j)**2*mat(3,1,1,1)**2
     +  +2.0/9.0*mat(1,1,1,1)**2*mat(3,2,4,j)**2-4.0/15.0*
     +  mat(1,2,4,j)*mat(3,1,1,1)*mat(1,1,1,1)*mat(3,2,4,j))
        SS = const*jstar(t,sigma,eps,pi,bolz)*(x+y)
        write(9,210) 'S3(',j-1,')=',SS
220   continue

c     calculate O single transition

      write(9,*)
      write(9,400) 'O transition'
      do 230 j = 3, 4
        x = p(j)*co(j)*mat(1,3,4,j)**2*mat(2,1,1,1)**2
        y = p(j)*co(j)*pc*(2.0/9.0*mat(1,3,4,j)**2*mat(3,1,1,1)**2
     +  +2.0/9.0*mat(3,3,4,j)**2*mat(1,1,1,1)**2-4.0/15.0*
     +  mat(1,3,4,j)*mat(3,1,1,1)*mat(3,3,4,j)*mat(1,1,1,1))
        OS = const*jstar(t,sigma,eps,pi,bolz)*(x+y)
        write(9,210) 'O3(',j-1,')=',OS
230   continue

c     calculate Q+S double transition

      write(9,*)
      write(9,400) 'Q+S transition'
      do 260 v1 = 2, 4
        v2 = 5-v1
        do 250 j1 = 1, 6
          do 240 j2 = 1, 4
            x = p(j1)*p(j2)*cs(j2)*mat(2,1,v1,j1)**2*mat(1,2,v2,j2)**2
            y = p(j1)*p(j2)*cq(j1)*cs(j2)*(2.0/9.0*mat(1,1,v1,j1)**2*
     +      mat(3,2,v2,j2)**2+2.0/9.0*mat(3,1,v1,j1)**2*
     +      mat(1,2,v2,j2)**2-4.0/15.0*mat(1,1,v1,j1)*mat(3,2,v2,j2)
```

```
     +        *mat(3,1,v1,j1)*mat(1,2,v2,j2))
              QSD = const*jstar(t,sigma,eps,pi,bolz)*(x+y)
              write(9,270) 'Q',v1-1,'(',j1-1,')+S',v2-1,'(',j2-1,')=',QSD
240         continue
250       continue
260     continue
270     format(2x,a1,i1,a1,i1,a3,i1,a1,i1,a2,g11.4)

c       calculate Q+Q double transition

        write(9,*)
        write(9,400) 'Q+Q transition'
        v1 = 3
        v2 = 2
        do 290 j1 = 1, 6
          do 280 j2 = 1, 6
            x = p(j1)*p(j2)*(cq(j1)*mat(1,1,v1,j1)**2*mat(2,1,v2,j2)
     +      **2+cq(j2)*mat(2,1,v1,j1)**2*mat(1,1,v2,j2)**2)
            y = p(j1)*p(j2)*cq(j1)*cq(j2)*(2.0/9.0*(mat(1,1,v1,j1)**2
     +      *mat(3,1,v2,j2)**2+mat(3,1,v1,j1)**2*mat(1,1,v2,j2)**2)
     +      -4.0/15.0*mat(1,1,v1,j1)*mat(3,1,v2,j2)*mat(3,1,v1,j1)
     +      *mat(1,1,v2,j)
            QQD = const*jstar(t,sigma,eps,pi,bolz)*(x+y)
            write(9,270) 'Q',v1-1,'(',j1-1,')+Q',v2-1,'(',j2-1,')=',QQD
280       continue
290     continue

c       calculate S+S double transition

        write(9,*)
        write(9,400) 'S+S transition'
        do 330 v1 = 1, 2
          v2 = 5-v1
          do 320 j1 = 1, 4
            do 310 j2 = 1, 4
              y = p(j1)*p(j2)*cs(j1)*cs(j2)*(2.0/9.0*(mat(1,2,v1,j1)
```

```
     +       **2*mat(3,2,v2,j2)**2+mat(3,2,v1,j1)**2*
     +       mat(1,2,v2,j2)**2)-4.0/15.0*mat(1,2,v1,j1)*
     +       mat(3,2,v1,j1)*mat(1,2,v2,j2)*mat(3,2,v2,j2))
             SSD = const*jstar(t,sigma,eps,pi,bolz)*y
             write(9,270) 'S',v2-1,'(',j2-1,')+S',v1-1,'(',j1-1,')=',SSD
310        continue
320      continue
330    continue
       close(9)
       end

       real function jstar(t,sigma,eps,pi,bolz)
c      function to evaluate the integral J* for h2
c      rmass is the reduced mass of the interacting pair (in
c      atomic mass unit)
c      sigma is the intermolecular separation (in angstrom)
c      eps is the depth of the potential well (in ergs)
c      k=1.380658e-16 erg/k
c      h=6.6260755e-27 erg.s
c      N=6.0221367e+23 /mol
c      lambda=h**2*N*1.0e+16/(2.0*rmass*eps*sigma**2)

       real *8 rmass,lambda,ts,jstar0,jstar1,jstar2
       real *8 v0,v1,v2,v3,v4,g0,g1,g2

       rmass = 1.00
       lambda = 2.64409e-13/(2.0*rmass*eps*sigma**2)

       ts = t*bolz/eps
       jstar0 = 0.0
       jstar1 = 0.0
       jstar2 = 0.0
       do 300 x = 0.5, 20.0, 0.005
         v0 = 4.0*(x**(-12) - x**(-6))
         v1 =-24.0*(2.0*x**(-13) - x**(-7))
         v2 = 24.0*(26.0*x**(-14) - 7.0*x**(-8))
```

```
      v3 =-672.0*(13.0*x**(-15) - 2.0*x**(-9))
      v4 = 2016.0*(65.0*x**(-16) - 6.0*x**(-10))
      g0 = exp(-v0/ts)
      g1 = g0/(24.0*pi**2*ts**2)*(-(v2+2.0*v1/x)+v1**2/(2.0*ts))
      g2 = g0/(192.0*pi**4*ts**3)*(-(v4+4.0*v3/x)/5.0+(9.0*v2**2
     +  +12.0*v1*v3+44.0*v1*v2/x+(2.0*v1/x)**2)/(30.0*ts)
     +  -(11.0*v2*v1**2+10.0*v1**3/x)/(30.0*ts**2)+v1**4
     +  /(24.0*ts**3))
      jstar0 = jstar0 + x**(-6)*g0*0.005
      jstar1 = jstar1 + x**(-6)*g1*0.005
      jstar2 = jstar2 + x**(-6)*g2*0.005
300   continue
      jstar = 12*pi*(jstar0+lambda*jstar1+lambda**2*jstar2)
      return
      end

c     calculate clebsch-gordan coefficients

      real function cq(j)

      cq = j*(j-1.0)/(2.0*j-3.0)/(2.0*j+1.0)
      end

      real function cs(j)

      cs = 3.0*j*(j+1.0)/2.0/(2.0*j-1.0)/(2.0*j+1.0)
      end

      real function co(j)

      co = 3.0*(j-1.0)*(j-2.0)/2.0/(2.0*j-3.0)/(2.0*j-1.0)
      end
```

A.2 Non-Linear Least Squares Fit to Experimental Profile

```
c       NON-LINEAR LEAST SQUARES FIT TO EXPERIMENTAL PROFILE
c       OF A SYNTHETIC QUADRUPOLAR AND OVERLAP SPECTRUM,
c       CONSIDER SINGLE AND DOUBLE TRANSITIONS INDIVIDUALLY
c       ---------------------------------------------------
        implicit real*8 (a-h,o-z)
        integer nqs,nqd,no,n,np,i1,i2,i3,i4,i5,i6,i7,i8,ip,in
        common riqs(50),fqs(50),riqd(100),fqd(100),rio(10),fo(10),a(10),
     1  nqs,nqd,no,i1,i2,i3,i4,i5,i6,i7,i8,t
        real*8 x(300),y(300),dvp(10),dvn(10),vsep(10),vsen(10),
     1  dvpm,dvnm,xx
        character*20 calfil, obsfil
        character*60 head
c
c       read the calculated data
c
        write (6,*) 'enter filename for calculated data'
        read 15, calfil
15      format (A20)
        open (unit = 8,file = calfil,status = 'old')
        rewind (8)
c       read the specification of the calculated data file
        read (8,51) head
        read (8,52) t
c       read freq.(fqs) and relat. intn.(riqs) of quad. single trans.
        read (8,53) nqs
        do 60 i = 1, nqs
          read (8,*) fqs(i),riqs(i)
60      continue
c       read freq.(fqd) and relat. intn.(riqd) of quad. double trans.
        read (8,54) nqd
        do 70 i = 1, nqd
          read (8,*) fqd(i),riqd(i)
70      continue
```

```
c       read freq.(fo) and relat. intn.(rio) of overlap trans.
        read (8,55) no
        do 80 i = 1, no
         read (8,*) fo(i),rio(i)
80      continue
51      format (A60)
52      format ('temperature =', F7.2)
53      format ('No. of quad. single tran. =', I3)
54      format ('No. of quad. double tran. =', I3)
55      format ('No. of overlap lines =', I3)
c
c       read intensities y and frequencies x of observed data
c
        write (6,*) 'enter filename for observed data'
        read 15, obsfil
        if ((obsfil .eq. 'none') .or. (obsfil .eq. 'q')) go to 990
        open (unit = 9,file = obsfil,status = 'old')
        rewind (9)
c       read the specification of the observed data file
        do 90 i = 1, 2
        read (9,51) head
90      continue
56      format ('No. of observed lines =', I3)
        read (9,56) n
        do 100 i = 1, n
        read (9,*) x(i),y(i)
100     continue
c
c       here read all of adjustable parameters
c
        np = 0
        write (6,*) 'intracollisional half-width at half-height dd?'
        read *, xx
        np = np+1
        i1= np
        a(i1) = xx
```

```
c
      write (6,*) 'intercollisional half-width at half-height dc?'
      read *, xx
      np = np+1
      i2 = np
      a(i2) = xx
c
      write (6,*) 'quadrupolar half-width at half-height dq?'
      read *, xx
      np = np+1
      i3 = np
      a(i3) = xx
c
      write (6,*) 'adjustable relative intensity of quad. single tran.?'
      read *, xx
      np = np+1
      i4 = np
      a(i4) = xx
c
      write (6,*) 'adjustable relative intensity of quad. double tran.?'
      read *, xx
      np = np+1
      i5 = np
      a(i5) = xx
c
      write (6,*) 'adjustable relative intensity of over. tran.?'
      read *, xx
      np = np+1
      i6 = np
      a(i6) = xx
c
      write (6,*) 'frequency shift of quad. tran.?'
      read *, xx
      np = np+1
      i7 = np
      a(i7) = xx
```

```
c
      write (6,*) 'frequency shift of overlap tran.?'
      read *, xx
      np = np+1
      i8 = np
      a(i8) = xx
c
c     calculate standard error
c
      vse = 0
      do 200 i = 1, n
        xi = x(i)
        call cal(xi,af)
        vse = vse+(y(i)-af*x(i))**2
200   continue
      aerr = vse/(n-np)
      aerr = sqrt(aerr)
      write (6,205) (a(i), i = 1, np)
      write (6,225) aerr
205   format (3(2x,f7.3)/,5(2x,g10.3))
215   format (2(4(x,g10.3)/))
225   format (x,'standard error =', E14.7/)
c
c     adjust all of parameters to get the best fit
c
      vsem = vse
      write (6,*) 'the increment of the adjustable parameters'
      read *, h
321   h = 0.8d0*h
      if (h .ge. 0.00001) then
        go to 322
      else
        go to 990
      end if
322   continue
      do 300 j = 1, np
```

```
        a(j) = a(j)*(1.d0+h)
        vse = 0
        do 310 i = 1, n
          xi = x(i)
          call cal(xi,af)
          vse = vse+(y(i)-af*x(i))**2
310     continue
        dvp(j) = vse-vsem
        a(j) = a(j)/(1.d0+h)
        vsep(j) = vse
300   continue
      write (6,215) (dvp(j), j = 1, np)
      dvpm = dvp(1)
      ip = 1
      do 320 k = 2, np
        if (dvp(k) .lt. dvpm) then
          dvpm = dvp(k)
          ip = k
        end if
320   continue
      do 400 j = 1, np
        a(j) = a(j)*(1.d0-h)
        vse = 0
        do 410 i = 1, n
          xi = x(i)
          call cal(xi,af)
          vse = vse+(y(i)-af*x(i))**2
410     continue
        dvn(j) = vse-vsem
        a(j) = a(j)/(1.d0-h)
        vsen(j) = vse
400   continue
      write (6,215) (dvn(j), j = 1, np)
      dvnm = dvn(1)
      in = 1
      do 420 k = 2, np
```

```
        if (dvn(k) .lt. dvnm) then
          dvnm = dvn(k)
          in = k
        end if
420     continue
        if (dvpm .le. dvnm ) then
          if (dvpm .lt. 0. ) then
            a(ip) = a(ip)*(1.d0+h)
            write (6,205) (a(i), i = 1, np)
            aerr = vsep(ip)/(n-np)
            aerr = sqrt(aerr)
            write (6,225) aerr
            vsem = vsep(ip)
            go to 322
          else
            go to 321
          end if
        else
          if (dvnm .lt. 0.) then
            a(in) = a(in)*(1.d0-h)
            write (6,205) (a(i), i = 1, np)
            aerr = vsen(in)/(n-np)
            aerr = sqrt(aerr)
            write (6,225) aerr
            vsem = vsen(in)
            go to 322
          else
            go to 321
          end if
        end if
990     stop
        end

        subroutine cal(xi,af)
        implicit real*8 (a-h,o-z)
        real *8 r,asqt,adqt,afqt,xt,rn,afot
```

```
      common riqs(50),fqs(50),riqd(100),fqd(100),rio(10),fo(10),a(10),
     1 nqs,nqd,no,i1,i2,i3,i4,i5,i6,i7,i8,t

      r = 1.43883204d0/t

c     Quadrupolar contribution

      asqt = 0.d0
      do 450 j = 1, nqs
        xt = xi-fqs(j)+a(i7)
        rn = a(i4)*riqs(j)*quad(xt,r,a(i3))
        asqt = asqt+rn
450   continue
      adqt = 0.d0
      do 460 j = 1, nqd
        xt = xi-fqd(j)+a(i7)
        rn = a(i5)*riqd(j)*quad(xt,r,a(i3))
        adqt = adqt+rn
460   continue
      afqt = asqt+adqt
c     Overlap contribution
      afot = 0.d0
      do 500 j = 1, no
        xt = xi-fo(j)+a(i8)
        rn = a(i6)*rio(j)*over(xt,r,a(i1),a(i2))
        afot = afot+rn
500   continue
      af = afqt+afot
      end

c     for Lorentz line shape function
      real*8 function quad(dv,r,a3)
      implicit real*8 (a-h,o-z)
      wq = 1.d0/(1.d0+(dv/a3)**2)
      quad = wq/(1.d0+dexp(-r*dv))
      end
```

```
c       for Birnbaum-Cohen line shape function
        real*8 function quad(dv,r,a3,a4)
        implicit real*8 (a-h,o-z)
        za = 1.0d0+(dv/a3)**2
        zb = (a3/a4)**2+(a3*r/2)**2
        z = dsqrt(za*zb)
        ra = 1.68986e-12/a3/za
        rb = dexp(a3/a4+dv*r/2)
        quad = ra*rb*xK1(z)
        end

        real*8 function xK1(x)
        implicit real*8 (a-h,o-z)
        real*8 I1, K1
c       routine calculates modified bessel function of second kind
        if (x .le. 2) then
        t1 = (x/3.75)**2
        I1 = 0.5+t1*(0.87890594+t1*(0.51498869+t1*(0.15084934
     1  +t1*(0.02658733+t1*(0.00301532+t1*(0.00032411))))))
        I1 = I1*x
        t1 = x*x/4.0
        K1 = x*dlog(x/2.0)*I1+1.0
        xK1 = K1+t1*(0.15443144+t1*(-0.67278579+t1*(-0.18156897
     1  +t1*(-0.01919402+t1*(-0.00110404+t1*(-0.00004686))))))
        else
        t1 = (2.0/x)
        K1 = 1.25331414+t1*(0.23498619+t1*(-0.03655620+t1*
     1  (0.01504268+t1*(-0.00780353+t1*(0.00325614+t1*
     1  (-0.00068245))))))
        xK1 = K1*dsqrt(x)/dexp(x)
        end if
        end

        real*8 function over(dv,r,a1,a2)
        implicit real*8 (a-h,o-z)
```

```
      xt = 2.d0*dv/al

c     routine calculates mod. bessel fn of the 2nd kind order 2
c     for intracollisional line shape function
c
      xt = dabs(xt)
      if (xt .gt. 0.0) go to 600
      res = 2.d0
      go to 850
600   if (xt .gt. 2.0) go to 800
      u = (xt/3.75)**2
      ai= 1.d0+u*(3.5156229+u*(3.0899424+u*(1.2067492
     1 +u*(0.2659732+u*(0.0360768+u*(0.0045813))))))
      ai1 = 0.5d0+u*(0.87890594+u*(0.51498869+u*(0.15084934
     1 +u*(0.02658733+u*(0.00301532+u*(0.00032411))))))
      xr = (xt/2.d0)**2
      ab1 = 1.d0+xr*(0.15443144+xr*(-0.67278579+xr*(-0.18156897
     1 +xr*(-0.01919402+xr*(-0.00110404+xr*(-0.00004686))))))
     2 +0.5d0*xt**2*dlog(xr)*ai1
      ab1 = ab1*2.d0
      ab2 = -0.5d0*ai*dlog(xr)-0.57721566+xr*(0.42278420
     1 +xr*(0.23069756+xr*(0.03488590+xr*(0.00262698
     2 +xr*(0.00010750+xr*(0.00000740))))))
      res = ab1+ab2*xt**2
      go to 850
800   xr=2.d0/xt
      ab1 = 1.25331414+xr*(0.23498619+xr*(-0.03655620+xr*(0.01504268
     1 +xr*(-0.00780353+xr*(0.00325614+xr*(-0.00068245))))))
      ab1 = 2.d0*ab1*xt**0.5d0*dexp(-1.d0*xt)
      ab2 = 1.25331414+xr*(-0.07832358+xr*(0.02189568+xr*(-0.01062446
     1 +xr*(0.00587872+xr*(-0.00251540+xr*(0.00053208))))))
      ab2 = ab2*xt**1.5d0*dexp(-1.d0*xt)
      res = ab1+ab2
850   continue
```

```
w = res

wov = w*(1.d0-(1.d0/(1.d0+(dv/a2)**2)))

over = wov/(1.d0+dexp(-dv*r))
end
```

Appendix B

MATRIX ELEMENTS OF MOLECULAR HYDROGEN

v \ J	0	1	2	3	4	5
			quadrupole matrix elements			
			Q branch			
0	0.483600	0.484700	0.487000	0.490400	0.495000	0.500600
1	0.087900	0.088000	0.088100	0.088400	0.088600	0.089000
2	-0.011190	-0.011230	-0.011300	-0.011410	-0.011550	-0.011730
3	0.001597	0.001605	0.001620	0.001643	0.001674	0.001712
4	-0.000308	-0.000310	-0.000314	-0.000320	-0.000329	-0.000339
5	0.000072	0.000073	0.000074	0.000076	0.000079	0.000083
			S branch			
0	0.485200	0.487300	0.490500	0.494700	0.000000	0.000000
1	0.078400	0.072100	0.065900	0.059800	0.000000	0.000000
2	-0.011650	-0.011830	-0.011920	-0.011930	0.000000	0.000000
3	0.001932	0.002133	0.002315	0.002476	0.000000	0.000000
4	-0.000433	-0.000513	-0.000591	-0.000665	0.000000	0.000000
5	0.000121	0.000154	0.000187	0.000219	0.000000	0.000000
			O branch			
0	0.000000	0.000000	0.000000	0.000000	0.000000	0.000000

1	0.000000	0.000000	0.097700	0.104300	0.111000	0.117700
2	0.000000	0.000000	-0.010530	-0.010070	-0.009500	-0.008870
3	0.000000	0.000000	0.001239	0.000989	0.000734	0.000477
4	0.000000	0.000000	-0.000184	-0.000103	-0.000025	0.000052
5	0.000000	0.000000	0.000026	-0.000003	-0.000030	-0.000055

polarizability matrix elements

Q branch

0	5.413800	5.423400	5.442600	5.471400	5.509500	5.557000
1	0.739230	0.740270	0.742340	0.745440	0.749530	0.754620
2	-0.071270	-0.071500	-0.071960	-0.072660	-0.073580	-0.074740
3	0.009930	0.009970	0.010040	0.010140	0.010290	0.010460
4	-0.002320	-0.002330	-0.002350	-0.002380	-0.002410	-0.002460
5	0.000740	0.000740	0.000740	0.000750	0.000760	0.000770

S branch

0	5.427200	5.444500	5.470500	5.505100	0.000000	0.000000
1	0.633760	0.564950	0.497700	0.432110	0.000000	0.000000
2	-0.070180	-0.068130	-0.065150	-0.061300	0.000000	0.000000
3	0.010490	0.010520	0.010270	0.009780	0.000000	0.000000
4	-0.002440	-0.002420	-0.002310	-0.002110	0.000000	0.000000
5	0.000740	0.000700	0.000630	0.000520	0.000000	0.000000

O branch

0	0.000000	0.000000	0.000000	0.000000	0.000000	0.000000
1	0.000000	0.000000	0.848060	0.921530	0.995660	1.070360
2	0.000000	0.000000	-0.070190	-0.068110	-0.065030	-0.061010
3	0.000000	0.000000	0.008830	0.007820	0.006610	0.005240
4	0.000000	0.000000	-0.002040	-0.001770	-0.001460	-0.001110
5	0.000000	0.000000	0.000660	0.000580	0.000480	0.000370

anisotropic polarizability matrix elements

Q branch

0	2.023800	2.031600	2.047300	2.070800	2.102200	2.141500

1	0.610010	0.611750	0.615240	0.620490	0.627410	0.636120
2	-0.012220	-0.012430	-0.012850	-0.013490	-0.014370	-0.015480
3	-0.005670	-0.005680	-0.005680	-0.005670	-0.005680	-0.005670
4	0.001970	0.001970	0.001980	0.001990	0.001980	0.001990
5	-0.000760	-0.000760	-0.000770	-0.000780	-0.000790	-0.000800

S branch

0	2.035100	2.050000	2.072500	2.102500	0.000000	0.000000
1	0.570810	0.546300	0.523230	0.501520	0.000000	0.000000
2	-0.020970	-0.026350	-0.031430	-0.036230	0.000000	0.000000
3	-0.003720	-0.002400	-0.001090	-0.000220	0.000000	0.000000
4	0.001610	0.001340	0.001050	0.000750	0.000000	0.000000
5	-0.000690	-0.000630	-0.000550	-0.000480	0.000000	0.000000

O branch

0	0.000000	0.000000	0.000000	0.000000	0.000000	0.000000
1	0.000000	0.000000	0.654360	0.685910	0.719310	0.754860
2	0.000000	0.000000	-0.002890	0.003770	0.010740	0.017970
3	0.000000	0.000000	-0.007610	-0.008890	-0.010150	-0.011410
4	0.000000	0.000000	0.002280	0.002450	0.002610	0.002750
5	0.000000	0.000000	-0.000820	-0.000850	-0.000870	-0.000890